AD_____

Award Number: DAMD17-03-1-0565

TITLE: Centrosome Defects, Genetic Instability and Breast Cancer Progression

PRINCIPAL INVESTIGATOR: Stephanie Mirabelle
Stephen Doxsey, Ph.D.

CONTRACTING ORGANIZATION: University of Massachusetts Medical School
Worcester, MA 01605

REPORT DATE: August 2006

TYPE OF REPORT: Annual Summary

PREPARED FOR: U.S. Army Medical Research and Materiel Command
Fort Detrick, Maryland 21702-5012

REPORT DOCUMENTATION PAGE

Form Approved
OMB No. 0704-0188

1. REPORT DATE	2. REPORT TYPE	3. DATES COVERED
01-08-2006	Annual Summary	21 Jul 2003 – 20 Jul 2006

4. TITLE AND SUBTITLE

Centrosome Defects, Genetic Instability and Breast Cancer Progression

5a. CONTRACT NUMBER

5b. GRANT NUMBER
DAMD17-03-1-0565

5c. PROGRAM ELEMENT NUMBER

6. AUTHOR(S)
Stephanie Mirabelle
Stephen Doxsey, Ph.D.

5d. PROJECT NUMBER

5e. TASK NUMBER

5f. WORK UNIT NUMBER

7. PERFORMING ORGANIZATION NAME(S) AND ADDRESS(ES)

University of Massachusetts Medical School
Worcester, MA 01605

8. PERFORMING ORGANIZATION REPORT NUMBER

9. SPONSORING / MONITORING AGENCY NAME(S) AND ADDRESS(ES)
U.S. Army Medical Research and Materiel Command
Fort Detrick, Maryland 21702-5012

10. SPONSOR/MONITOR'S ACRONYM(S)

11. SPONSOR/MONITOR'S REPORT NUMBER(S)

12. DISTRIBUTION / AVAILABILITY STATEMENT
Approved for Public Release; Distribution Unlimited

13. SUPPLEMENTARY NOTES
Original contains colored plates: ALL DTIC reproductions will be in black and white.

14. ABSTRACT

Breast cancer is the most prevalent of all cancers and it is the second most common cause of cancer death amongst women. Centrosome defects have been implicated in cancer formation and can be detected very early in this process. The centrosome protein pericentrin is overexpressed in many cancers including breast cancer. We found that down regulation of pericentrin leads to cytokinesis defects and aneuploidy. Pericentrin overexpression leads to an increase in the number of multinucleated cells, suggesting a defect in cytokinesis. In addition to the cytokinesis defects, pericentrin knock down also induce a G0/G1 arrest that is p53-p38 dependent. Moreover, pericentrin knockdown affects cilia formation in epithelial cells. Also, knock down of several other centrosome proteins leads to aG1 arrest and affects cilia formation in epithelial cells. We conclude that pericentrin affects cytokinesis, G1progression and differentiation. Defects during mitosis, as well as loss of checkpoints and uncontrolled cell division are the first steps in cancer formation. Understanding those events will be a major advance in breast cancer research.

15. SUBJECT TERMS
Centrosome defects, genetic instability, breast cancer progression

16. SECURITY CLASSIFICATION OF:				18. NUMBER OF PAGES	19a. NAME OF RESPONSIBLE PERSON
a. REPORT	b. ABSTRACT	c. THIS PAGE			19b. TELEPHONE NUMBER *(include area code)*
U	U	U	UU	84	USAMRMC

Standard Form 298 (Rev. 8-98)
Prescribed by ANSI Std. Z39.18

TABLE OF CONTENTS

Introduction.

Aneuploidy, an abnormal number of chromosomes (non-euploid), is a hallmark of breast carcinoma that correlates with defects in centrosomes and a poor prognosis and appears to contribute to tumor progression (Hoskins and Weber 1994; Fujii, Marsh et al. 1996). Aneuploidy and centrosome defects can occur by failure of cytokinesis, the final stage of cell division. They can also occur by improper spindle assembly. Centrosomes are microtubule-organizing centers in human cells involved not only in organizing mitotic spindles, but also in cytokinesis, the G1/G0 checkpoint, cell cycle progression and differentiation, all those being parameters relevant to breast cancer (Hinchcliffe 2003; Doxsey, McCollum et al. 2005; Doxsey, Zimmerman et al. 2004). Pericentrin is a centrosome protein whose overexpression induces supernumerary and structurally aberrant centrosomes, dysfunctional mitotic spindles and growth in soft agar(Purohit, Tynan et al. 1999). Pericentrin is overexpressed in some breast cancers(Lingle, Lutz et al. 1998). A better understanding of the role of pericentrin and other centrosome proteins in cytokinesis and spindle function will be important for understanding breast tumor formation. The main goal of this project is to understand potential mechanisms that generate aneuploidy and their relationship to breast cancers. We are testing the role of pericentrin and other centrosome proteins by RNAi-mediated depletion on several functions associated with breast cancer, as a complement to our original focus on pericentrin overexpression studies.

Body.

In the last year we have studied the role of pericentrin and other centrosome proteins in generating aneuploidy, a common defects in most aggressive breast cancers. These studies are discussed below.

Centriolin-anchoring of exocyst and SNARE complexes at the midbody is required for secretory vesicle-mediated abscission during cytokinesis (Appendix 1).

The terminal step in cytokinesis called abscission, requires resolution of the membrane connection between two prospective daughter cells. Centriolin is a coiled-coil midbody and centrosome protein required for abscission. Here we show that centriolin interacts with proteins that associate with vesicle targeting exocyst complexes and vesicle fusion SNARE complexes. Both complexes require centriolin for localization to a unique ring structure at the central midbody. Disruption of either complex by RNA interference disrupts the final stages of cytokinesis. When the exocyst is disrupted, v-SNARE-containing vesicles accumulate at the midbody ring. V-SNAREs co-localize with GFP-labeled secretory vesicles, which move to the midbody ring asymmetrically from one prospective daughter cell. The GFP signal is rapidly lost and the cell separates into two daughters at the site of vesicle delivery. We propose that centriolin anchors protein complexes required for vesicle target specificity and fusion, and coordinates events leading to abscission.

Centrosome protein depletion induces cell cycle arrest in normal cells and severe defects in tumor cells (Appendix 2).

Centrosomes organize the microtubule cytoskeleton for both interphase and mitotic functions. They are implicated in cell cycle progression but the mechanism is unknown. Here we show that depletion of 14/15 centrosome proteins arrests human diploid cells in G_1 with reduced Cdk2-cyclin A activity; expression of a dominant-negative centrosome construct gives similar results. Cell cycle arrest is always accompanied by defects in centrosome structure and centrosome function (duplication, primary cilia assembly). The arrest occurs from within G_1, ruling out contributions from mitosis and cytokinesis. The arrest requires p38, p53 and p21, and is preceded by p38-dependent activation and centrosomal recruitment of p53. p53-deficient tumor cells fail to arrest, leading to centrosome and spindle dysfunction and aneuploidy. We propose that loss of centrosome integrity activates a checkpoint that inhibits G_1/S progression. This model satisfies the definition of checkpoint in having three elements: a perturbation that is sensed, a transducer (p53) and a receiver (p21). These results stress the importance of the centrosome in cell cycle control, an idea for which there is currently little data. Moreover, breast cancer cells, which frequently exhibit p53 loss or dysfunction, show profound changes in centrosome number and size (Lingle, Lutz et al. 1998; Lingle and Salisbury 1999; Borresen-Dale 2003). It is possible failure to arrest under these conditions could propagate centrosome defects in subsequent divisions leading to aneuploidy and breast tumor progression.

Pericentrin binds a protein of a nuclear remodeling complex (Appendix 3).

Pericentrin is an integral centrosomal component that anchors regulatory and structural molecules to centrosomes. In a yeast two-hybrid screen with pericentrin we identified chromodomain helicase DNA-binding protein 4 (CHD4/Mi2b). CHD4 is part of the multiprotein nucleosome remodelling deacetylase (NuRD) complex. We show that many NuRD components interacted with pericentrin following immunoprecipitation of endogenous proteins and they localized to centrosomes and midbodies. Over-expression of the pericentrin-binding domain of CHD4 or another family member (CHD3) dissociated pericentrin from centrosomes. Depletion of CHD3, but not CHD4, by RNA interference dissociated pericentrin, gamma-tubulin and other centrosome components from centrosomes. Microtubule nucleation/organization, cell morphology and nuclear centration were disrupted in CHD3-depleted cells. Spindles were disorganized, the majority showing a prometaphase-like configuration and mitotic spindle defects. These defects often led to chromosome missegregation and aneuploidy. Time-lapse imaging revealed mitotic failure prior to chromosome segregation and cytokinesis failure. Failure of cytokinesis is a second mechanism that leads to aneuploidy through disruption of the CHD3/4-pericentrin interaction. We conclude that pericentrin forms a complex(es) with CHD3 and CHD4, but a distinct CHD3-pericentrin complex is required for centrosomal anchoring of pericentrin/gamma tubulin and for centrosome and genome integrity.

Key research accomplishments.

- Pericentrin knock down leads to late cytokinesis defects and aneuploidy, a common phenotype of aggressive breast cancers.

- Pericentrin binds the nuclear remodeling complex protein CHD3/4 and disruption of this interaction leads to centrosome defect and aneuploidy, common phenotypes of aggressive breast cancers.

- Centriolin depletion causes cytokinesis failure leading to aneuploidy.

- The mechanism of cytokinesis failure in centriolin depletions is surprising: loss of secretory vesicle fusion at the site of cell-cell cleavage.

- Depletion of several centrosome proteins induces a G0/G1 p53-, p38, p21-dependent arrest in normal retinal epithelial cell line.

- Tumor cell lines lacking p53 do not arrest but propagate the defects induced by centrosome protein depletion including centrosome damage, ciliary defects and centrosome duplication defects.

Reportable Outcomes

Manuscripts

A. Gromley, C. Yeaman, J. Rosa, S. Redick. C. Chen, S. Mirabelle, M. Guha, J. Sillibourne, and S. Doxsey. Centriolin anchoring of exocyst and SNARE complexes at the midbody is required for secretory-vesicle-mediated abscission. Cell **123**(1): 75-87, Oct. 2005.

K. Mikule, P. Kaldis, A. Jurczyk, S. Mirabelle, S. Doxsey. Centrosome protein depletion activates a p53-, p38-, p21-dependent checkpoint that triggers G1 arrest through inhibition of cyclinA-Cdk2. Nature Cell Biology, in revision.

Chromatin remodeling proteins interact with pericentrin and the centrosome to regulate centrosome integrity and spindle function. James Sillibourne Manish Singh, Stephanie Mirabelle and Stephen Doxsey. Mol Boil Cell, in revision.

Presentations

Poster presentation 2004, Centriolin-anchoring of exocyst and SNARE complexes at the midbody is required for localized secretion and abscission during cytokinesis, A. Gromley, C. Yeaman, A. Jurczyk, S. Mirabelle, S. Riddick, S. J. Doxsey, 44th ASCB Meeting, Washington DC.

Poster presentation 2005, “Centrosome genes involved in cytokinesis, genetic fidelity and potentially tumorigenesis”, S. Mirabelle, S. Doxsey, 2005 Era of Hope meeting, Philadelphia

Conclusions

I have contributed to work showing that pericentrin depletion induces cytokinesis failure. This results in aneuploidy, a hallmark of aggressive breast cancer. I have also contributed to work showing that another centrosome protein called centriolin contributes to aneuploidy through a similar mechanism. Moreover, this work uncovers a surprising mechanism for the final stages of cytokinesis, namely secretory vesicle movement and fusion at the site of cell-cell cleavage. I have worked on a study that investigates a surprising pericentrin-interacting protein; a nuclear remodeling complex component called CHD3/4 and contributed to work showing that this interaction is important for the integrity of centrosomes and the fidelity of chromosome segregation and genomic stability. We showed that depletion of CHD3/4 leads to multipolar spindles and aneuploidy by a mechanism different from pericentrin depletion. In conclusion, my work has focused on understanding mechanisms that control aneuploidy, a common phenotype of aggressive breast cancers. The Doxsey laboratory will follow up on the finding that cells lacking p53 seem to die when centrosome proteins are depleted, whereas normal cells arrest.

References

Borresen-Dale, A. L. (2003). "TP53 and breast cancer." Hum Mutat **21**(3): 292-300.

Doxsey, S., D. McCollum, et al. (2005). "Centrosomes in cellular regulation." Annu Rev Cell Dev Biol **21**: 411-34.

Doxsey, S., W. Zimmerman, et al. (2005). "Centrosome control of the cell cycle." Trends Cell Biol **15**(6): 303-11.

Fujii, H., C. Marsh, et al. (1996). "Genetic divergence in the clonal evolution of breast cancer." Cancer Res **56**(7): 1493-7.

Gromley, A., C. Yeaman, et al. (2005). "Centriolin anchoring of exocyst and SNARE complexes at the midbody is required for secretory-vesicle-mediated abscission." Cell **123**(1): 75-87.

Hinchcliffe, E. H. (2003). "Cell cycle: seeking permission from the mother centriole." Curr Biol **13**(16): R646-8.

Hoskins, K. and B. L. Weber (1994). "The biology of breast cancer." Curr Opin Oncol **6**(6): 554-9.

Jurczyk, A., A. Gromley, et al. (2004). "Pericentrin forms a complex with intraflagellar transport proteins and polycystin-2 and is required for primary cilia assembly." J Cell Biol **166**(5): 637-43.

Lingle, W. L., W. H. Lutz, et al. (1998). "Centrosome hypertrophy in human breast tumors: implications for genomic stability and cell polarity." Proc Natl Acad Sci U S A **95**(6): 2950-5.

Lingle, W. L. and J. L. Salisbury (1999). "Altered centrosome structure is associated with abnormal mitoses in human breast tumors." Am J Pathol **155**(6): 1941-51.

Pazour, G. J. (2004). "Intraflagellar transport and cilia-dependent renal disease: the ciliary hypothesis of polycystic kidney disease." J Am Soc Nephrol **15**(10): 2528-36.

Pazour, G. J., S. A. Baker, et al. (2002). "The intraflagellar transport protein, IFT88, is essential for vertebrate photoreceptor assembly and maintenance." J Cell Biol **157**(1): 103-13.

Pazour, G. J. and J. L. Rosenbaum (2002). "Intraflagellar transport and cilia-dependent diseases." Trends Cell Biol **12**(12): 551-5.

Pazour, G. J., J. T. San Agustin, et al. (2002). "Polycystin-2 localizes to kidney cilia and the ciliary level is elevated in orpk mice with polycystic kidney disease." Curr Biol **12**(11): R378-80.

Purohit, A., S. H. Tynan, et al. (1999). "Direct interaction of pericentrin with cytoplasmic dynein light intermediate chain contributes to mitotic spindle organization." J Cell Biol **147**(3): 481-92.

Quarmby, L. M. and J. D. Parker (2005). "Cilia and the cell cycle?" J Cell Biol **169**(5): 707-10.

Zimmerman, W. C., J. Sillibourne, et al. (2004). "Mitosis-specific anchoring of gamma tubulin complexes by pericentrin controls spindle organization and mitotic entry." Mol Biol Cell **15**(8): 3642-57.

Appendix 1

Dear Contract Specialist,

I worked in the areas covered by this grant from 11/7/2004 to 7/20/06. While I made progress during this time, I decided to leave science and begin a career in teaching high school. For this reason I have returned to France and will no longer continue work in cell biology or breast cancer. If you have further questions, please contact my P.I. during the time of this grant, Dr. Stephen Doxsey.

Thank you for your support.

Stephanie Mirabelle

Cell, Vol. 123, 75–87, October 7, 2005, Copyright ©2005 by Elsevier Inc. DOI 10.1016/j.cell.2005.07.027

Centriolin Anchoring of Exocyst and SNARE Complexes at the Midbody Is Required for Secretory-Vesicle-Mediated Abscission

Adam Gromley,[1,3] Charles Yeaman,[2] Jack Rosa,[1] Sambra Redick,[1] Chun-Ting Chen,[1] Stephanie Mirabelle,[1] Minakshi Guha,[1] James Sillibourne,[1] and Stephen J. Doxsey[1,*]
[1]Program in Molecular Medicine
University of Massachusetts Medical Center
Worcester, Massachusetts 01605
[2]Department of Anatomy and Cell Biology
University of Iowa
Iowa City, Iowa 52242

Summary

The terminal step in cytokinesis, called abscission, requires resolution of the membrane connection between two prospective daughter cells. Our previous studies demonstrated that the coiled-coil protein centriolin localized to the midbody during cytokinesis and was required for abscission. Here we show that centriolin interacts with proteins of vesicle-targeting exocyst complexes and vesicle-fusion SNARE complexes. These complexes require centriolin for localization to a unique midbody-ring structure, and disruption of either complex inhibits abscission. Exocyst disruption induces accumulation of v-SNARE-containing vesicles at the midbody ring. In control cells, these v-SNARE vesicles colocalize with a GFP-tagged secreted polypeptide. The vesicles move to the midbody ring asymmetrically from one prospective daughter cell; the GFP signal is rapidly lost, suggesting membrane fusion; and subsequently the cell cleaves at the site of vesicle delivery/fusion. We propose that centriolin anchors protein complexes required for vesicle targeting and fusion and integrates membrane-vesicle fusion with abscission.

Introduction

Cytokinesis is a fundamental process that results in division of a single cell with replicated DNA into two daughters with identical genomic composition (see (Glotzer, 2001, 2005; Guertin et al., 2002). Early events in animal cell cytokinesis include assembly and contraction of the actomyosin ring to form the cleavage furrow. Continued furrowing results in constriction of the plasma membrane to form a narrow cytoplasmic bridge between the two nascent daughter cells. Within this intercellular bridge are bundled microtubules and a multitude of proteins that together form the midbody. In a poorly understood final step called abscission, the cell cleaves at the intercellular bridge to form two daughter cells.

Membrane trafficking is required for late stages of cytokinesis (Albertson et al., 2005; Finger and White, 2002; Jurgens, 2005; Papoulas et al., 2004; Strickland and Burgess, 2004). In *C. elegans* embryos, inhibition of Golgi secretion by brefeldin A (BFA) resulted in late-stage cytokinesis defects (Skop et al., 2001). More recent studies in mammalian cells using dominant-negative approaches showed that the membrane-fusion-inducing SNARE components, syntaxin-2 and endobrevin/VAMP8, are required for a final step in cell cleavage (Low et al., 2003). Endocytic traffic also plays a role in cytokinesis. Recycling endosomes and associated components localize to the midbody and are required for cell cleavage (Monzo et al., 2005; Wilson et al., 2005; Thompson et al., 2002). However, little is known about the spatial and temporal control of dynamic membrane compartments and molecules during abscission or how these activities are coordinated to achieve cell cleavage.

The role of membrane-vesicle-tethering exocyst complexes in animal cell abscission is poorly understood. The exocyst is a multiprotein complex that targets secretory vesicles to distinct sites on the plasma membrane. In the budding yeast *S. cerevisiae*, exocyst components localize to the mother-bud neck, the site of cytokinesis (Finger et al., 1998; Mondesert et al., 1997). Exocyst disruption results in accumulation of vesicles at this site (Salminen and Novick, 1989) and impairs actomyosin-ring contraction and cell cleavage (Dobbelaere and Barral, 2004; Verplank and Li, 2005). In the fission yeast *S. pombe*, exocyst components localize to the actomyosin ring (Wang et al., 2002). Mutants for the exocyst component Sec8 accumulate 100 nm "presumptive" secretory vesicles near the division septum and cannot complete extracellular separation of the two daughter cells. A screen for cytokinesis mutants in *Drosophila melanogaster* identified the exocyst component sec5 (Echard et al., 2004), and proteomic analysis of the midbody in mammalian cells showed that the exocyst protein sec3 is at the midbody (Skop et al., 2004). Mammalian exocyst components are involved in secretion in polarized epithelial cells (Yeaman et al., 2004) and localize to the midbody (Skop et al., 2004; Wilson et al., 2005), but the function of the exocyst during cytokinesis is unclear.

Components of membrane-vesicle-tethering and -fusion complexes have been identified in some organisms and linked to cytokinesis, but the pathway that integrates these complexes with vesicle trafficking during cell cleavage is unknown. Little is known about how SNAREs and the exocyst are anchored at the midbody or how they modulate membrane-vesicle organization and fusion to coordinate abscission. Moreover, the origin and dynamics of membrane compartments involved in abscission have not been investigated. In this manuscript, we describe a multistep pathway for abscission that requires a scaffold protein to anchor

*Correspondence: stephen.doxsey@umassmed.edu
[3]Present address: Department of Genetics and Tumor Cell Biology, St. Jude Children's Research Hospital, Memphis, Tennessee, 38105.

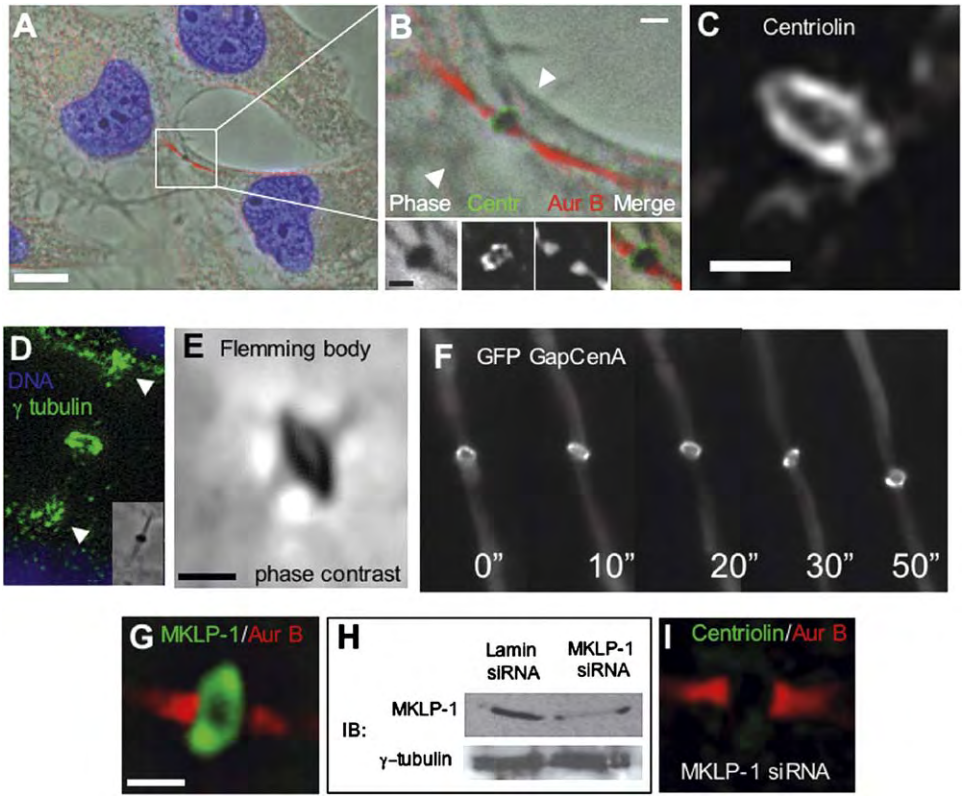

Figure 1. Centriolin Localizes to a Midbody Ring

(A) Immunofluorescence/phase image of HeLa cell during cytokinesis showing the phase-dense Flemming body within the larger diameter of the plasma membrane (arrowheads in [B]).

(B and C). Boxed region enlarged with insets (B) to show the centriolin ring (Centr, enlarged in [C]) as part of the Flemming body (phase) and flanked bilaterally by Aurora B (Aur B).

(D) γ-tubulin localizes to the midbody ring (inset, Flemming body) and sites of presumed microtubule minus ends (arrowheads).

(E) The Flemming body forms a ring.

(F) GFP-tagged GAPCenA localizes to the midbody ring and is highly dynamic (time in s).

(G–I) MKLP-1 localizes to the midbody ring (G) and, upon depletion, mislocalizes centriolin from the midbody (I). Immunoblots (IB) from cells treated with siRNAs targeting MKLP-1 or lamin A/C (control) (H). γ-tubulin, loading control. Scale bars in (A), 10 μm; (B), 5 μm; (C), (E), and (G), 1 μm.

SNARE and exocyst complexes at a unique midbody site and also requires asymmetric transport and fusion of secretory vesicles at this site.

Results

Centriolin Is Part of a Ring-like Structure at the Central Midbody during Cytokinesis

We previously showed that centriolin localized to the midbody during cytokinesis (Gromley et al., 2003). Using high-resolution deconvolution microscopy, we now demonstrate that centriolin is part of a unique ring-like structure within the central portion of the midbody, which we call the midbody ring (observed in ~75% of all telophase cells, Figures 1A–1C). The midbody ring was 1.5–2 μm in diameter (Figure 1C), contained γ-tubulin (Figure 1D), and colocalized with the phase-dense Flemming body (Figure 1B, inset) (Paweletz, 1967). In fact, high-magnification phase-contrast imaging revealed that the Flemming body was organized into a ring-like structure (Figure 1E). The midbody ring was flanked by Aurora B kinase, which colocalized with microtubules on either side of the ring (Figure 1B, inset). Several other proteins localized to the midbody ring including ectopically expressed GFP-GAPCenA, a GTPase-activating protein previously shown to localize to centrosomes (Cuif et al., 1999). Time-lapse imaging of GFP-GAPCenA and other proteins in living cells showed that the midbody ring was dynamic, moving between cells and tipping from side to side to reveal the ring structure (Figure 1F; see also Movie S1 in the Supplemental Data available with this article online). In addition, midbody-ring localization of GFP-GAPCenA confirmed the ring structure seen by immunofluorescence microscopy and demonstrated that there were no antibody penetration problems in this midbody region as seen for other antigens (Saxton and McIntosh, 1987). The midbody ring was distinct from the actomyosin ring and did not change in diameter during cytokinesis (Figures 1A and 1B). It appeared during the early stages of actomyosin-ring constriction and persisted until after cell cleavage (see below).

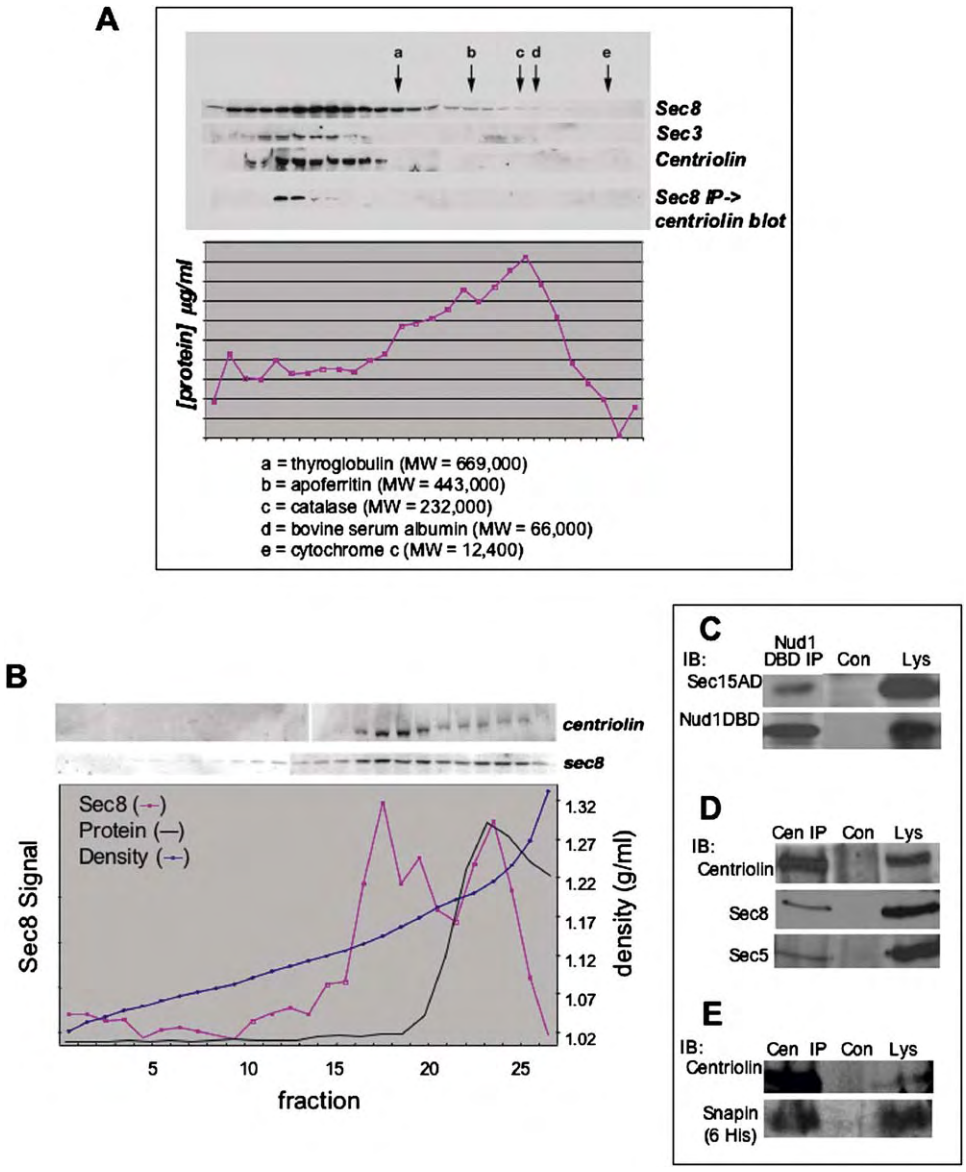

Figure 2. Centriolin Interacts with Exocyst Components and Snapin

(A) Gel filtration (Superose 6) using MDCK cell lysates shows that centriolin coelutes with peak exocyst fractions (top). Immunoprecipitation (IP) of sec8 coprecipitates centriolin. Graph, total protein profile; markers a–e are indicated.

(B) Following isopycnic centrifugation (iodixanol), centriolin comigrates in peak fractions containing sec8 (upper panels). Graph shows sec8 levels, iodixanol density, and total protein.

(C) Immunoprecipitation (IP) of Nud1-DBD (DBD antibody) pulls down sec15-AD (left). DBD, DNA binding domain; AD, activation domain; Con, control beads; Lys, lysate.

(D) Endogenous exocyst components coimmunoprecipitate with endogenous centriolin (Cen IP).

(E) Endogenous centriolin immunoprecipitates (Cen IP) overexpressed His_6-tagged snapin.

The centralspindlin components MKLP-1/CHO1/ZEN-4 (Figure 1G) and MgcRacGAP/CYK-4 (data not shown) also localized to the midbody ring and appeared earlier than centriolin during actomyosin-ring constriction. Depletion of MKLP-1 by RNAi to 18% of control levels (n = 2 experiments) prevented recruitment of centriolin to the ring (Figures 1H and 1I). In contrast, depletion of centriolin had no effect on the localization of MKLP-1 or MgcRacGAP (data not shown). These data suggested that centralspindlin anchored centriolin to the midbody ring.

Centriolin Interacts with the Exocyst Complex and the SNARE-Associated Protein Snapin and Is in Membrane-Associated Cytoplasmic Fractions

To determine the molecular function of centriolin in cytokinesis, we performed a yeast two-hybrid screen using a 120 amino acid domain of centriolin that is required for the cytokinesis function of centriolin and shares homology with budding- and fission-yeast genes (Nud1/Cdc11) involved in cytokinesis and mitotic exit (Gromley et al., 2003). A screen of approximately 12 million clones from a human testis cDNA library

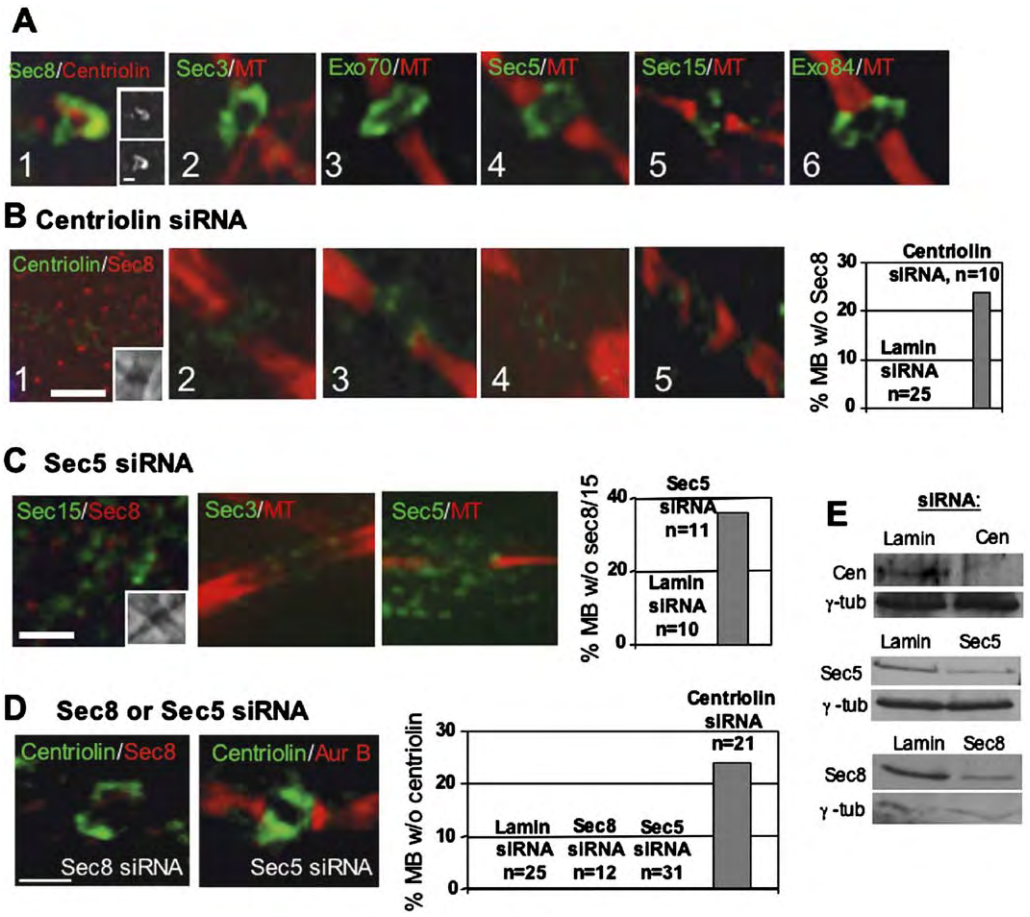

Figure 3. Exocyst Localization to the Midbody Ring Is Centriolin Dependent

(A) Immunofluorescence images of exocyst components (green) costained with centriolin antibodies (panel 1) or with anti-α-tubulin antibody (red) to visualize microtubules (MTs, panels 2–6). Panel 1 inset: top, sec8; bottom, centriolin.

(B) Cells depleted of centriolin lack midbody-associated exocyst. Images labeled as in A1–A5; B1 inset, Flemming body. Graph, percentage of midbodies (MB) without (w/o) sec8 signal following treatment with siRNAs targeting lamin A/C or centriolin; other cells have reduced levels (see text).

(C) siRNA depletion of sec5 disrupts the exocyst from midbodies costained with two exocyst proteins (C1 inset, phase) or one exocyst protein and microtubules (C2–C3). Graph, percentage of midbodies (MB) lacking sec5 staining in cells treated with lamin A/C or sec5 siRNAs.

(D) Exocyst disruption by siRNAs does not affect centriolin midbody localization. Graph, percentage of midbodies (MB) lacking centriolin stain following treatment of indicated siRNAs. Scale bar equals 1 μm (all panels).

(E) Immunoblots showing reduction of proteins targeted by siRNAs. γ-tubulin (γ-tub), loading control. Cen, centriolin.

yielded two potential interacting proteins: sec15, a member of the exocyst complex, and snapin, a SNARE-associated protein.

Additional biochemical analysis confirmed the yeast two-hybrid interactions and demonstrated that centriolin was in a large complex associated with membranes (Figure 2). The centriolin Nud1 domain fused to the DNA binding domain (DBD) and sec15 fused to the activation domain (AD) were coexpressed in the same yeast cells. Immunoprecipitation of the Nud1 fusion protein effectively coprecipitated the sec15 fusion protein (Figure 2C). To test whether other members of the exocyst complex were bound to centriolin, we immunoprecipitated endogenous centriolin from HeLa cell lysates with affinity-purified centriolin antibodies and showed that sec8 and sec5 coprecipitated (Figure 2D). Gel filtration experiments (Superose 6) using MDCK cell lysates demonstrated that centriolin coeluted with fractions containing the exocyst complex (detected with antibodies to sec8 and sec3, Figure 2A). Centriolin was eluted as a single peak that overlapped with peaks of sec3 and sec8. We next asked if centriolin coimmunoprecipitated with the exocyst. Antibodies to sec8 were added to each of the fractions from the gel filtration column, and immune complexes were collected and probed with affinity-purified centriolin antibodies as described (Gromley et al., 2003). Centriolin was found only in fractions containing exocyst components (Figure 2A). The centriolin-containing fractions eluted earlier than the peak of sec 3 or sec8, suggesting that the exocyst fraction to which centriolin was bound was different from the cytosolic and lateral plasma-membrane fractions of the exocyst (Yeaman et al., 2004). The exocyst-centriolin fractions did not cofractionate with the

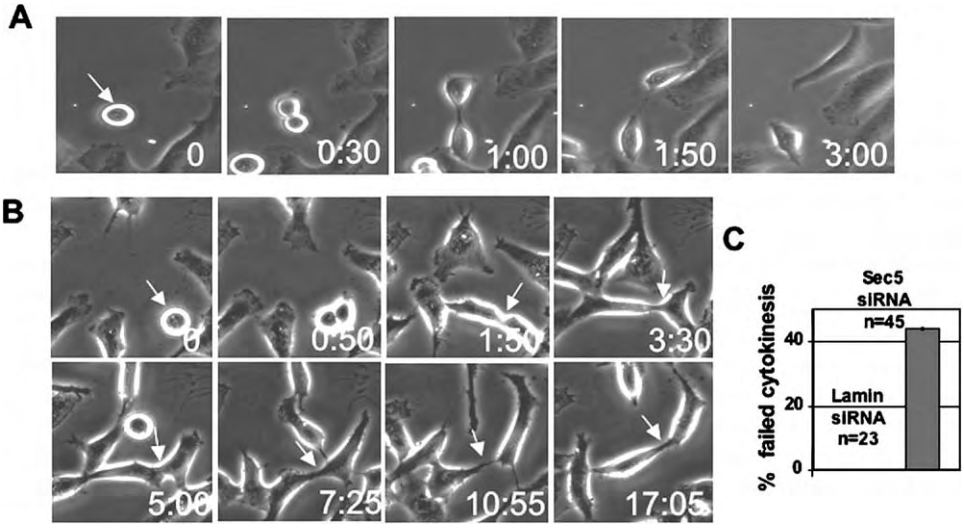

Figure 4. Exocyst Disruption Induces Cytokinesis Defects

(A) Time-lapse images of a HeLa cell treated with lamin A/C siRNAs showing a mitotic cell entering mitosis (arrow), forming a cleavage furrow, and cleaving into two separate cells in 3 hr. Time, hr:min.

(B) A cell depleted of sec5 enters mitosis (arrow), forms a cleavage furrow with normal timing (~50 min), and remains interconnected by a thin intercellular bridge for over 17 hr (panels 1:50 through 17:05).

(C) Graph shows percentage of mitotic cells that fail cytokinesis; many others are delayed (see text).

bulk of the cellular protein and eluted considerably earlier than thyroglobulin (MW 669,000) suggesting it was part of a large complex.

Since the exocyst associates with membrane vesicles, we next tested whether centriolin was also present in membranous fractions. Cell homogenates were prepared in the absence of detergent and underlain at the bottom of linear iodixanol gradients. Isopycnic centrifugation was performed, and fractions were probed for both centriolin and the exocyst component sec8. Centriolin "floated up" to fractions lighter than the cytosol having a buoyant density of $\delta \sim 1.14$ g/ml (Figure 2B). The centriolin peak cofractionated with a major peak of Sec8 that was slightly less dense than the junction-associated peak of Sec8 described previously in confluent MDCK cells ($\delta \sim 1.16$ g/ml; Yeaman et al., 2004). Little to no centriolin was observed at other positions in the gradient or in the major protein peak, suggesting that most if not all centriolin was associated with membranes. Taken together, the density gradient, immunoprecipitation, and chromatography data support the conclusion that centriolin associates with the exocyst in a very large complex bound to cellular membranes. The yeast two-hybrid interaction between centriolin and the low-abundance protein snapin was confirmed by showing that endogenous centriolin coimmunoprecipitated a His_6-tagged snapin fusion protein expressed in HeLa cells (Figure 2E) and by the centriolin-dependent midbody localization of snapin (see below).

The Exocyst Complex Colocalizes with Centriolin at the Midbody Ring

Further support for the centriolin-exocyst interaction was obtained by showing that exocyst-complex components localized to the midbody ring with centriolin. HeLa cells were colabeled with antibodies against one of several exocyst components (sec3, sec5, sec8, sec15, exo70, or exo84) and either microtubules or centriolin (Figure 3A). We found that all these exocyst components localized to the midbody ring during cytokinesis and formed a ring-like structure similar to that seen for centriolin. In fact, double-stained images revealed considerable overlap between sec8 and centriolin, indicating that they were part of the same structure (Figure 3A, panel 1). We also showed that a myc-tagged form of sec8 localized to the midbody ring when expressed in HeLa cells (Figure S1), confirming the localization seen with antibodies directed to the endogenous protein.

Midbody Localization of the Exocyst Is Disrupted in Cells Depleted of Centriolin

We next tested whether centriolin was required for midbody-ring localization of the exocyst. siRNA-mediated depletion of centriolin resulted a in ~70% reduction in centriolin protein levels and complete loss of midbody staining in 24% of cells compared with control cells treated with lamin siRNA (Figures 3B and 3E). Immunofluorescence quantification of midbody signals performed as in our previous studies (Gromley et al., 2003) demonstrated that many of the remaining centriolin-depleted cells had lower levels of midbody staining than controls (48%, n = 23 cells), bringing the total percentage of midbody depleted cells to 72%. Cells that lacked detectable midbody-associated centriolin usually lacked midbody labeling of sec8 (10/10, Figure 3B, panels 1 and 6). Although other exocyst components could not be costained with centriolin because all were detected with rabbit antibodies like centriolin, all were lost from or reduced at midbodies in centriolin-depleted cells (Figure 3B, panels 2–5). For example,

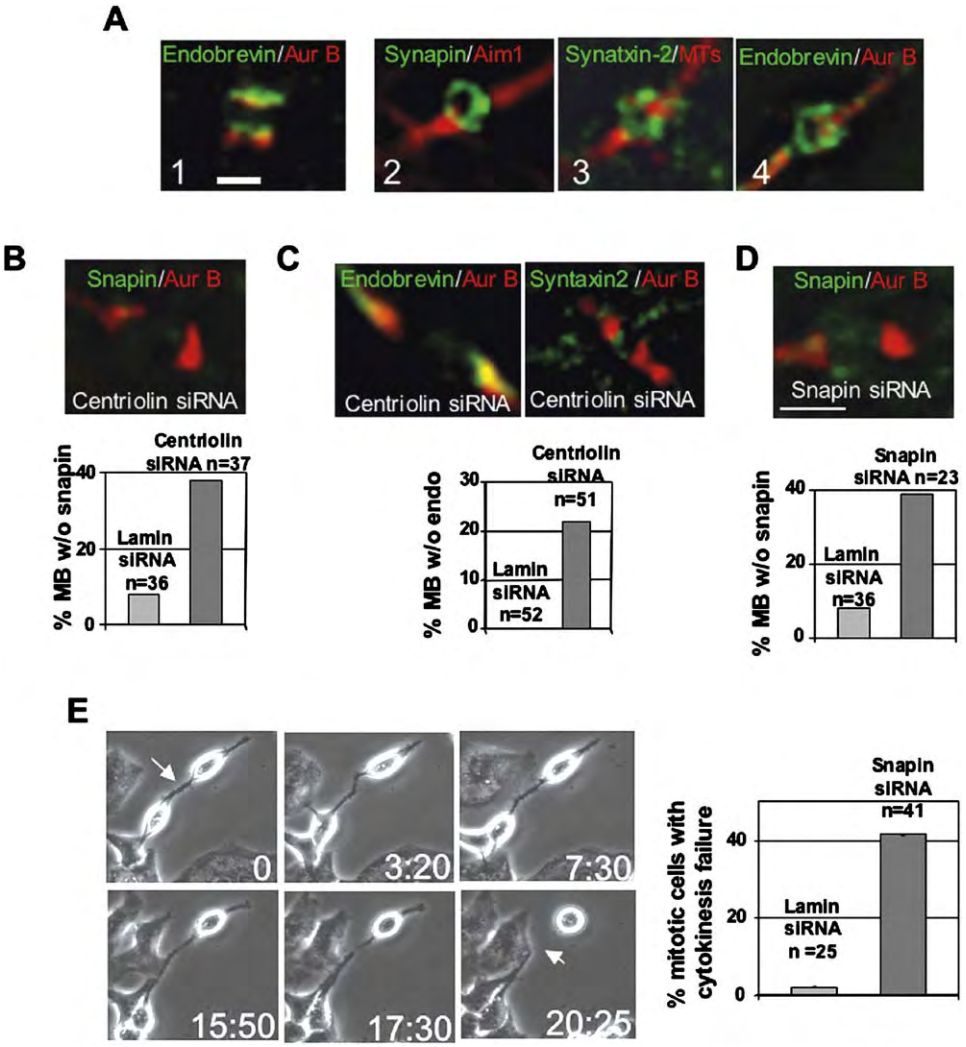

Figure 5. Centriolin siRNA Mislocalizes Midbody-Ring-Associated SNAREs and Snapin, which Disrupts Cytokinesis When Depleted

(A) Endobrevin/VAMP8 (1) localizes adjacent to the midbody ring when snapin is on the ring (2). Later, when the midbody diameter is thin (0.5–1 μm), endobrevin/VAMP8 and syntaxin-2 localize to the ring (3 and 4).

(B) Centriolin-depleted cell shows loss of snapin from the midbody ring (green). Graph, percentage of midbodies lacking snapin after siRNA depletion of proteins.

(C) Centriolin-depleted cells lose SNARE proteins from the midbody ring. Graph, percentage of midbodies lacking endobrevin/VAMP8 staining after indicated siRNAs treatments. Endo, endobrevin.

(D) Snapin-depleted cells show loss of snapin from the midbody ring. Graph, percentage of midbodies lacking snapin after indicated siRNA treatments.

(E) A snapin-depleted cell in cytokinesis (0) remains connected by a thin intercellular bridge for >17 hr before separating (20:25) (time, hr:min). Graph, percentage of mitotic cells that failed cytokinesis.

Exo84 was undetectable at midbodies in 22% of centriolin-depleted cells (n = 9 cells) or had levels below the lowest control midbody staining in 42% of centriolin-depleted cells (n = 19 cells). Significant reduction in midbody staining of centriolin and other exocyst components was observed with a second siRNA targeting a different centriolin sequence (Gromley et al., 2003) (data not shown).

To test whether centriolin was dependent on the exocyst complex for localization to the midbody, we initially targeted sec5 for siRNA depletion. Recent studies showed that mutants of sec5 in *D. melanogaster* disrupted exocyst function (Murthy and Schwarz, 2004) and that RNAi-mediated depletion of sec5 inhibited exocyst-dependent processes in vertebrate cells (Prigent et al., 2003). We found that depletion of sec5 resulted in loss of midbody-associated sec5 as well as other exocyst components, including sec3, sec8, and sec15 (Figures 3C and 3E). These results show that sec5 depletion disrupts midbody-ring localization of the exocyst. In contrast, neither sec5 nor sec8 loss from the midbody affected the association of centriolin with the midbody ring (Figures 3D and 3E). These data demonstrate that centriolin is required for midbody localiza-

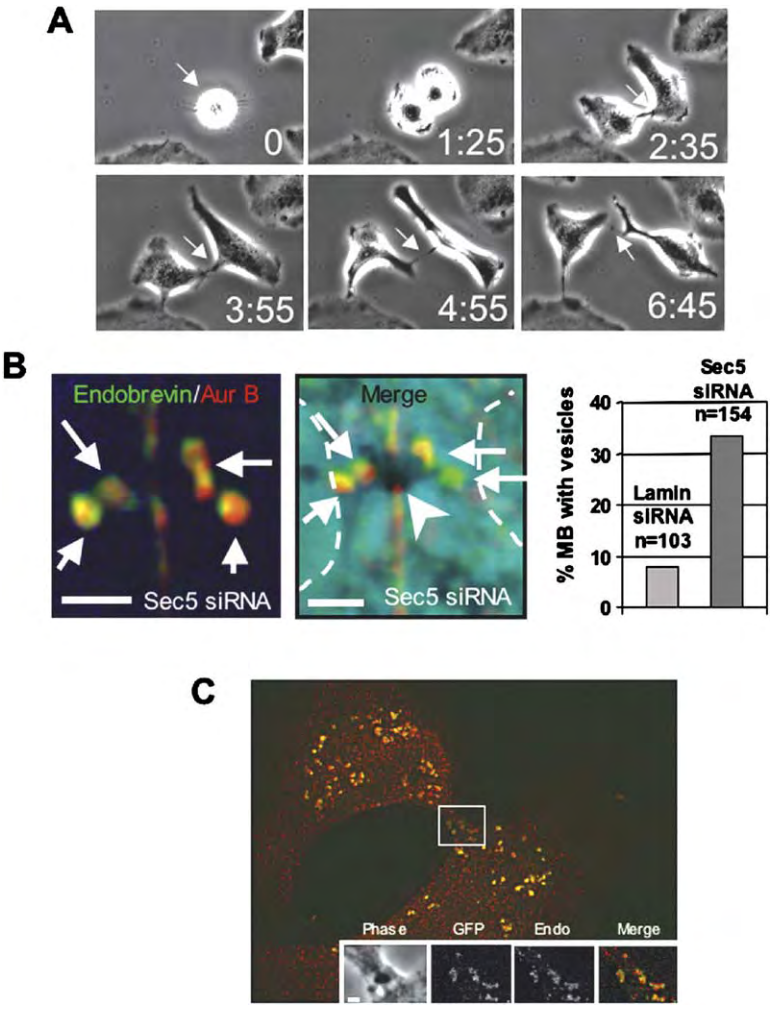

Figure 6. Disruption of the Exocyst Results in Accumulation of Secretory Vesicles at the Midbody Ring

(A) A mitotic cell (0, arrow) treated with BFA exits mitosis and forms a cleavage furrow with normal timing but arrests with a thin intercellular bridge that connects the two daughters (panels 2:35 through 6:45).

(B) sec5 siRNA-treated cells accumulate endobrevin/VAMP8-containing vesicle-like structures (arrows) at the Flemming body (arrowhead, panel 2). Dotted lines, plasma membrane. Graph, percentage of cells with endobrevin/VAMP8 vesicles at the midbody following indicated siRNA treatments. Scale bars, 2 μm.

(C) Endobrevin/VAMP8 (green) localizes to luminal-GFP secretory vesicles (red). Box at midbody is enlarged in insets. Endo, endobrevin/VAMP8.

tion of the exocyst, while localization of centriolin appears to be independent of the exocyst.

Disruption of the Exocyst Causes Failure at the Final Stages of Cytokinesis

Localization of the exocyst to the midbody and its interaction with centriolin suggested that the complex might play a role in cytokinesis. To examine this, we disrupted the midbody-associated exocyst using siRNAs targeting sec5 and examined cytokinesis by time-lapse imaging over a 20 hr time period. We found that over half the cells exhibited severe cytokinesis defects, including failure in the final abscission step (42%, Figures 4B and 4C, Movie S3) and delays during cytokinesis (24%, n = 18) compared with control lamin siRNA-treated cells (Figures 4A and 4C, Movie S2). Some cells remained interconnected by thin cytoplasmic bridges (Figure 4B, panel 17:05 and Movie S3) and sometimes entered one or more additional rounds of mitosis while still connected to their partner cells. Sec5-depleted cells viewed for an additional 24 hr showed a similar level of cytokinesis defects (data not shown), suggesting that nearly all cells in the culture experienced cytokinesis problems over time. Cytokinesis defects were also observed when the exocyst was disrupted by siRNA depletion of sec15 and sec8 (data not shown). Cells remained healthy, as no differences in cell morphology or mitochondrial function were observed. These data show that disruption of the exocyst produces late-stage cytokinesis defects similar to centriolin (Gromley et al., 2003) and demonstrates a requirement for the exocyst in the final stages of animal cell cytokinesis.

Snapin and SNARE Components Localize to the Midbody Ring in a Centriolin-Dependent Manner

Snapin was originally considered to be a neuron-specific protein, but recent studies demonstrated that it is also expressed in nonneuronal cells (Buxton et al., 2003). Snapin may facilitate assembly of SNARE complexes and may define a limiting step in vesicle fusion mediated by PKA phosphorylation (Chheda et al., 2001). Although the role of snapin in neurotransmission has been questioned (Vites et al., 2004), recent results indicate that it is essential for this process (Thakur et al., 2004). The role of snapin in cytokinesis is currently unknown. Using previously characterized antibodies to snapin (Thakur et al., 2004), we demonstrated that the

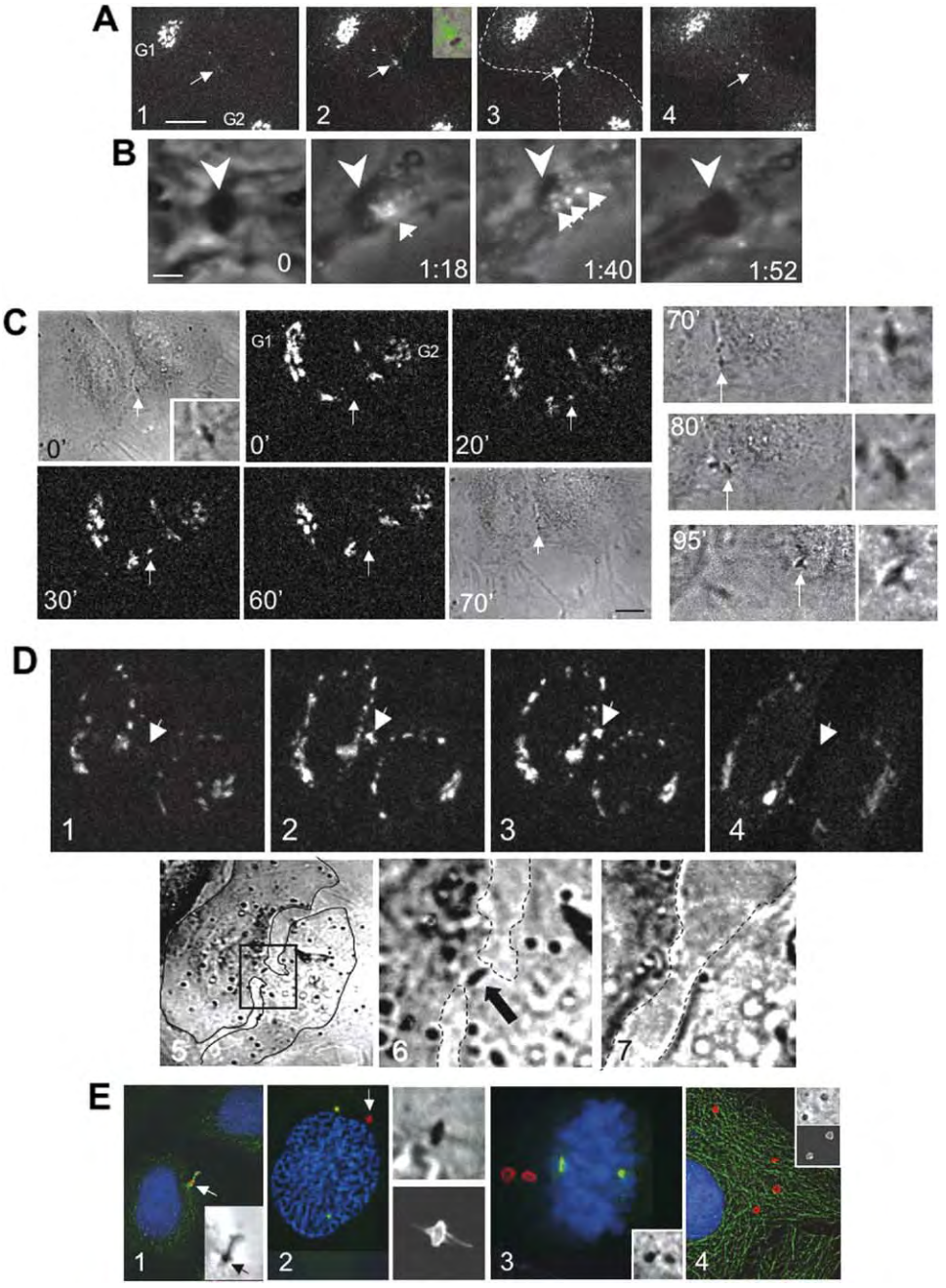

Figure 7. Asymmetric Delivery of Secretory Vesicles to One Side of the Flemming Body Is Followed by Abscission at This Site

(A) A dividing HeLa cell expressing luminal GFP accumulates secretory vesicles on one side of the Flemming body (arrows in 2 and 3, inset). In panel 1, most luminal-GFP signal is in Golgi complexes (G1 and G2). The signal appears transiently at one side of the midbody (2 and 3, arrows; Movie S5) and is lost, although Golgi signal remains (4). Scale bar in panel 1, 10 μm.

(B) Higher-magnification images of another cell (see Movie S6) showing unidirectional delivery of luminal-GFP-containing vesicles from one nascent daughter cell to one side of the Flemming body (arrowhead). GFP vesicles move to the Flemming body from the cell on the right (1:18 and 1:40, arrows; see Movie S6) and quickly disappear (1:52), presumably due to vesicle fusion with the plasma membrane and diffusion of the signal into the extracellular space. Phase and GFP signals are overlaid. Time, hr:min. Scale bar in panel 1, 1 μm.

(C) Lum-GFP vesicle delivery to the Flemming body (0'–30', arrows) followed by signal loss (60', at arrow) and abscission (80' and 95'). Phase-contrast images were taken after disappearance of GFP signal. Enlargements of Flemming body are shown to the right of each low-magnification image in 70'–95'. Scale bar at 70': 10 μm for 0'–95' and 2 μm for enlargements in 70'–95'.

(D) Lum-GFP vesicle delivery to one side of the midbody (panels 1–3) followed by disappearance of the GFP signal (panel 4) and abscission (loss of intercellular bridge, panels 5–7, arrows). The box in panel 5 is enlarged in panel 6. Solid and dotted lines show cell boundaries.

(E) Postmitotic cell (1) showing microtubules (green, GT335 antibody) of the intercellular bridge (phase-contrast image, inset) attached to one of the two daughter cells; no detectable midbody microtubules are seen on the other cell. Microtubules are on both sides of the midbody ring (arrow, red, MKLP-1) and Flemming body (inset, phase), showing that the midbody with attached microtubules was delivered to one daughter cell. Prophase HeLa cell (2) with condensing chromatin (blue) and two centrosomes (green) has a midbody ring and lateral material

protein localized to the midbody ring at the same time as the exocyst and shortly after centriolin (Figure 5A, panel 2).

Previous immunofluorescence studies showed that the v-SNARE endobrevin/VAMP8 and t-SNARE syntaxin-2 were enriched in the region of the midbody flanking the Flemming body and coincident with microtubules and Aurora B staining (Low et al., 2003). Using the same antibodies, we confirmed the localization pattern of endobrevin/VAMP8 (Figure 5A, panel 1) and syntaxin-2 (data not shown). Very late in cytokinesis, the intercellular bridge narrows to ~0.5 μm, and microtubule bundles are reduced in diameter to 0.2–0.5 μm. At this time, endobrevin/VAMP8 and syntaxin-2 joined centriolin, snapin, and the exocyst at the midbody ring (Figure 5A, panels 3 and 4). siRNA depletion of centriolin eliminated the midbody-ring localization of snapin (>35% of cells, Figure 5B), endobrevin/VAMP8 (>20% of cells, Figure 5C), and syntaxin-2 (Figure 5C). Of the remaining cells, 24% and 36% showed midbody staining levels below those of controls for snapin (n = 22) and endobrevin/VAMP8 (n = 25), respectively. As shown earlier, midbody-ring integrity was not compromised under these conditions, as MKLP-1 and MgcRacGAP remained at this site in cells with reduced centriolin. These results indicated that centriolin was required for midbody-ring localization of v- and t-SNARE proteins and the SNARE-associated protein snapin.

Snapin Depletion Mislocalizes the Protein from the Midbody and Induces Cytokinesis Defects

Midbodies in 41% of snapin-depleted cells showed no detectable snapin staining (Figure 5D). Time-lapse imaging over a 22 hr period showed that 40% of snapin-depleted cells experienced late-stage cytokinesis failure (Figure 5E, Movie S4). Other cells showed long delays and often remained connected by a thin intercellular bridge (data not shown). When cultures were imaged for an additional 24 hr, we observed multicellular syncytia resulting from multiple incomplete divisions and additional individual cells undergoing cytokinesis failure. This suggested that most cells in the population ultimately failed cytokinesis and that some failed multiple times. Occasionally, cells separated when one of the attached daughters re-entered mitosis, possibly due to tensile forces generated by cell rounding during mitosis (Figure 5E, Movie S4). These results demonstrated that snapin was necessary for abscission and suggested that it functioned by anchoring SNARE complexes at the midbody.

Disruption of the Exocyst Results in Accumulation of Secretory Vesicles at the Midbody

We next tested whether the late-stage cytokinesis defects observed in this study resulted from changes in membrane trafficking to the midbody. As a first test of this idea, we used brefeldin A, which disrupts cytokinesis in *C. elegans* presumably due to inhibition of post-Golgi secretory-vesicle trafficking (Skop et al., 2001). In HeLa cells treated with brefeldin A, we observed late-stage cytokinesis defects (Figure 6A) that were similar to those observed following depletion of centriolin. Many cells were delayed in or failed cytokinesis (n = 9/13 cells in two separate experiments). This suggested that post-Golgi vesicle trafficking was involved in late-stage cytokinesis events in vertebrate cells, although brefeldin A is known to affect other membrane-trafficking pathways (Antonin et al., 2000).

Based on the localization of the exocyst to the midbody ring, we reasoned that the vesicle-tethering function of the complex might be operating at this site to facilitate fusion of v-SNARE-containing vesicles at the late stages of cytokinesis. To test this idea, we depleted cells of sec5 to disrupt exocyst complexes and examined the localization of v-SNARE (endobrevin/VAMP8) containing vesicles. We observed a collection of small, spherical endobrevin/VAMP8-containing structures resembling vesicles at the midbody (Figure 6B, panel 1, arrows) that were positioned around the phase-dense Flemming body (Figure 6B, arrowhead, panel 2). Although these structures were occasionally seen in control lamin A/C siRNA-treated cells, they were significantly increased in sec5-depleted cells (Figure 6B, graph).

To determine whether the endobrevin/VAMP8-containing structures were secretory vesicles, we used a more specific marker for the secretory pathway. We expressed a GFP-tagged construct containing an amino-terminal signal peptide that targets the protein to the lumen of the ER (lum-GFP) (Blum et al., 2000) and lacks retention and retrieval motifs, so it would not be expected to target to endosomes, multivesicular bodies, or lysosomes. The lum-GFP was efficiently secreted from nondividing MDCK cells following a 19°C *trans*-Golgi network block and release from the block in the presence of protein-synthesis inhibitors (C.Y., unpublished data). When we expressed lum-GFP, numerous GFP-containing vesicles were observed in the cytoplasm. Following fixation and staining for endobrevin/VAMP8, we found that most of the endobrevin/VAMP8 vesicles colabeled with lum-GFP throughout the cytoplasm (Figure 6C) and within the intercellular bridge during late stages of cytokinesis (Figure 6C, insets). This observation demonstrates that the v-SNARE-containing vesicles that accumulated following disruption of the exocyst are secretory vesicles, an observation similar to that seen in studies in exocyst mutants of *S. cerevisiae* where vesicles dock normally but fail to fuse with the plasma membrane (Guo et al., 2000)

Asymmetric Delivery of Secretory Vesicles to the Midbody Is Followed by Abscission

At early stages of cytokinesis, we observed numerous GFP-labeled secretory vesicles in Golgi complexes and

stained with MKLP-1 (arrow, red) and in enlargement (bottom right); the Flemming body with flanking material is enlarged at upper right. Metaphase cell (3) with two midbody rings stained for MKLP-1 (red). Inset, two Flemming bodies corresponding to the two MKLP-1-stained structures. Centrosomes, green; DNA, blue. Interphase cell (4) showing four MKLP-1-stained midbody rings (red). Two are enlarged in lower inset and colocalize with phase-dense Flemming bodies (upper inset). DNA, blue; microtubules, green.

cell bodies of nascent daughter cells but few within intercellular bridges (Figure 7A, panel 1). However, at a late stage of cytokinesis when the intercellular bridge narrowed to a diameter of ~2 μm and the midbody microtubule bundle was reduced to a diameter of 0.5–1 μm, GFP secretory vesicles accumulated in the intercellular bridge near the midbody ring (Figure 7A, Movie S5). Higher-magnification imaging of another cell at a similar cell-cycle stage revealed labeled secretory vesicles moving suddenly and rapidly (within 20 min) from the cell bodies into the intercellular bridge and up to the midbody ring (Figure 7B, Movie S6). In 11/11 cells, the vesicles were delivered primarily if not exclusively from one of the nascent daughter cells (Figure 7B, center panels). Vesicles packed into the region adjacent to the phase-dense Flemming body (Figure 7B, panels 2 and 3, large arrowhead; Movie S6). Within 20 min, the GFP signal disappeared (Figure 7B, last panel and Figure 7A, last panel), suggesting that the vesicles fused with the plasma membrane, releasing the GFP signal into the extracellular space where it was free to diffuse. Loss of the GFP signal was not due to photobleaching because GFP-labeled vesicles in cell bodies adjacent to the intercellular bridge and in the Golgi complex retained the signal. We next examined the relationship between vesicle delivery to the midbody and abscission. We found that, shortly after the GFP signal was lost from the midbody region, the cell cleaved on the side of the Flemming body that received the GFP vesicles (6/6 cells from four experiments, Figure 7C). The cell on the opposite side received the Flemming body (Figure 7C, 70'–95' and Figure 7D). In some cases, the Flemming body moved around rapidly after abscission on the cell surface (Movie S7), suggesting that the structure was not anchored at a discrete point on the new daughter cell. Postdivision midbodies contained multiple midbody-ring components and retained microtubules from both sides of the midbody ring (Figure 7E, panel 1). They persisted for some time after abscission, consistent with previous results (Mishima et al., 2002), and were often present in multiple copies, suggesting that they were retained through several cell cycles (Figure 7E, panels 2–4). These structures were seen on ~35% of HeLa cells and often retained features of the Flemming body and midbody ring, including MKLP-1 staining, Aurora B staining, phase-dense Flemming bodies, and localization to the plasma membrane (Figure 7E, data not shown). This suggested that supernumerary midbodies represent structures from previous divisions similar to the bud scars observed in yeast (Chen and Contreras, 2004).

Discussion

A Model for the Final Stage of Cytokinesis

This study defines several distinct molecular and structural steps during the late stages of cytokinesis (Figure 8). During cleavage-furrow ingression, MKLP-1 and MgcRacGAP arrive at the midbody ring (Figure 8A). When the intercellular bridge forms, centriolin localizes to the ring (Figure 8B), followed by snapin and exocyst proteins (Figure 8C). When the diameter of the midbody microtubule bundle and the intercellular bridge are reduced to ~0.5–1 μm, endobrevin/VAMP8 (v-SNARE) and syntaxin-2 (t-SNARE) move to the midbody ring. The v-SNAREs are part of secretory vesicles that move asymmetrically into the intercellular bridge predominantly from one nascent daughter cell; binding to v-SNAREs may incorporate t-SNAREs into this organization. The vesicles pack into the area adjacent to the ring and appear to fuse, releasing their contents into the extracellular space (lum-GFP, Figures 8D and 8E). Vesicle fusion with the plasma membrane may be initiated near the midbody ring where v- and t-SNAREs are localized. This could be followed by additional fusion events between vesicles and the plasma membrane as well as vesicle-vesicle fusion events (homotypic) mediated by SNAP23/25, a v-SNARE involved in compound exocytosis (Takahashi et al., 2004) (Figures 8F and 8G). Abscission then occurs at the site of vesicle fusion, and the entire midbody remains with the daughter cell opposite the fusion site (Figure 8H). Abscission could be triggered by arrival of v- and t-SNAREs at the midbody ring; release of SNAP23/25 from lipid rafts (Takahashi et al., 2004; Takeda et al., 2004); phosphorylation of snapin by PKA, which mediates its binding to the t-SNARE complex (Buxton et al., 2003; Chheda et al., 2001); or another event. Dynamic movement of the postabscission midbody ring suggests connections to motile forces within the cell, although this remains to be determined.

Asymmetric Delivery of Secretory Vesicles Marks the Site of Abscission

It is remarkable that secretory vesicles loaded with luminal GFP move into the intercellular bridge from only one of the two prospective daughter cells. The mechanism of this asymmetric vesicle delivery is unknown. It is tempting to speculate that a signal, negative or positive, emanates asymmetrically from one centrosome in the dividing cell. Centrosomes in the two prospective daughter cells are different in that one was "born" from the older centriole in the previous cell division during the centrosome duplication process (Doxsey, 2001). Consistent with this idea is the asymmetric spindle-pole body (SPB) localization of budding- and fission-yeast proteins that control mitotic exit and cytokinesis (Doxsey et al., 2005; Grallert et al., 2004; Molk et al., 2004). In *S. pombe*, inhibitors of mitotic exit (Cdc16p and Byr4p) localize to the "old" SPB while activators of mitotic exit (Cdc7p and presumably Sid1p and Cdc14p) localize to the new SPB (Grallert et al., 2004). The relevance of this localization in both yeasts is still unknown. Further studies will be required to determine the role of centrosome protein asymmetry in the unidirectional delivery of secretory vesicles and abscission in animal cells. It has been suggested that the mother centriole moves to the intercellular bridge in telophase cells to coordinate the final steps in cytokinesis (Piel et al., 2001), although this was not consistently observed in this study (data not shown) or another that investigated several cell lines (RPE-1, Ptk-1, CV-1, NRK-52E; A. Khodjakov, personal communication).

The final stages of cytokinesis in animal cells share features with cell division in higher plants. Higher plant cells cannot divide using an actomyosin-based cleavage furrow due to the presence of a nonpliant cell wall,

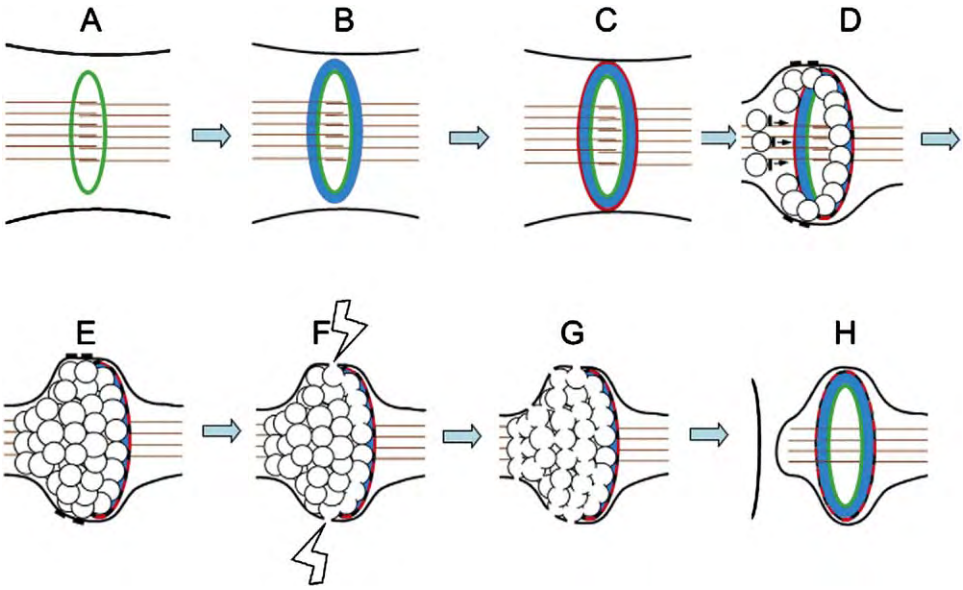

Figure 8. Model Depicting Vesicle-Mediated Abscission during Cytokinesis

(See text for details.)

(A) MKLP-1 and MgcRacGAP (green) arrive at midbody ring after cleavage furrowing has progressed. Microtubules, brown; plasma membrane, upper and lower lines.

(B and C) Centriolin moves to ring ([B], blue) and anchors sec15, other exocyst components, and snapin ([C], red).

(D) When midbody microtubules are reduced and the membrane constricted, v- and t-SNAREs ([D], black) move to the midbody ring from one prospective daughter cell. v-SNAREs presumably move with vesicles and bind there in a centriolin-dependent manner; t-SNAREs on the plasma membrane could bind through v-SNAREs.

(E) Vesicles heterogeneous in diameter pack asymmetrically into the intercellular bridge adjacent to the midbody ring.

(F and G) Vesicles adjacent to the ring containing SNARES and exocyst fuse with the plasma membrane (F) as well as at other plasma-membrane sites and with one another (G).

(H) Abscission follows at the site of membrane fusion, and the midbody is retained by the daughter cell opposite the fusion site. The released midbody ring contains multiple midbody-ring proteins and usually retains microtubule bundles from both sides of the ring. (In this model, the apparent "layering" of components is a simplification to depict arrival of different components at the midbody.)

so they accomplish cell division by constructing a new membrane at the division plane, called the cell plate, that is independent of the plasma membrane and is established by microtubule-dependent delivery and fusion of vesicles at this site (Albertson et al., 2005; Finger and White, 2002; Jurgens, 2005). Our data show that the coordinated delivery of vesicles to the midbody ring during the late stages of cytokinesis is also required for the final stages of cell division in animal cells. However, we still do not understand the mechanism of secretory-vesicle delivery to the midbody, the role of microtubules in this process, or the precise contribution of vesicle transport and fusion to abscission. The presence of vesicles with heterogeneous diameters adjacent to the midbody ring prior to abscission is consistent with a model in which some vesicles fuse together prior to fusion with the plasma membrane. This would be analogous to the cell plate in plant cells. The enodocytic pathway also appears to play a role in cell cleavage as components (dynamin, FIP3, Rab11) and compartments (endosomes) involved in this pathway affect the late stages of cytokinesis (Thompson et al., 2002; Wilson et al., 2005). Recycling endosomes have been shown to move from both prospective daughter cells to the midbody during cytokinesis then return to the daughter-cell cytoplasm (Wilson et al., 2005). It is still unclear how recycling endosomes participate in abscission and how the bidirectional movement of endosomes into the intercellular bridge is related to the unidirectional movement of secretory vesicles to this site in our study.

Structure and Persistence of the Midbody Ring

We have shown that many proteins localize to the midbody ring and that the phase-dense Flemming body is also organized into the shape of a ring. This is consistent with earlier ultrastructural studies that describe cytoplasmic channels coursing through the central midbody (Mullins and Biesele, 1977). The ring structure bears a resemblance to bud scars of *S. cerevisiae,* which serve as markers for longevity (Chen and Contreras, 2004). The midbody ring in animal cells is inherited by the daughter cell that lies opposite the site of vesicle delivery and appears to persist, as it is often seen in mitotic cells prior to cytokinesis and found in multiple copies in interphase cells (Figure 7E) (Mishima et al., 2002). Shortly after abscission, the midbody ring contains microtubules that extend from both sides of the ring. This suggests that dissolution of microtubule bundles adjacent to the midbody ring is not an absolute requirement for the final stage of cytokinesis but rather that abscission can result in transfer of the entire mid-

body and associated microtubules into one daughter cell.

Experimental Procedures

Cell Culture and Transfections

The cells used primarily in this study were diploid, telomerase-immortalized human RPE cells (hTERT-RPE-1s, Clontech Laboratories, Inc.) (Morales et al., 1999) and HeLa cells. All cells were grown as previously described (American Type Culture Collection). HeLa cells were transfected as previously described (Lipofectamine, Invitrogen).

Immunofluorescence

Cells were prepared for immunofluorescence, imaged, and deconvolved (Metamorph, Universal Imaging Corp.) using either formaldehyde, formaldehyde followed by methanol, or methanol alone as previously described (Dictenberg et al., 1998). All immunofluorescence images are two-dimensional projections of three-dimensional reconstructions to ensure that all stained material was visible in two-dimensional images. Quantification of signals produced by immunofluorescence staining for various midbody antigens was performed as described for centrosome protein quantification in our earlier studies (Gromley et al., 2003).

Antibodies

Antibodies to the following proteins were used: sec3, sec5, sec8, sec10, exo70, exo84, and sec15 (Yeaman, 2003); centriolin (Gromley et al., 2003); α-tubulin, γ-tubulin, α-His_6, and α-myc (Sigma-Aldrich); Aurora B (Transduction Laboratories); MKLP-1, GAL4 transactivation domain (AD), and GAL4 DNA binding domain (DBD) (Santa Cruz Biotechnology, Inc.); and GT335 for stabilized microtubules (Gromley et al., 2003).

Yeast Two-Hybrid Screen

Yeast two-hybrid library screens were performed following the manufacturer's instructions using a human testis Matchmaker Pre-Transformed Two-Hybrid Library (Matchmaker GAL4 Yeast Two-Hybrid System, Clontech). False positives were eliminated by mating each clone with strains expressing either lamin C or the DNA binding domain alone and plating on quadruple dropout media.

siRNAs

Two siRNAs targeting centriolin and one targeting lamin A/C were used as described (Gromley et al., 2003). Additional siRNAs targeted nucleotides in the following proteins: MKLP-1 (189–207), sec5 (260–278), sec8 (609–627), and snapin (312–330). Cells were examined 24–48 hr after siRNA treatment. siRNAs were used at 10–50 nM, and Lipofectamine was the delivery agent (Gromley et al., 2003).

Brefeldin A Treatment

HeLa cells were treated with 5–10 μg/ml brefeldin A (Sigma-Aldrich) and imaged.

Immunoprecipitations

Antibodies to centriolin or exocyst were added to hTERT-RPE cell extracts and incubated at 4°C overnight. The lysis buffer included 50 mM Tris-HCl (pH 7.5), 10 mM Na_2HPO_4 (pH 7.2), 1 mM EDTA, 150 mM NaCl, 1% IGEPAL CA-1630, and protease inhibitors (Mini tablets, Roche Diagnostics, Mannheim, Germany). Superose 6 samples were incubated with antibodies to sec3 and sec8, bound to protein A/G beads (Santa Cruz Biotechnology, Inc.) at 4°C for 2 hr (Yeaman, 2003), and exposed to SDS-PAGE and immunoblotting (Harlow and Lane, 1988).

Time-Lapse Imaging

Time-lapse imaging of cytokinesis was performed using a wide-field microscope (Gromley et al., 2003), and images were taken every 5 min for 18–24 hr. For luminal-GFP-expressing cells (Figure 7B), two concurrent time-lapse programs were used (GFP, phase contrast), and images were taken every 2 min for 3–4 hr. A PerkinElmer spinning-disc confocal microscope with an UltraVIEW CSU-10 head was used for Figures 7A, 7C, and 7D. Images were taken every 5 min and captured on an ORCA-AG cooled CCD camera. Images of GFP-GAPCenA-expressing cells were taken every 10 min on a Zeiss Axiophot microscope equipped with a Hamamatsu digital camera. Mitochondria function was assessed by Mitotracker staining (Molecular Probes).

Exocyst Fractionation

For isopycnic centrifugation, membrane compartments containing exocyst fractions were prepared as described (Grindstaff et al., 1998; Yeaman, 2003). For size-exclusion chromatography, cells were extracted with MEBC buffer (0.5% Nonidet P-40, 50 mM Tris-HCl [pH 7.5], 100 mM NaCl) containing protease inhibitors (0.1 mM Na_3VO_4; 50 mM NaF; 1 mM Pefabloc [Boehringer Mannheim]; and 10 μg/ml each of leupeptin, antipain, chymostatin, and pepstatin A) for 10 min at 4°C. Lysates were first sedimented in a Microfuge (Beckman Instruments, Fullerton, California) for 10 min and then for 30 min at 100,000 × g, passed through a 0.22 μm filter (Millipore), and loaded on a Superose 6 HR 10/30 column (200 μl, 10 mm × 30 cm; Pharmacia Biotech, Inc.) equilibrated in MEBC buffer and 1 mM dithiothreitol with 0.1 mM Pefabloc. Proteins were eluted (0.3 ml/min) at 17°C in 0.5 ml fractions, the concentration of protein in the fractions was determined, and the fractions were used for various assays (fractions 7–30).

Supplemental Data

Supplemental Data include one figure and seven movies and can be found with this article online at http://www.cell.com/cgi/content/full/123/1/75/DC1/.

Acknowledgments

We thank Dan McCollum, Yu-Li Wang, Ted Salmon, and Bill Theurkauf for useful discussions. We thank Z. Sheng (NINDS, NIH) (snapin), T. Wiembs (Lerner Institute, Cleveland) (endobrevin/VAMP8 and syntaxin-2) and M. Glotzer (IMP, Vienna) (MKLP-1, MgcRacGAP) for antibodies. This work was supported in part by grants from the National Institutes of Health to S.J.D. (GM51994) and from the Department of Defense to C.Y. (DAMD-17-03-1-0187).

Received: August 18, 2004
Revised: June 3, 2005
Accepted: July 27, 2005
Published: October 6, 2005

References

Albertson, R., Riggs, B., and Sullivan, W. (2005). Membrane traffic: a driving force in cytokinesis. Trends Cell Biol. *15*, 92–101.

Antonin, W., Holroyd, C., Tikkanen, R., Honing, S., and Jahn, R. (2000). The R-SNARE endobrevin/VAMP-8 mediates homotypic fusion of early endosomes and late endosomes. Mol. Biol. Cell *11*, 3289–3298.

Blum, R., Stephens, D.J., and Schulz, I. (2000). Lumenal targeted GFP, used as a marker of soluble cargo, visualises rapid ERGIC to Golgi traffic by a tubulo-vesicular network. J. Cell Sci. *113*, 3151–3159.

Buxton, P., Zhang, X.M., Walsh, B., Sriratana, A., Schenberg, I., Manickam, E., and Rowe, T. (2003). Identification and characterization of Snapin as a ubiquitously expressed SNARE-binding protein that interacts with SNAP23 in non-neuronal cells. Biochem. J. *375*, 433–440.

Chen, C., and Contreras, R. (2004). The bud scar-based screening system for hunting human genes extending life span. Ann. N Y Acad. Sci. *1019*, 355–359.

Chheda, M.G., Ashery, U., Thakur, P., Rettig, J., and Sheng, Z.H. (2001). Phosphorylation of Snapin by PKA modulates its interaction with the SNARE complex. Nat. Cell Biol. *3*, 331–338.

Cuif, M.H., Possmayer, F., Zander, H., Bordes, N., Jollivet, F., Couedel-Courteille, A., Janoueix-Lerosey, I., Langsley, G., Bornens, M., and Goud, B. (1999). Characterization of GAPCenA, a GTPase

activating protein for Rab6, part of which associates with the centrosome. EMBO J. *18*, 1772–1782.

Dictenberg, J., Zimmerman, W., Sparks, C., Young, A., Vidair, C., Zheng, Y., Carrington, W., Fay, F., and Doxsey, S.J. (1998). Pericentrin and gamma tubulin form a protein complex and are organized into a novel lattice at the centrosome. J. Cell Biol. *141*, 163–174.

Dobbelaere, J., and Barral, Y. (2004). Spatial coordination of cytokinetic events by compartmentalization of the cell cortex. Science *305*, 393–396.

Doxsey, S. (2001). Re-evaluating centrosome function. Nat. Rev. Mol. Cell Biol. *2*, 688–698.

Doxsey, S., McCollum, D., and Theurkauf, W. (2005). Centrosomes in cellular regulation. Annu. Rev. Cell Dev. Biol. *21*, 688–698. in press.

Echard, A., Hickson, G.R., Foley, E., and O'Farrell, P.H. (2004). Terminal cytokinesis events uncovered after an RNAi screen. Curr. Biol. *14*, 1685–1693.

Finger, F.P., and White, J.G. (2002). Fusion and fission: membrane trafficking in animal cytokinesis. Cell *108*, 727–730.

Finger, F.P., Hughes, T.E., and Novick, P. (1998). Sec3p is a spatial landmark for polarized secretion in budding yeast. Cell *92*, 559–571.

Glotzer, M. (2001). Animal cell cytokinesis. Annu. Rev. Cell Dev. Biol. *17*, 351–386.

Glotzer, M. (2005). The molecular requirements for cytokinesis. Science *307*, 1735–1739.

Grallert, A., Krapp, A., Bagley, S., Simanis, V., and Hagan, I.M. (2004). Recruitment of NIMA kinase shows that maturation of the S. pombe spindle-pole body occurs over consecutive cell cycles and reveals a role for NIMA in modulating SIN activity. Genes Dev. *18*, 1007–1021.

Grindstaff, K.K., Yeaman, C., Anandasabapathy, N., Hsu, S.C., Rodriguez-Boulan, E., Scheller, R.H., and Nelson, W.J. (1998). Sec6/8 complex is recruited to cell-cell contacts and specifies transport vesicle delivery to the basal-lateral membrane in epithelial cells. Cell *93*, 731–740.

Gromley, A., Jurczyk, A., Sillibourne, J., Halilovic, E., Mogensen, M., Groisman, I., Blomberg, M., and Doxsey, S. (2003). A novel human protein of the maternal centriole is required for the final stages of cytokinesis and entry into S phase. J. Cell Biol. *161*, 535–545.

Guertin, D.A., Trautmann, S., and McCollum, D. (2002). Cytokinesis in eukaryotes. Microbiol. Mol. Biol. Rev. *66*, 155–178.

Guo, W., Sacher, M., Barrowman, J., Ferro-Novick, S., and Novick, P. (2000). Protein complexes in transport vesicle targeting. Trends Cell Biol. *10*, 251–255.

Harlow, E., and Lane, D. (1988). Antibodies: A Laboratory Manual (Cold Spring Harbor, NY: Cold Spring Harbor Laboratory Press).

Jurgens, G. (2005). Plant cytokinesis: fission by fusion. Trends Cell Biol. *15*, 277–283.

Low, S.H., Li, X., Miura, M., Kudo, N., Quinones, B., and Weimbs, T. (2003). Syntaxin 2 and endobrevin are required for the terminal step of cytokinesis in mammalian cells. Dev. Cell *4*, 753–759.

Mishima, M., Kaitna, S., and Glotzer, M. (2002). Central spindle assembly and cytokinesis require a kinesin-like protein/RhoGAP complex with microtubule bundling activity. Dev. Cell *2*, 41–54.

Molk, J.N., Schuyler, S.C., Liu, J.Y., Evans, J.G., Salmon, E.D., Pellman, D., and Bloom, K. (2004). The differential roles of budding yeast Tem1p, Cdc15p, and Bub2p protein dynamics in mitotic exit. Mol. Biol. Cell *15*, 1519–1532.

Mondesert, G., Clarke, D.J., and Reed, S.I. (1997). Identification of genes controlling growth polarity in the budding yeast Saccharomyces cerevisiae: a possible role of N-glycosylation and involvement of the exocyst complex. Genetics *147*, 421–434.

Monzo, P., Gauthier, N.C., Keslair, F., Loubat, A., Field, C.M., Le Marchand-Brustel, Y., and Cormont, M. (2005). Clues to CD2-associated protein involvement in cytokinesis. Mol. Biol. Cell *16*, 2891–2902. 10.1091/mbc.E04-09-0773

Morales, C.P., Holt, S.E., Ouellette, M., Kaur, K.J., Yan, Y., Wilson, K.S., White, M.A., Wright, W.E., and Shay, J.W. (1999). Absence of cancer-associated changes in human fibroblasts immortalized with telomerase. Nat. Genet. *21*, 115–118.

Mullins, J.M., and Biesele, J.J. (1977). Terminal phase of cytokinesis in D-98s cells. J. Cell Biol. *73*, 672–684.

Murthy, M., and Schwarz, T.L. (2004). The exocyst component Sec5 is required for membrane traffic and polarity in the Drosophila ovary. Development *131*, 377–388.

Papoulas, O., Hays, T.S., and Sisson, J.C. (2004). The golgin Lava lamp mediates dynein-based Golgi movements during Drosophila cellularization. Nat. Cell Biol. *7*, 612–618. 10.1038/ncb1264

Paweletz, N. (1967). On the function of the 'Flemming body' during division of animal cells. Naturwissenschaften *54*, 533–535.

Piel, M., Nordberg, J., Euteneuer, U., and Bornens, M. (2001). Centrosome-dependent exit of cytokinesis in animal cells. Science *291*, 1550–1553.

Prigent, M., Dubois, T., Raposo, G., Derrien, V., Tenza, D., Rosse, C., Camonis, J., and Chavrier, P. (2003). ARF6 controls post-endocytic recycling through its downstream exocyst complex effector. J. Cell Biol. *163*, 1111–1121.

Salminen, A., and Novick, P.J. (1989). The Sec15 protein responds to the function of the GTP binding protein, Sec4, to control vesicular traffic in yeast. J. Cell Biol. *109*, 1023–1036.

Saxton, W.M., and McIntosh, J.R. (1987). Interzone microtubule behavior in late anaphase and telophase spindles. J. Cell Biol. *105*, 875–886.

Skop, A.R., Bergmann, D., Mohler, W.A., and White, J.G. (2001). Completion of cytokinesis in C. elegans requires a brefeldin A-sensitive membrane accumulation at the cleavage furrow apex. Curr. Biol. *11*, 735–746.

Skop, A.R., Liu, H., Yates, J., Meyer, B.J., and Heald, R. (2004). Dissection of the mammalian midbody proteome reveals conserved cytokinesis mechanisms. Science *305*, 61–66. Published online May 27, 2004..

Strickland, L.I., and Burgess, D.R. (2004). Pathways for membrane trafficking during cytokinesis. Trends Cell Biol. *14*, 115–118.

Takahashi, N., Hatakeyama, H., Okado, H., Miwa, A., Kishimoto, T., Kojima, T., Abe, T., and Kasai, H. (2004). Sequential exocytosis of insulin granules is associated with redistribution of SNAP25. J. Cell Biol. *165*, 255–262.

Takeda, T., Kawate, T., and Chang, F. (2004). Organization of a sterol-rich membrane domain by cdc15p during cytokinesis in fission yeast. Nat. Cell Biol. *6*, 1142–1144.

Thakur, P., Stevens, D.R., Sheng, Z.H., and Rettig, J. (2004). Effects of PKA-mediated phosphorylation of Snapin on synaptic transmission in cultured hippocampal neurons. J. Neurosci. *24*, 6476–6481.

Thompson, H.M., Skop, A.R., Euteneuer, U., Meyer, B.J., and McNiven, M.A. (2002). The large GTPase dynamin associates with the spindle midzone and is required for cytokinesis. Curr. Biol. *12*, 2111–2117.

Verplank, L., and Li, R. (2005). Cell cycle-regulated trafficking of Chs2 controls actomyosin ring stability during cytokinesis. Mol. Biol. Cell *16*, 2529–2543.

Vites, O., Rhee, J.S., Schwarz, M., Rosenmund, C., and Jahn, R. (2004). Reinvestigation of the role of snapin in neurotransmitter release. J. Biol. Chem. *279*, 26251–26256.

Wang, H., Tang, X., Liu, J., Trautmann, S., Balasundaram, D., McCollum, D., and Balasubramanian, M.K. (2002). The multiprotein exocyst complex is essential for cell separation in Schizosaccharomyces pombe. Mol. Biol. Cell *13*, 515–529.

Wilson, G.M., Fielding, A.B., Simon, G.C., Yu, X., Andrews, P.D., Hames, R.S., Frey, A.M., Peden, A.A., Gould, G.W., and Prekeris, R. (2005). The FIP3-Rab11 protein complex regulates recycling endosome targeting to the cleavage furrow during late cytokinesis. Mol. Biol. Cell *16*, 849–860.

Yeaman, C. (2003). Ultracentrifugation-based approaches to study regulation of Sec6/8 (exocyst) complex function during development of epithelial cell polarity. Methods *30*, 198–206.

Yeaman, C., Grindstaff, K.K., and Nelson, W.J. (2004). Mechanism of recruiting Sec6/8 (exocyst) complex to the apical junctional complex during polarization of epithelial cells. J. Cell Sci. *117*, 559–570.

Loss of centrosome integrity induces p38/p53/p21-dependent G_1/S arrest

Keith Mikule, Benedicte Delaval, Phil Kaldis+, Agata Jurcyzk, Stephanie Mirabelle, Alexey Khodjakov* and Stephen Doxsey

Program in Molecular Medicine, University of Massachusetts Medical School, Worcester, Massachusetts 01605, +National Cancer Institute, Fredrick, Maryland 21702, *Wadsworth Center, Albany, New York 12201

[5]Correspondence:

Stephen Doxsey

University of Massachusetts Medical School

Program in Molecular Medicine

373 Plantation Street

Worcester, Massachusetts 01605

Ph: 508-856-1613

Fx: 508-856-4289

EM: Stephen.Doxsey@umassmed.edu

Text 3518 words; 8 Figures; 4 supplemental figures

Running title: Centrosome-triggered G_1 arrest.

Abstract

Centrosomes organize the microtubule cytoskeleton for both interphase and mitotic functions. They are implicated in cell cycle progression but the mechanism is unknown. Here we show that depletion of 14/15 centrosome proteins arrests human diploid cells in G_1 with reduced Cdk2-cyclin A activity; expression of a dominant-negative centrosome construct gives similar results. Cell cycle arrest is always accompanied by defects in centrosome structure and function (duplication, primary cilia assembly). The arrest occurs from within G_1, ruling out contributions from mitosis and cytokinesis. The arrest requires p38, p53 and p21, and is preceded by p38-dependent activation and centrosomal recruitment of p53. p53-deficient cells fail to arrest, leading to centrosome and spindle dysfunction and aneuploidy. We propose that loss of centrosome integrity activates a checkpoint that inhibits G_1/S progression. This model satisfies the definition of checkpoint in having three elements: a perturbation that is sensed, a transducer (p53) and a receiver (p21).

The centrosome is best known for its microtubule organizing function. However, centrosomes contain hundreds of structural and regulatory proteins with diverse functions suggesting roles in numerous cellular activities[1]. Animal cell centrosomes are structurally complex organelles comprised of two microtubule–shaped centrioles surrounded by a protein matrix (pericentriolar material, PCM) and other structural elements. Like DNA replication, the centrosome duplication process occurs once per cell cycle, is semi-conservative, initiates in G_1 and is controlled by the same cyclin-dependent kinases (Cdk2-cyclin A/E)[2,3]. A single interphase centrosome yields two mature centrosomes at mitosis, which participate in organization of bipolar spindles and segregation of chromosomes. Most human carcinomas are characterized by aberrant centrosomes[4,5], which are thought to organize dysfunctional spindles and contribute to genetic instability.

Recent studies indicate that centrosomes play a role in cytokinesis and that disruption of this function is associated with cell cycle arrest. For example, when centrosomes are removed[6,7] or disrutped[8,9] cytokinesis is impaired and cells undergo G_1 arrest. In contrast, cell cycle progression is not affected in cells with extra centrosomes, extra nuclei or after pharmacological disruption of cytokinesis[10,11]. Taken together, these results indicate that the centrosome-associated G_1 arrest occurs only when centrosomes are absent or compromised. Other studies demonstrate that progression from G_1 into S phase and other cell cycle transitions requires binding of cell cycle regulatory molecules to centrosomes[12,13]. However, little is known about the mechanism by which centrosomes contribute to the G_1- to S-phase transition.

Results

Centrosome protein depletion reduces centrosomal levels of targeted proteins and induces G_1 arrest

To address the role of centrosomes in cell cycle progression, we targeted fifteen centrosome proteins for depletion by small-interfering RNAs (siRNAs). We used human

diploid epithelial cells (RPE-1) and confirmed results with three other human diploid cell lines (see Materials and Methods). Targeted proteins included integral centrosome/centriole components as well as regulatory proteins that affect centrosome function; three non-centrosomal proteins served as negative controls including the intermediate filament protein lamin and the actin-associated protein zyxin. Indirect immunofluorescence staining of individual cells revealed a substantial reduction in the centrosome-associated fraction of all targeted centrosome proteins (Fig. 1a, Supplementary Fig. 1 a-c), even though many have significant cytoplasmic fractions (e.g. centrin is >90% cytoplasmic). Western blots of whole cell lysates showed reduction in the global level of targeted proteins (Supplemental Fig. 1d).

Depletion of 14/15 centrosome proteins induced G_1 arrest (Fig. 1). Cells failed to reach confluency, exhibited a low mitotic index, did not progress into S phase (BrdU-negative, Fig. 1b) and showed reduced reactivity for the proliferating antigen Ki-67 (Fig. 1c)[14]. To more precisely define the stage of cell cycle arrest, we treated cells with nocodazole to depolymerize microtubules, activate the spindle assembly checkpoint and induce accumulation of cells in G_2/M with 4N DNA content. Remarkably, centrosome-depleted cells were retained in the G_1 peak with 2N DNA content and did not shift to the G_2/M peak as did control cells (Fig. 1d). Depletion of all centrosome proteins except one induced G_1 arrest (Fig. 1b, d). Cells treated with siRNAs targeting control proteins or the centrosome protein ninein[15] continued to cycle normally. Ninein had no effect on cell cycle progression (or associated defects, see below) despite the fact that it was significantly reduced at centrosomes following treatment with two independent siRNAs (Supplemental Fig. 1c). Whether the lack of cell cycle arrest in ninein-depleted cells was due to insufficient protein reduction or a lack of ninein involvement in this pathway was not determined. Targeted centrosome proteins were localized to different centrosomal sites including the PCM, centrioles, the mother centriole or subdistal appendages. This suggested that a single centrosome substructure was not involved in the arrest.

G_1 arrest is specifically suppressed by re-expression of the target protein

In addition to the several control proteins targeted in our siRNA experiments (above), we performed other experiments to demonstrate that the cell cycle arrest was specific for centrosome proteins. We first tested whether G_1 arrest could be suppressed by re-expression of the targeted protein. We used a siRNA that targeted the 5' untranslated region (UTR) of endogenous centrin 2**,** but did not target GFP-centrin 2 produced from a plasmid (Fig.2). GFP-centrin 2 localized to centrosomes in RPE cells(Fig. 2b). As expected, the UTR-directed siRNA successfully depleted endogenous centrin 2 but not GFP-centrin 2 as determined by immunoblotting and immunofluorescence microscopy (Fig. 2a, b). Cell cycle analysis demonstrated that control cells depleted of GFP-centrin 2 arrested, whereas most cells ectopically expressing GFP-centrin 2 continued to cycle (Fig. 2c). However, when GFP-centrin 2-expressing cells were treated with a siRNA that targeted both endogenous centrin 2 and GFP-centrin 2 (Fig.2b), G_1 arrest was induced (Fig. 2a-c). This demonstrated that centrin 2 was specifically required for cell cycle progression and suggested that localization of the protein to centrosomes was important for this function.

In a separate experiment, cells were kept under sustained cell cycle arrest (for 10 days) by repeated treatment with siRNAs targeting pericentrin (Supplemental Fig. 2). When siRNAs were washed out, cells resumed cycling only after pericentrin was re-expressed and localized properly to centrosomes. These two 'rescue' experiments demonstrate that centrosome protein depletion induces a specific and reversible G_1 arrest.

Mislocalization of pericentrin from centrosomes by expression of a dominant-negative construct induces G_1 arrest

To more specifically test whether loss of protein from centrosomes induced G_1 arrest, we expressed the C-terminus of pericentrin (Peri-CT), which acts in a dominant negative manner by disrupting the centrosome–bound fraction of endogenous pericentrin[16]**.** Most cells expressing RFP-tagged Peri-CT were unable to incorporate BrdU after a 24-hour

pulse, whereas those expressing RFP alone were mostly BrdU-positive (Fig. 3a, 17% vs. 98% BrdU+, n=50 cells). This experiment demonstrates that cell cycle arrest can be induced by ectopic expression of a centrosome protein, in addition to centrosome protein depletion.

Previous studies demonstrated that cell cycle arrest could be induced by centrosome-specific antibodies. Microinjection of antibodies to PCM-1 disrupted centrosome structure and induced G_1 arrest in mouse embryos[17], and microinjection of centriolin antibodies induced a G_1-like arrest in Xenopus embryos[9]. Thus, G_1 arrest can be induced by centrosome protein depletion, overexpression or antibody binding in both cultured cells and multicellular organisms. Cell cycle arrest by three independent methods for targeting centrosome proteins in three different experimental systems argues that this phenomenon is specific for centrosomes.

G_1 arrest can be induced in postmitotic cells from within G_1

We next tested if G_1 arrest was a consequence of mitotic defects. In the experiment shown in Figure 3a, we identified cells by time lapse imaging as they completed cytokinesis[18], then microinjected them with a plasmid containing the dominant-negative pericentrin construct to induce protein expression in G_1. As described earlier (Fig. 3a), G_1- stage pericentrin-expressing cells never entered S-phase, whereas control cells continued to cycle, demonstrating that arrest was induced in postmitotic cells. In a second strategy, cells were accumulated in G_0/G_1 by serum withdrawal then treated with siRNAs to deplete pericentrin. Subsequently, bulk cellular proteins were labeled by a fluorescent dye (CFDA-SE) that becomes halved after each cell division[19,20] and serum was added to release cells from the G_0/G_1 arrest. Nearly all control cells divided at least once within 24 hours, whereas ~40% of pericentrin-depleted cells did not divide at all during the same time period (Fig. 3b). These two independent approaches demonstrate that G_1 arrest can be induced from within G_1, and that perturbation of mitotic events, such as spindle function and cytokinesis, are not required to trigger the arrest.

G_1 arrest occurs in late G_1 with reduced Cdk2-cyclin A activity, and is suppressed by blocking the Cdk inhibitor, p21

To more accurately determine the cell cycle stage and molecular mechanism of the G_1 arrest, we examined the levels and activity of Cdk-cyclin complexes. Immunoprecipitations from pericentrin-depleted cells showed that Cdk2-cyclin A activity but not cyclin A levels, was diminished in pericentrin depleted cells compared with controls (Fig. 3c, data not shown). Similar results were obtained for several centrosome proteins (Fig. 3c, third panel). The diminished Cdk2 activity in the absence of a change in cyclin A levels suggested the presence of a Cdk inhibitory activity. In fact, human cells null for the Cdk inhibitor p21 suppressed the cell cycle arrest (HCT116 p21-/-, Fig. 3d), suggesting a role for p21 in the inhibition of Cdk2-cyclinA complexes[21] and a molecular mechanism for the arrest.

G_1 arrested cells have defects in centrosome structure/organization

Because disruption of centrosome proteins induced G_1 arrest from within G_1, we examined G_1 arrested cells for defects in centrosome structure and organization. Immunofluorescence imaging using markers for centrioles and PCM revealed three categories of structural defects: centriole loss, centriole separation and apparent centriole fragments. Importantly, all centrosome protein depletions analyzed that showed cell cycle arrest, also showed centrosome defects in one or more of these categories when compared to controls (10/10). In Fig. 4a we present data for the centrosome defect that exhibited the highest increase over control levels for each centrosome protein analyzed; quantitative data for each of the three individual assays is presented in Supplemental Fig. 3. Some protein depletions induced defects in all three categories (e.g. GCP2) and others in only one or two (e.g. δ tubulin, centriole separation, PCM1, centriole loss, Supplemental Fig. 3.). Aberrant centrosomes did not result from cell cycle arrest, as they were not detected in cells arrested by other means (e.g. serum deprivation, hydroxyurea).

The use of centriole markers in immunofluorescence studies allowed us to identify a reduction in centriole number in G_1 arrested cells from two to one. Eight of nine centrosome protein depletions exhibited this phenotype (excluding ninein, Supplementary Fig. 3b). In addition, separated centrioles were observed in 6/9 centrosome protein depletions (Supplementary Fig. 3c). In control siRNA treated cells, centrioles were closely opposed (0-2 μm) compared with widely separated centrioles in centrosome protein-depleted cells (5-8 μm).

Apparent centriole fragments were also observed by immunofluorescence. These structures stained positively for centriole proteins (centrin) and often for a marker for stabilized tubulin (polyglutamylated tubulin), but not for PCM proteins (pericentrin, γ tubulin, Fig. 4b). They were heterogeneous in size, smaller than centrioles and found in the vicinity of the centrosome. They were observed in 4/6 centrosome protein depletions tested (Supplementary Fig. 3a). A few of the very same structures were examined at higher resolution by correlative electron microscopy (EM)[22]. This revealed elements that appeared to be disorganized microtubule-like structures (Fig. 4c). Two cells had three GFP-centrin dots and all appeared to be incomplete microtubule-like structures by EM; a third cell showed no structural correlates by EM and could represent less complete centriole structures as described previously[22]**.** These data suggested that centrosome protein depletion induced formation of centriole intermediates analogous to abnormal centrioles produced by mutation of genes involved in centriole duplication[23,24]. Taken together, the results from these three assays show that centrosome defects accompany G_1 arrest for all centrosome depletions analyzed here, suggesting a strong link between these phenotypes.

G_1 arrested cells exhibit defects in centrosome function

We reasoned that defects in centrosome structure/organization could perturb centrosome functions known to occur in G_1, namely centrosome duplication and primary cilia assembly. In fact, previous studies showed that loss of centrioles, as described above, was associated with improper centrosome duplication[25,26]. To test for defects in centrosome

duplication we first treated U2OS cells with hydroxyurea to induce S phase arrest and multiple rounds of centrosome duplication[27]. All centrosome protein depletions analyzed here, that induced cell cycle arrest and centrosome defects, also inhibited formation of supernumerary centrosomes and supernumerary centrioles (6/6, Fig. 5a, b). In addition, supernumerary centrosomes/centrioles that occur naturally in U2OS cells (without added hydroxyurea) were reduced to more normal or lower than normal numbers (supplemental Fig. 3d). These two assays show that centrosomes with abnormal structure were unable to duplicate properly.

We next tested the ability of centrosomes depleted of centrosome protein to assemble primary cilia. Primary cilia are solitary microtubule-based structures that require functional centrosomes for their assembly[28] serve as environmental sensors and are implicated in human disease[29]. siRNAs targeting 10 proteins that induced G_1 arrest inhibited primary cilia formation (Fig. 5c). This loss of functional integrity was consistent with the observed defects in centrosome structure (Fig. 4a).

All centrosome protein depletions tested that lead to G_1 arrest also showed defects in centrosome structure/organization and centrosome function. This correlation is remarkable and suggests that defects in centrosome structure and function are tightly linked to centrosome-associated G_1 arrest.

G_1 arrest requires p53 and p38

We next investigated regulatory molecules and pathways that could control cell cycle progression in centrosome protein depleted cells. Immunofluorescence imaging and biochemical strategies, demonstrated that the p53 tumor suppressor accumulated in nuclei of siRNA treated cells prior G_1 arrest (Fig. 6a); p53 did not translocate to nuclei in lamin siRNA-treated control cells (Fig. 6 a). Translocation of p53 into the nucleus is consistent with its activation[30,31] and indicates a role for the protein in G_1 arrest. In fact, cell lines with compromised p53 (HCT116 p53-/-, HeLa, Saos-2, Fig 6b, supplemental Fig. 4a) did

not undergo G_1 arrest whereas cells with wild type p53 arrested normally (RPE-1, BJ-1, HME-1, HCT-116, Fig. 1, Fig. 3d).

It is possible that p53-deficient cell lines acquire additional genetic changes that contribute to cell cycle arrest in a p53-independent manner. To overcome this potential problem, we depleted p53 acutely using siRNAs in cells concurrently depleted of centrosome proteins and found that G_1 arrest was also suppressed under these conditions (Fig. 6c, supplemental Fig. 4b,c). p53 activation is sometimes linked to DNA damage[32]. However, we found no evidence for DNA damage in cells depleted of centrosome proteins using an immunofluorescence assay for 53BP1, an early marker for double-strand DNA breaks[33]. In contrast, robust 53BP1 staining was observed when DNA was damaged by etoposide and hydroxyurea (supplemental Fig. 4d). These results demonstrate that G_1 arrest induced by centrosome protein depletion is p53-dependent and occurs without detectable DNA damage.

p53 activity is modulated by multiple signal transduction pathways[34] including p38. p38 is a member of a pathway that responds to cellular stress and is linked to the cell cycle through senescence and differentiation pathways[35]. In cells depleted of centrosome proteins, we found that p53 was activated on serine-33 ($p53^{P\text{-}ser33}$), a residue known to be phosphorylated by p38 (Fig. 7)[36]. This phosphorylation was not observed in ninein-depleted or control siRNA treated cells (Fig. 7a). Consistent with the lack of detectable DNA damage in centrosome protein depleted cells, we did not detect phosphorylation on serine-15 of p53 by the DNA damage-associated ATM kinase (data not shown).

We next tested whether p38 was required for the centrosome associated G_1 arrest. We first showed that SB202190 and another inhibitor of the α and β isoforms of p38 (SB203580)[37] suppressed the G_1 arrest (Fig. 7b,) and reduced nuclear translocation of $p53^{P\text{-}ser33}$ if added prior to centrosome protein depletion, but not after (data not shown). In contrast, an inhibitor of the MEK signal transduction pathway (MAPK) had no effect on cell cycling. We confirmed pharmacological suppression of the G_1 arrest by siRNA-mediated depletion of p38 α (Fig 7c).

The p38-activated form of p53 accumulates at centrosomes prior to G_1 arrest

Immunofluorescence imaging demonstrated that prior to G_1 arrest, the p38-phosphorylated form of p53 ($p53^{P\text{-}ser33}$) concentrated at centrosomes in response to centrosome protein depletion but not control protein depletion (lamin, Fig. 8a). Centrosome accumulation of $p53^{P\text{-}ser33}$ occurred prior to its nuclear translocation (Fig. 8a, 24h), suggesting a multi-step pathway for activation and nuclear entry of p53. We also found that activated p38 was detectable at centrosomes in mitotic and most interphase cells (Fig. 8b). In summary, we show that p38 localizes to centrosomes, that $p53^{P\text{-}ser33}$ accumulates at centrosomes specifically in response to centrosome protein depletion and that both proteins are required for the centrosome-associated cell cycle arrest. These observations are consistent with a role for p53 and p38 in transmitting signals from the centrosome to the cell cycle machinery (p21-cyclinA-Cdk2 complexes) as part of a cell cycle checkpoint that monitors changes in centrosome integrity and controls G_1 to S phase progression. Consistent with this model are previous studies showing that p38 activates p53[36], that p53 activates p21 [38,39] and that p21 inhibits Cdk2-cyclin complexes[21].

Discussion

This study represents an extensive analysis of centrosome protein depletion in vertebrate cells. The original goal was to identify centrosome proteins involved in cell cycle progression. We unexpectedly found that nearly all centrosome genes tested induced G_1 arrest when depleted or overexpressed. Also unexpected was the observation that defects in centrosome structure and G_1 centrosome functions always accompanied cell cycle arrest, suggesting a link between these phenotypes (see below). This work uncovers two functions that are common to many centrosome proteins (centrosome duplication, primary cilia assembly); no common mitotic function was identified in this study (data not shown). We propose that these G_1 functions are core functions of centrosomes in vertebrate cells.

Possible mechanism of cell cycle arrest

The concordance of three distinct phenotypes--defective centrosome structure, centrosome dysfunction and G_1 arrest--is remarkable and provides a strong argument for a causal relationship. Based on these observations, we propose that cell cycle arrest is triggered by defects in centrosome structure and/or function. Consistent with this idea, was the observation that the centrosome-bound fraction of targeted proteins was always reduced following centrosome protein depletion or expression of the pericentrin dominant-negative construct. Moreover, none of three phenotypes was observed following depletion of control proteins or the centrosome protein ninein. The ability to induce G_1 arrest from within G_1 is consistent with disruption of centrosome/centriole structure and G_1-associated centrosome functions within G_1. Finally, specific recruitment of regulatory molecules to centrosomes (e.g. p53) in response to centrosome protein depletion is also consistent with a role for centrosomes in the cell cycle arrest pathway.

Work from other studies supports the idea that cell cycle progression is linked to centrosomes. For example, cell cycle arrest was observed in cultured cells following centrosome disruption by laser ablation[6] or microsurgery[7], and in mouse oocytes following microinjection of anti-PCM-1 antibodies[17]. Disruption of centrosome structure in all systems could logically lead to defects in centrosome functions such as duplication and primary cilia assembly, as described in this study. In fact, links between premature centriole separation and aberrant centrosome duplication, and between defective centrosome duplication and cilia assembly, have been demonstrated previously in vertebrate cells and organisms[40]. Taken together, this earlier work and work presented here provides a strong link between defective centrosomes and cell cycle arrest.

The structural defects in centrosomes observed following depletion of centrosome proteins could arise in a number of ways including production of centrosome duplication intermediates that fail to assemble into mature organelles, defects in parent centrosomes/centrioles that occur prior to G_1, or the inability to remodel centrosomes during centrosome duplication[41]. We propose that most if not all centrosome proteins are

required, perhaps as parts of an assembly line, to complete the construction of a functional centrosome. Master regulators likely control the overall process (e.g. Plk4[26,42])

Is there a centrosome damage checkpoint?

Our results suggest the presence of a novel cell cycle checkpoint that prevents cells from entering S phase when defects in centrosome structure and/or function are detected. Consistent with a checkpoint is the observation that centrosome-protein-depleted cells arrest with 'centrosome damage' (structural/functional defects) and re-enter the cell cycle only after target protein levels are restored. As with other checkpoints, cell cycle arrest can be overcome by depleting/inhibiting elements of the checkpoint pathway (p53, p38, p21). In this regard, our data satisfy the definition of checkpoint as having three elements: a change in a condition that is sensed (perturbation of centrosome structure/function), a transducing system (p38/p53) and a receiver element (p21).

Abrogation of the proposed centrosome damage checkpoint has deleterious downstream consequences. For example, in p53-deficient HeLa cells, depletion of proteins involved in centrosome duplication induces spindle defects, cytokinesis failure and aneuploidy (Plk4, centrin)[25,26]. In much the same way, p53-deficiency in many human tumors could abrogate the 'centrosome damage' checkpoint and contribute to centrosome defects, spindle dysfunction and aneuploidy [5,43].

The centrosome damage checkpoint has strong parallels with the DNA damage checkpoint

The proposed centrosome damage checkpoint and the DNA damage checkpoint appear to be activated by damage of a cellular structure and trigger cell cycle arrest prior to S phase entry. In response to DNA damage, signaling molecules such as ATM are recruited to damaged DNA. We propose that in response to centrosome damage, activated $p53^{P\text{-}ser33}$ accumulates on centrosomes; p38 is present continuously. DNA and centrosomes are the only cellular structures that are replicated once and only once during every cell cycle and

both are replicated semi-conservatively. Moreover, replication of both DNA and centrosomes is initiated at the same cell cycle stage (G_1) and controlled by some of the same regulatory molecules (Cdk2-cyclin A/E)[1]. Thus, it is possible that checkpoints that independently monitor centrosomes and DNA damage co-exist in G_1 to prevent entry into the next cell cycle with compromised structures. Additional studies will be required to identify other centrosome-associated molecules that are part of the checkpoint control pathway and to determine the precise mechanism of pathway activation. In vivo, the centrosome damage checkpoint could prevent cell cycling when centrosomes are compromised by certain pathogens[44-46] or other perturbations such as heat (data not shown)[47].

Methods

Antibodies

We are indebted to the following investigators for providing antibodies: GCP2 and 3 (T. Stearns); ninein (G. Chan); Nek2a and cNap1 (A. Fry); pericentrin B (T. Davis); PCM-1 (A. Merdes); 20H5 Centrin-2 (J. Salisbury); cdc14A and cdc14B (P. Jackson); polyglutamylated tubulin (GT335) antibody (P. Denoulet); $p53^{P\text{-}ser33}$ (Y. Taya); and 53BP1 (T. Halazonetis). Commercially available antibodies were also used: α-tubulin, γ-tubulin, ε tubulin, actin, BrdU (Sigma); Ki-67 (BD Biosciences); lamin A/C (Cell Signaling); p38, histone H1, zyxin, Nek2, δ tubulin, ε tubulin (Santa Cruz); Phospho-p38 (Thr180/Tyr182, Cell Signaling); p53 (ab-2), p53 (ab-6). Pericentrin A/B[28] 5051[48] and cyclins A2, B1, cdk1-2[49] have been described previously.

Cell culture, siRNA, transfection, and microinjection

These studies utilized primarily diploid, telomerase-immortalized RPE-1 cells (Clontech)[50], cell lines containing wild-type p53 (BJ-1, HCT116, IMR-90) or compromised p53 (Saos-2, HeLa, HCT116 p53 -/- [generous gift from B. Vogelstein]). HeLa and U2OS stably expressing GFP-centrin were prepared in our laboratory. Cells

were grown as described by American Type Culture Collection. For G_0/G_1 synchrony, cells were grown for 24h in media with reduced serum (0.25%) prior to experimentation. Targeted proteins were depleted with small-interfering RNAs (siRNAs) delivered to cells at 1-200 nM using Oligofectamine or Lipofectamine 2000 (Invitrogen) per manufacturers instructions. Synthetic double-stranded siRNAs (Dharmacon) were designed according to recently published suggestions[50] (siRNA sequences available on request). For "rescue" experiment siRNA we ordered Smart pool siRNA (Dharmacon) localized in the UTR region. Several genes were targeted with a second siRNA to eliminate possible non-specific effects. p38 (SB202190, Calbiochem) and MAPK (PD98059) inhibitors were used at 10μM and 50μM respectively. For telophase microinjection experiments, cells synchronized in mitosis via 10h nocodazole incubation (0.5 μg/mL), were microinjected into the nucleus 1h after release, with either a plasmid encoding RFP-peri-CT1, or a control RFP plasmid using an Eppendorf transjector 5246 and Micromanipulator (Brinkman). Immediately following microinjection, cells were incubated with 10 μM BrdU for 24h before fixation and staining. Alternatively, cells were transfected using calcium phosphate and incubated for 24h with BrdU followed by fixation and staining.

Immunofluorescence and immunoblotting

Cells were prepared for immunofluorescence, imaged, deconvolved (Meta-Morph; Universal Imaging Corp.), displayed as two-dimensional projections of three-dimensional reconstructions to visualize the entire cell volume, and quantified as previously described[51]. Pixel intensity profiles (total intensity plot) were constructed from maximal intensity projections using Meta-Morph. Crude cell lysates were analyzed for protein depletion. Cells were treated with siRNAs for 48-72h, harvested and lysed in phosphate-buffered saline (PBS) supplemented with 1% Triton X-100 and a cocktail of protease inhibitors. Cell lysates were clarified at top speed in a Microfuge for 15 min at 5°C. Protein concentration for each lysate was determined using Bio-Rad protein dye reagent, loads were adjusted and proteins were resolved by SDS-PAGE and analyzed by western blot.

Kinase assays and nuclear fractions

Immunoprecipitations and kinase assays were performed as previously described[49]. Affinity-purified cyclin A antibodies were cross-linked to Sepharose beads and incubated with cell lysates (100 to 300 μg proteins) for 3 hr before being washed 4X in buffer. Precipitated proteins were resuspended in 20 μl of 1X SDS-PAGE sample buffer for immunoblot analysis. For kinase assays, immunoprecipitation beads were dissolved in 5 μl kinase buffer with 10 mM DTT, and 20-50 μM ATP. Each sample was incubated with 5-10 μCi [γ-^{32}P]ATP (PE/NEN Life Sciences, #BLU-502A), 1.5 μg and histone H1 (Roche, #1004875) in a final volume of 16 μl for 30min at 30°C. Reactions were terminated with 8 μl 5X SDS-PAGE sample buffer and processed for autoradiography and quantified by phosphorimage analysis (Molecular Probes, Storm 820). Nuclear fractions were prepared by resuspending trypsinized cells in cold nuclear extraction buffer (320 mM sucrose, 5 mM $MgCl_2$, 10mM HEPES, 1% Triton X-100 at pH 7.4) by gentle vortexing, followed by incubation on ice for 10 min. Nuclei were then pelleted at 2000 x g and washed twice with nuclei extraction buffer without Triton X-100. Nuclei yield and integrity were confirmed by microscopic examination. All washes were combined to obtain the cytoplasmic fraction and both fractions were processed for immunoblot analysis (as above).

Flow Cytometry, BrdU assay, proliferation assay

Cells treated with siRNAs for 48-72 hours were exposed to 1-5 μg/ml nocodazole for 12h, removed from plates, and fixed in ethanol. Cells stained with propidium iodide were analyzed by flow cytometry (FACSCAN, Becton Dickinson) using FlowJo software (Tree Star, Inc.). BrdU labeling was performed essentially as described[52]. Cells were incubated with 10 μM BrdU for 16-24h before fixation in 4% formaldehyde for 2 min and post-fixation in 100% methanol. Generational tracking of cell populations by flow cytometry was accomplished by labeling cellular proteins with 2 μM carboxyfluoroscein diacetate, succinimidyl ester (CFDA-SE, Molecular Probes) for 5 min according to manufacturers specifications, so that each cell division results in halving of the total cellular fluorescence.

Centrosome duplication, primary cilia formation and quantification of centrosome defects

After 24h of siRNA-mediated depletion of centrosome proteins, U2OS cells were blocked in S-phase by incubation in hydroxyurea-containing growth media (4mM) for an additional 40h prior to fixation in 100% ice-cold methanol. To unambiguously identify centrioles in interphase, cells were pre-treated with nocodazole (5 μg/mL) for 2h or incubated on ice for 30 min to depolymerize microtubules before fixation. Centrioles from untreated U2OS cells in interphase and mitosis were also counted. The indicated antibodies were used to detect centrosomes and centrioles. Primary cilia were detected as described using GT335 antibody[28]. Briefly, cells were retransfected 48 h after the first siRNA transfection using Oligofectamine. At 72h, primary cilia were induced by culturing RPE1 cells in medium with 0.25% serum for 48h. For quantifying centrosome defects (Fig. 4a), three categories of centrosome defects were an analyzed (structure, separation, loss). For each depleted centrosome protein, the assay showing the largest difference compared to control was plotted as the fold difference and compared with ninein.

1. Doxsey, S., Zimmerman, W. & Mikule, K. Centrosome control of the cell cycle. *Trends Cell Biol* **15**, 303-11 (2005).

2. Hinchcliffe, E. H. & Sluder, G. "It takes two to tango": understanding how centrosome duplication is regulated throughout the cell cycle. *Genes Dev* **15**, 1167-81 (2001).

3. Lacey, K. R., Jackson, P. K. & Stearns, T. Cyclin-dependent kinase control of centrosome duplication. *Proc Natl Acad Sci U S A* **96**, 2817-22 (1999).

4. Pihan, G. A. et al. Centrosome defects and genetic instability in malignant tumors. *Cancer Res* **58**, 3974-85. (1998).

5. Nigg, E. A. Centrosome aberrations: cause or consequence of cancer progression? *Nat Rev Cancer* **2**, 815-25 (2002).

6. Khodjakov, A. & Rieder, C. L. Centrosomes enhance the fidelity of cytokinesis in vertebrates and are required for cell cycle progression. *J Cell Biol* **153**, 237-42 (2001).

7. Hinchcliffe, E. H., Miller, F. J., Cham, M., Khodjakov, A. & Sluder, G. Requirement of a centrosomal activity for cell cycle progression through G1 into S phase. *Science* **291**, 1547-50. (2001).

8. Keryer, G. et al. Dissociating the centrosomal matrix protein AKAP450 from centrioles impairs centriole duplication and cell cycle progression. *Mol Biol Cell* **14**, 2436-46 (2003).

9. Gromley, A. et al. A novel human protein of the maternal centriole is required for the final stages of cytokinesis and entry into S phase. *Journal of Cell Biology* **161**, 535-45 (2003).

10. Wong, C. & Stearns, T. Mammalian cells lack checkpoints for tetraploidy, aberrant centrosome number, and cytokinesis failure. *BMC Cell Biol* **6**, 6 (2005).

11. Uetake, Y. & Sluder, G. Cell cycle progression after cleavage failure: mammalian somatic cells do not possess a "tetraploidy checkpoint". *J Cell Biol* **165**, 609-15 (2004).

12. Kramer, A. et al. Centrosome-associated Chk1 prevents premature activation of cyclin-B-Cdk1 kinase. *Nat Cell Biol* (2004).

13. Matsumoto, Y. & Maller, J. L. A centrosomal localization signal in cyclin E required for Cdk2-independent S phase entry. *Science* **306**, 885-8 (2004).

14. Gerdes, J. et al. Cell cycle analysis of a cell proliferation-associated human nuclear antigen defined by the monoclonal antibody Ki-67. *J Immunol* **133**, 1710-5. (1984).

15. Hong, Y. R., Chen, C. H., Chuo, M. H., Liou, S. Y. & Howng, S. L. Genomic organization and molecular characterization of the human ninein gene. *Biochem Biophys Res Commun* **279**, 989-95. (2000).

16. Gillingham, A. K. & Munro, S. The PACT domain, a conserved centrosomal targeting motif in the coiled-coil proteins AKAP450 and pericentrin. *EMBO Rep* **1**, 524-9 (2000).

17. Balczon, R., Simerly, C., Takahashi, D. & Schatten, G. Arrest of cell cycle progression during first interphase in murine zygotes microinjected with anti-PCM-1 antibodies. *Cell Motility & the Cytoskeleton* **52**, 183-92 (2002).

18. Gromley, A. et al. Centriolin anchoring of exocyst and SNARE complexes at the midbody is required for secretory-vesicle-mediated abscission. *Cell* **123**, 75-87 (2005).

19. Bronner-Fraser, M. Alterations in neural crest migration by a monoclonal antibody that affects cell adhesion. *J Cell Biol* **101**, 610-7 (1985).

20. Nose, A. & Takeichi, M. A novel cadherin cell adhesion molecule: its expression patterns associated with implantation and organogenesis of mouse embryos. *J Cell Biol* **103**, 2649-58 (1986).

21. Sherr, C. J. & Roberts, J. M. CDK inhibitors: positive and negative regulators of G1-phase progression. *Genes Dev* **13**, 1501-12 (1999).

22. La Terra, S. et al. The de novo centriole assembly pathway in HeLa cells: cell cycle progression and centriole assembly/maturation. *J Cell Biol* **168**, 713-22 (2005).

23. Kirkham, M., Muller-Reichert, T., Oegema, K., Grill, S. & Hyman, A. A. SAS-4 is a C. elegans centriolar protein that controls centrosome size. *Cell* **112**, 575-87 (2003).

24. Leidel, S. & Gonczy, P. SAS-4 is essential for centrosome duplication in C elegans and is recruited to daughter centrioles once per cell cycle. *Developmental Cell* **4**, 431-9 (2003).

25. Salisbury, J. L., Suino, K. M., Busby, R. & Springett, M. Centrin-2 is required for centriole duplication in mammalian cells. *Curr Biol* **12**, 1287-92 (2002).

26. Bettencourt-Dias M, R.-M. A., Carpenter L, Riparbelli M, Lehmann L, Gatt MK, Carmo N, Balloux F, Callaini G, Glover DM. SAK/PLK4 Is Required for

Centriole Duplication and Flagella Development. *Curr Biol* **15** (24), 2199-207. (2005).

27. Balczon, R. et al. Dissociation of centrosome replication events from cycles of DNA synthesis and mitotic division in hydroxyurea-arrested Chinese hamster ovary cells. *Journal of Cell Biology* **130**, 105-15 (1995).

28. Jurczyk, A. et al. Pericentrin forms a complex with intraflagellar transport proteins and polycystin-2 and is required for primary cilia assembly. *Journal of Cell Biology* **166**, 637-43 (2004).

29. Pazour, G. J. & Witman, G. B. The vertebrate primary cilium is a sensory organelle. *Curr Opin Cell Biol* **15**, 105-10 (2003).

30. Rubbi, C. P. & Milner, J. Disruption of the nucleolus mediates stabilization of p53 in response to DNA damage and other stresses. *Embo J* **22**, 6068-77 (2003).

31. Appella, E. & Anderson, C. W. Post-translational modifications and activation of p53 by genotoxic stresses. *Eur J Biochem* **268**, 2764-72 (2001).

32. Zhan, Q., Carrier, F. & Fornace, A. J., Jr. Induction of cellular p53 activity by DNA-damaging agents and growth arrest. *Mol Cell Biol* **13**, 4242-50 (1993).

33. Wang, B., Matsuoka, S., Carpenter, P. B. & Elledge, S. J. 53BP1, a mediator of the DNA damage checkpoint. *Science* **298**, 1435-8 (2002).

34. Wu, G. S. The functional interactions between the p53 and MAPK signaling pathways. *Cancer Biol Ther* **3**, 156-61 (2004).

35. Yee, A. S. et al. The HBP1 transcriptional repressor and the p38 MAP kinase: unlikely partners in G1 regulation and tumor suppression. *Gene* **336**, 1-13 (2004).

36. Kishi, H. et al. Osmotic shock induces G1 arrest through p53 phosphorylation at Ser33 by activated p38MAPK without phosphorylation at Ser15 and Ser20. *J Biol Chem* **276**, 39115-22 (2001).

37. Lee, J. C. et al. A protein kinase involved in the regulation of inflammatory cytokine biosynthesis. *Nature* **372**, 739-46 (1994).

38. Harper, J. W., Adami, G. R., Wei, N., Keyomarsi, K. & Elledge, S. J. The p21 Cdk-interacting protein Cip1 is a potent inhibitor of G1 cyclin-dependent kinases. *Cell* **75**, 805-16 (1993).

39. el-Deiry, W. S. et al. WAF1, a potential mediator of p53 tumor suppression. *Cell* **75**, 817-25 (1993).

40. Dutcher, S. K. Elucidation of basal body and centriole functions in Chlamydomonas reinhardtii. *Traffic* **4**, 443-51 (2003).

41. Leidel, S., Delattre, M., Cerutti, L., Baumer, K. & Gonczy, P. SAS-6 defines a protein family required for centrosome duplication in C. elegans and in human cells. *Nature Cell Biology* **7**, 115-25 (2005).

42. Habedanck, R., Stierhof, Y. D., Wilkinson, C. J. & Nigg, E. A. The Polo kinase Plk4 functions in centriole duplication. *Nat Cell Biol* **7**, 1140-6 (2005).

43. Pihan, G. A. et al. Centrosome defects can account for cellular and genetic changes that characterize prostate cancer progression. *Cancer Res* **61**, 2212-9 (2001).

44. Grieshaber, S. S., Grieshaber, N. A., Miller, N. & Hackstadt, T. Chlamydia trachomatis causes centrosomal defects resulting in chromosomal segregation abnormalities. *Traffic* **7**, 940-9 (2006).

45. Ploubidou, A. et al. Vaccinia virus infection disrupts microtubule organization and centrosome function. *Embo J* **19**, 3932-44 (2000).

46. Jouvenet, N. & Wileman, T. African swine fever virus infection disrupts centrosome assembly and function. *J Gen Virol* **86**, 589-94 (2005).

47. Vidair, C. A., Doxsey, S. J. & Dewey, W. C. Thermotolerant cells possess an enhanced capacity to repair heat-induced alterations to centrosome structure and function. *Journal of Cellular Physiology* **163**, 194-203 (1995).

48. Tuffanelli, D. L., McKeon, F., Kleinsmith, D. M., Burnham, T. K. & Kirschner, M. Anticentromere and anticentriole antibodies in the scleroderma spectrum. *Arch Dermatol* **119**, 560-6 (1983).

49. Berthet, C., Aleem, E., Coppola, V., Tessarollo, L. & Kaldis, P. Cdk2 knockout mice are viable. *Curr Biol* **13**, 1775-85 (2003).

50. Morales, C. P. et al. Absence of cancer-associated changes in human fibroblasts immortalized with telomerase. *Nat Genet* **21**, 115-8 (1999).

51. Gromley, A. et al. A novel human protein of the maternal centriole is required for the final stages of cytokinesis and entry into S phase. *J Cell Biol* **161**, 535-45 (2003).

52. Kennedy, B. K., Barbie, D. A., Classon, M., Dyson, N. & Harlow, E. Nuclear organization of DNA replication in primary mammalian cells. *Genes Dev* **14**, 2855-68 (2000).

Acknowledgements

We thank Bill Theurkauf, Kip Sluder, Chuck Sherr and Courtney Havens for useful discussions on this work. This work was supported by funding from the National Institutes of Health (GM51994) to SJD and the Department of Defense to KM (DMAD17-03-1-0303) and AJ (DAMD17-03-1-056). The National Cancer Institute (PK) also supported this work.

Competing interest statement

The authors declare that they have no competing financial interests.

Figure legends

Figure 1 siRNA-mediated centrosome protein depletion triggers G_1 arrest. **a**, Semi-quantitative pixel intensity profiles of centrosomes produced from optically sectioned (Z-axis) fluorescence images show depletion of centrosomal PCM1 (inset, enlarged pixel intensity profile of centrosome). Profiles for other proteins in Supplementary Fig. 1. **b**, BrdU incorporation (16h pulse) in siRNA-treated (72 hour) cells, as indicated. **c,** Immunoflorescence images showing that Ki-67 staining is not present in nuclei of most GCP2 siRNA-treated cells (72h) but is present in cycling control cells (lamin). **d**, Flow cytometry profiles of cells treated with indicated siRNAs for 72h, and with nocodazole (+ noc) or DMSO (- noc) for the final 12h. Profiles representative of three experiments, >5000 cells/profile.

Figure 2 G_1 arrest can specifically be suppressed by overexpression of the target protein. **a,** Western blots from RPE and RPE/ GFP-Cetn2 cells treated with siRNAs as indicated and probed with centrin antibody (20H5) to show endogenous (middle panel) and overexpressed (upper panel) centrin. lamin, control. Cetn2 UTR siRNA targets only endogenous Cetn2, Cetn2 siRNA targets both endogenous Cetn2 and GFP-Cetn2. γ tubulin staining demonstrates equivalent loading conditions (lower panel). **b,** Immunofluorescence images taken from siRNA-treated RPE cells (72h, left column) show reduced level of endogenous Cetn2 protein (green) at the centrosome with both Cetn2 UTR siRNA and Cetn2 siRNA, when compared to normal levels obtained with lamin siRNA (insets, enlargements of indicated centrosomes). Immunofluorescence images taken from siRNA-treated RPE overexpressing GFP-Cetn2 (right columns) show reduced level of overexpressed GFP-Cetn2 at the centrosome with Cetn2 siRNA but not with Cetn2 UTR siRNA. Enlargements of centrosomes (right) from an overexpressing cell (ov, top inset from each picture) and a non overexpressing cell in the same field (E, endogenous, bottom inset). γ tubulin, centrosome marker (red). **c,** Quantification of BrdU incorporation (16h pulse) in siRNA-treated RPE and RPE overepressing GFP-Cetn2. Representative of 3 independent experiments.

Figure 3 G_1 arrest can be induced from within G_1, occurs in late G_1 with reduced Cdk2-cyclin A activity and is suppressed by deletion of the p21 gene. **a**, Cells microinjected in late telophase/early G_1 with plasmids encoding either the pericentrin C-terminus fused to RFP (Peri-CT1-RFP) or RFP alone, as indicated. BrdU was added at the time of injection and its incorporation was determined 24 hours later. Inset shows enlargement of the centrosome of a Peri-CT1-RFP expressing cell with no BrdU incorporation; nonexpressing cells in the same field incorporate BrdU. Quantification of these results shows that most Peri-CT1-RFP expressing cells do not incorporate BrdU. **b,** Cells accumulated in G_1/G_0 with low serum were loaded with a fluorescent probe that enables tracking of population doublings then treated with the indicated siRNAs to deplete proteins within G_1. Flow cytometry was performed on one set of samples prior to addition of siRNA to serve as a nondivided control population (green trace). Other samples were treated with indicated siRNAs for 72h and serum was added during the last 24 hours to induce cycling. Flow cytometry profiles show that a population of pericentrin siRNA-treated cells retain the original label showing they did not divide (left, red trace within green), whereas control cells divided at least once (blue trace). Graph (right) shows percentage of cells that failed to divide. All results are representative of three experiments. **c**, Cyclin A immunoprecipitations and cdk2 IP-kinase assays from cells treated with indicated siRNAs (left). Top panels, autoradiographs of histone H1 phosphorylation from cyclin A immunoprecipitations; bottom panels, immunoblots for cdk2. Results representative of three experiments. Graphs (right) show quantification of histone H1 phosphorylation by cdk2 after normalizing for cdk2 levels. Phosphorimager units (PI). ss=serum starved 0.25% serum. **d**, BrdU incorporation (16h pulse) in HCT116 and HCT116 p21 -/- cells as indicated following 60h siRNA-treatments as indicated.

Figure 4 G_1 arrested cells show defects in centrosome structure/organization. **a,** Quantification of cells with defects in centrosome structure/organization following siRNA treatment of the indicated proteins (fold difference normalized to GFP and compared to ninein, see Materials and Methods for details) **b,** Immunofluorescence images of apparently incomplete centrosome-like structures that stain for centriole

markers (centrin, CETN and polyglutamylated tubulin, Glut-tub) but not for PCM markers (pericentrin, peri or γ tubulin) in RPE-1 cells stably expressing GFP-centrin2 and depleted of the indicated centrosome proteins. **c**, Correlative electron microscopy of incomplete centrosome-like structures in serial sections (i-v) seen by immunofluorescence (vi, arrows) and the two parent centrioles (arrowheads, daughter centriole: ii, iii, mother centriole: iv, v). Enlargement of box in v shows mother centriole (vii, center) and incomplete centrosome-like structures (above and below).

Figure 5 G_1 arrested cells exhibit defects in centrosome function. **a,** Immunofluorescence images of centrosomes in control (lamin siRNA, lam) and GCP3 depleted U2OS cells following treatment with hydroxyurea (48h) to induce S-phase arrest and supernumerary centrosomes. **b,** Graph shows numbers of centrosomes (grey) and centrioles (black) in hydroxyurea-treated U2OS cells following siRNA treatment (64h) of the indicated proteins. Overduplication, > 2 γ tubulin dots (centrosome), > 4 centrin dots (centrioles). n=200 cells/ bar. **b**, Immunofluorescence images (top) and quantification (bottom) of primary cilia assembly in cells depleted of the indicated proteins. Cells were stained with an antibody to polyglutamylated tubulin (Glut tub) and γ tubulin (γ tub). Adjacent insets show staining for Glut tub, left and γ tub, right. > 200 cells /bar, normalized to 100% in control (lamin), mean of 3 experiments ± standard deviation. Nin, ninein, cetn2, centrin, centrio, centriolin.

Figure 6 G_1 arrest induced by centrosome protein depletion is p53-dependent. **a**, Immunofluorescence images (left) showing nuclear accumulation of p53 in GCP2 siRNA-treated cells but not controls. Immunoblots (right) of cytoplasmic (cytopl) and nuclear (nuc) extracts of siRNA-treated cells showing p53 nuclear accumulation after pericentrin siRNA treatment but not after lamin siRNA treatment. Histone H1 (H1), loading control. **b**, Immunofluorescence images and quantification of BrdU incorporation (16 h pulse) in siRNA-treated cultures (60 h) of HCT116 p53 -/- cells; compare images with control HCT 116 wild type cells in Fig. 3d. **c,** Immunoblot from p53 siRNA-treated and control cells (upper panels). Actin, control. Flow cytometry profiles (lower panel) of

asynchronous (-noc) and nocodazole-treated (+ noc, 12h) cells treated simultaneously with two siRNAs as indicated, >5000 cells/trace. Results representative of at least two experiments.

Figure 7 G_1 arrest induced by centrosome protein depletion is p38-dependent. **a,** Immunoblot showing phospho-ser33-p53, p53 and α tubulin (loading control) in cells treated with siRNAs. **b**, Flow cytometry profiles of inhibitor-treated cells and inhibitor-treated cells depleted of GCP3 collected in the absence or presence of nocodazole (noc-12h). Representative of three experiments, >5000 cells/trace. **c**,. Western blot showing depletion of p38 (upper left panel). Graph showing quantification of BrdU positive cells (bottom left, normalized to untreated) after depletion of pericentrin alone (peri), or in tandem with p38 (p38/peri). Results representative of three experiments. Immunofluorescence images (right) showing BrdU incorporation in cells depleted of p38 and GCP2 (p38/GCP2) or GCP2 alone.

Figure 8 The p38-activated form of p53 accumulates at the centrosome prior to G_1 arrest. **a,** Immunofluorescence images showing $p53^{P\text{-}ser33}$ concentrated at centrosomes in response to centrosome protein depletion (siRNA GCP2) 48h after siRNA but not control protein depletion (lamin). Kinetic experiment (times after release from serum starvation are indicated) show p53 concentration at centrosomes (4-24h) before the nuclear staining becomes prominent (24h). **b,** Immunofluorescence images showing phospho-p38 at the centrosome of a mitotic (top inset) and interphase cell (bottom inset).

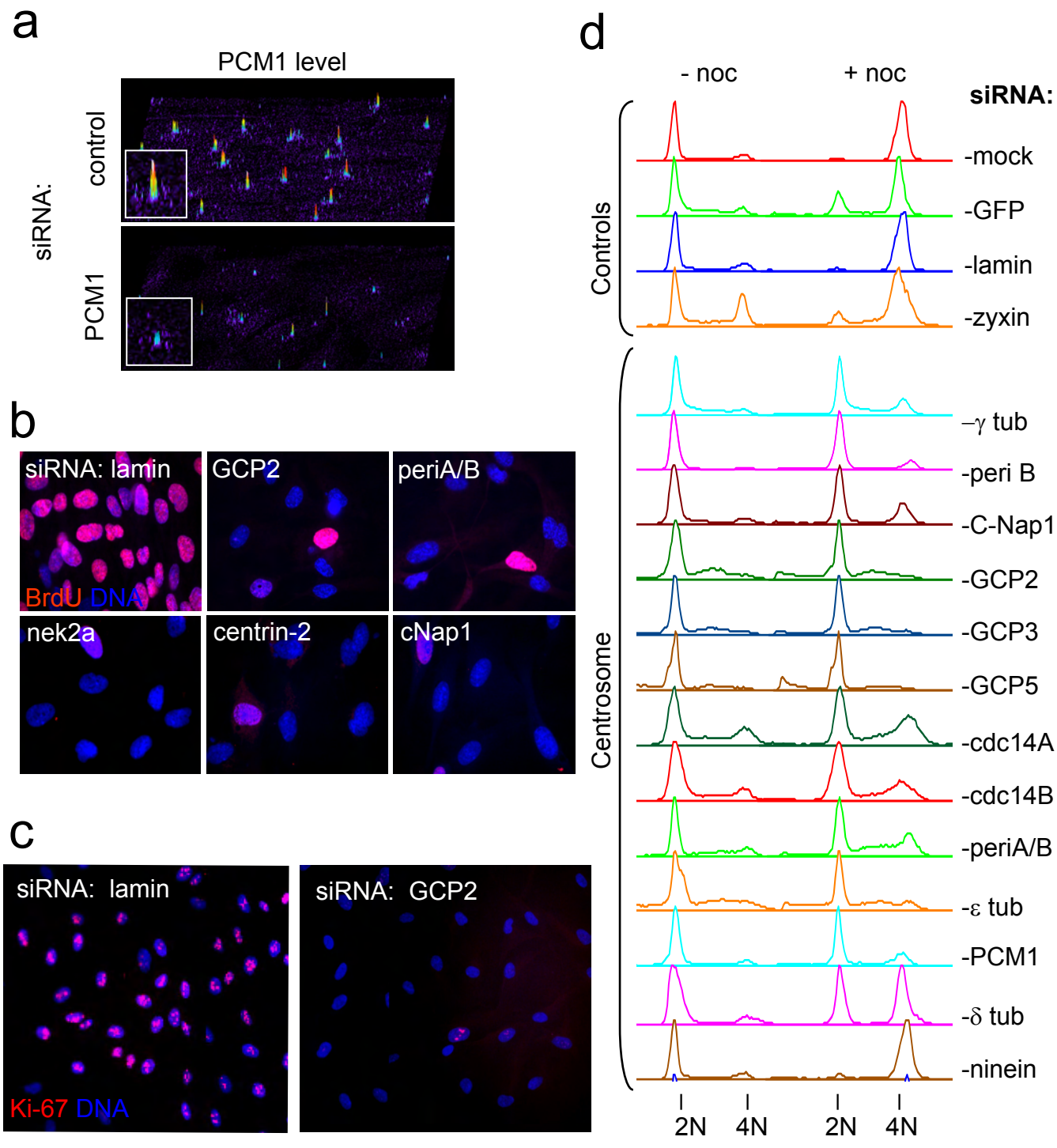
a
PCM1 level
siRNA:
control
PCM1
b
siRNA: lamin
GCP2
periA/B
BrdU DNA
nek2a
centrin-2
cNap1
c
siRNA: lamin
siRNA: GCP2
Ki-67 DNA
d
- noc
+ noc
siRNA:
Controls
-mock
-GFP
-lamin
-zyxin
Centrosome
–γ tub
-peri B
-C-Nap1
-GCP2
-GCP3
-GCP5
-cdc14A
-cdc14B
-periA/B
-ε tub
-PCM1
-δ tub
-ninein
2N
4N
2N
4N

Fig. 1

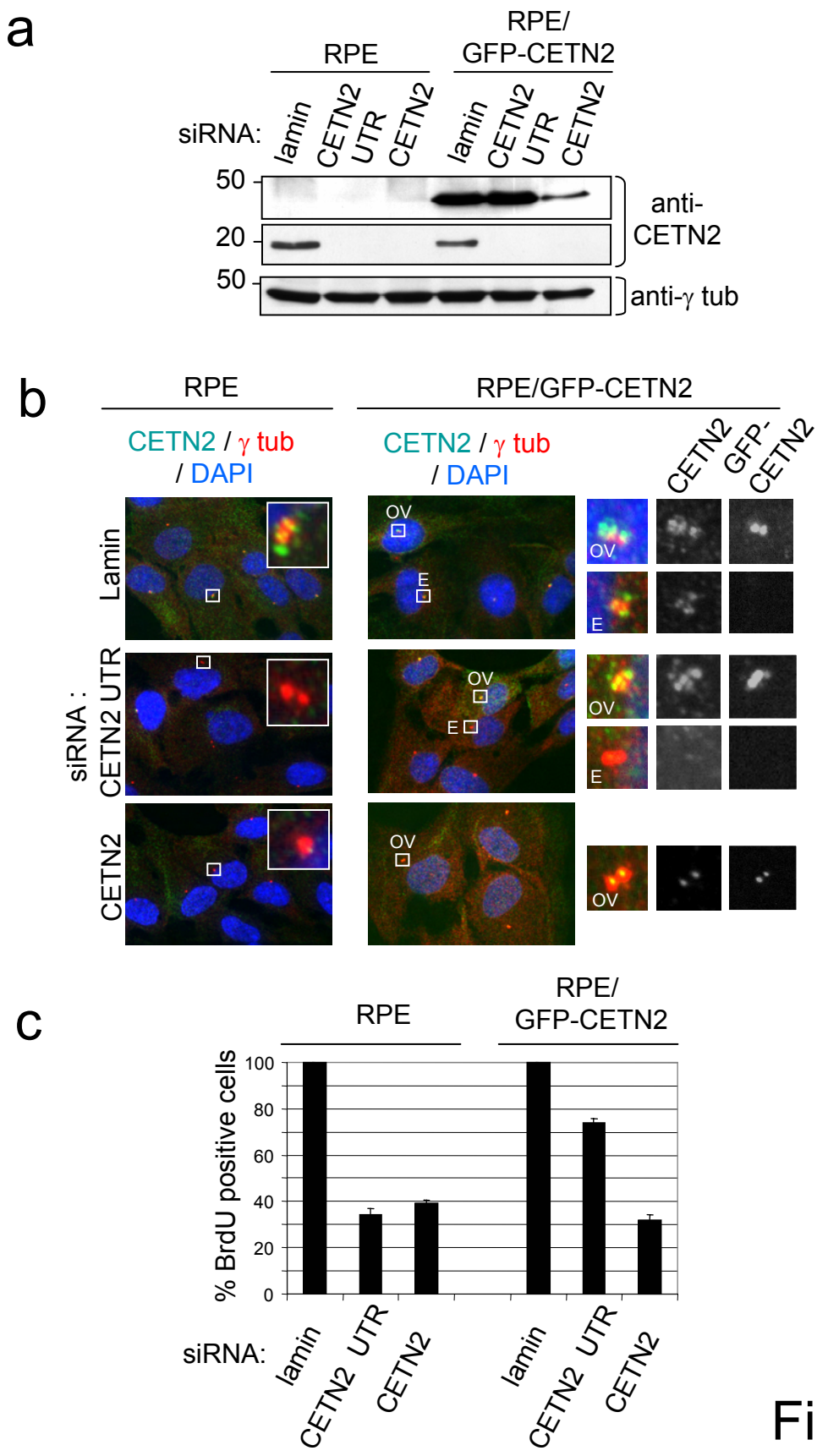
a
RPE
RPE/
GFP-CETN2
siRNA:
lamin
CETN2 UTR
CETN2
lamin
CETN2 UTR
CETN2
50
20
50
anti-
CETN2
anti-γ tub
b
RPE
RPE/GFP-CETN2
CETN2 / γ tub
/ DAPI
CETN2 / γ tub
/ DAPI
CETN2
GFP-
CETN2
Lamin
siRNA :
CETN2 UTR
CETN2
OV
E
c
RPE
RPE/
GFP-CETN2
% BrdU positive cells
100
80
60
40
20
0
siRNA:
lamin
CETN2 UTR
CETN2
lamin
CETN2 UTR
CETN2

Fig. 2

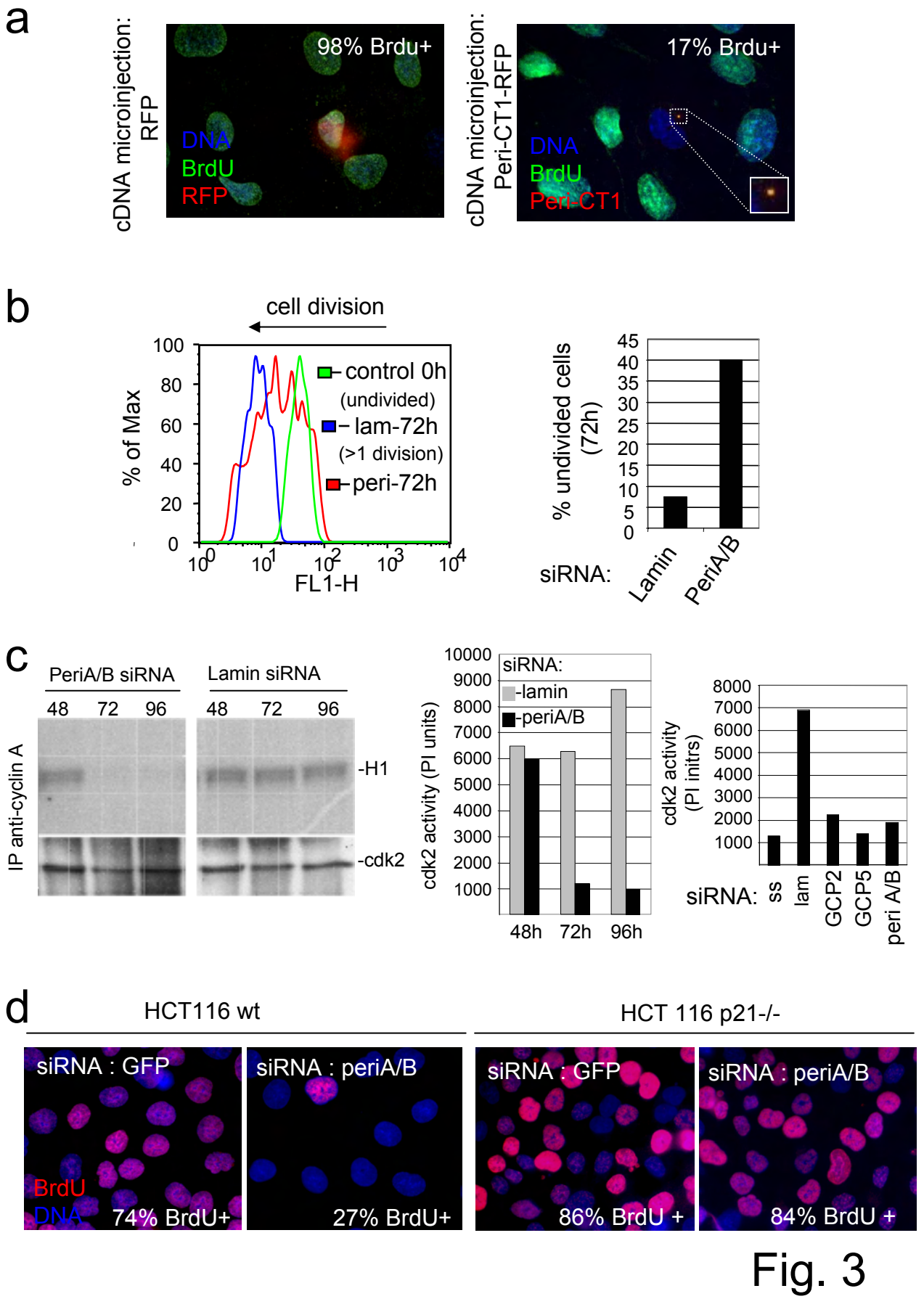
a
cDNA microinjection: RFP
98% Brdu+
DNA
BrdU
RFP
cDNA microinjection: Peri-CT1-RFP
17% Brdu+
DNA
BrdU
Peri-CT1
b
cell division
% of Max
control 0h
(undivided)
lam-72h
(>1 division)
peri-72h
FL1-H
% undivided cells (72h)
siRNA:
Lamin
PeriA/B
c
PeriA/B siRNA
Lamin siRNA
48 72 96
48 72 96
IP anti-cyclin A
-H1
-cdk2
cdk2 activity (PI units)
siRNA:
-lamin
-periA/B
48h 72h 96h
cdk2 activity (PI initrs)
siRNA: ss lam GCP2 GCP5 peri A/B
d
HCT116 wt
HCT 116 p21-/-
siRNA : GFP
BrdU
DNA
74% BrdU+
siRNA : periA/B
27% BrdU+
siRNA : GFP
86% BrdU +
siRNA : periA/B
84% BrdU +

Fig. 3

a

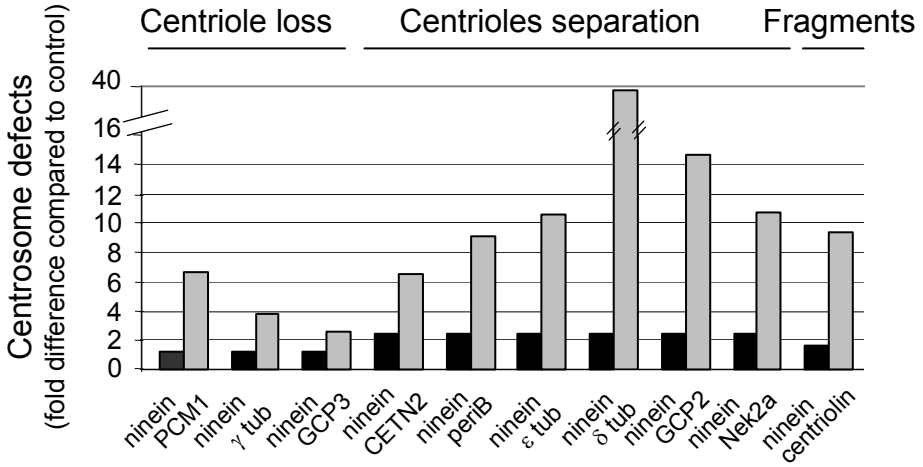
Centriole loss
Centrioles separation
Fragments
Centrosome defects
(fold difference compared to control)
40
16
14
12
10
8
6
4
2
0
ninein
PCM1
ninein
γ tub
ninein
GCP3
ninein
CETN2
ninein
periB
ninein
ε tub
ninein
δ tub
ninein
GCP2
ninein
Nek2a
ninein
centriolin

b

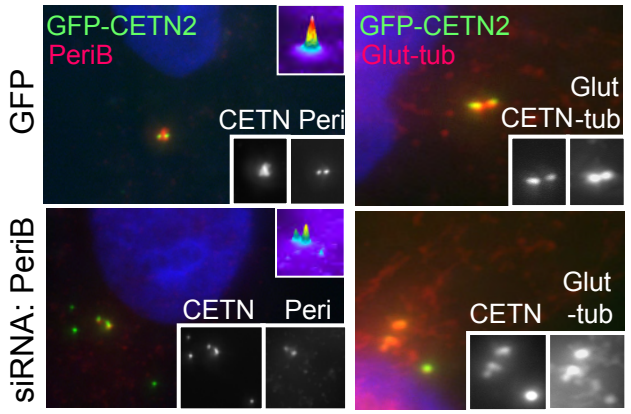
GFP
siRNA: PeriB
GFP-CETN2
PeriB
CETN Peri
GFP-CETN2
Glut-tub
Glut
CETN-tub
CETN
Peri
CETN
Glut
-tub

c

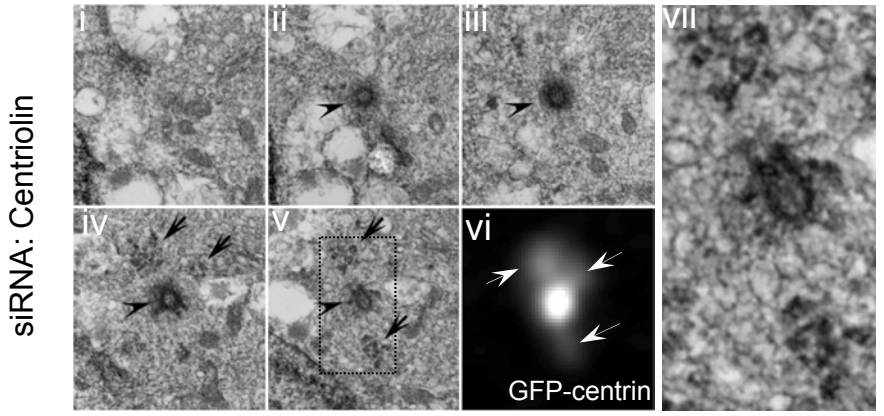
siRNA: Centriolin
i
ii
iii
vii
iv
v
vi
GFP-centrin

Fig. 4

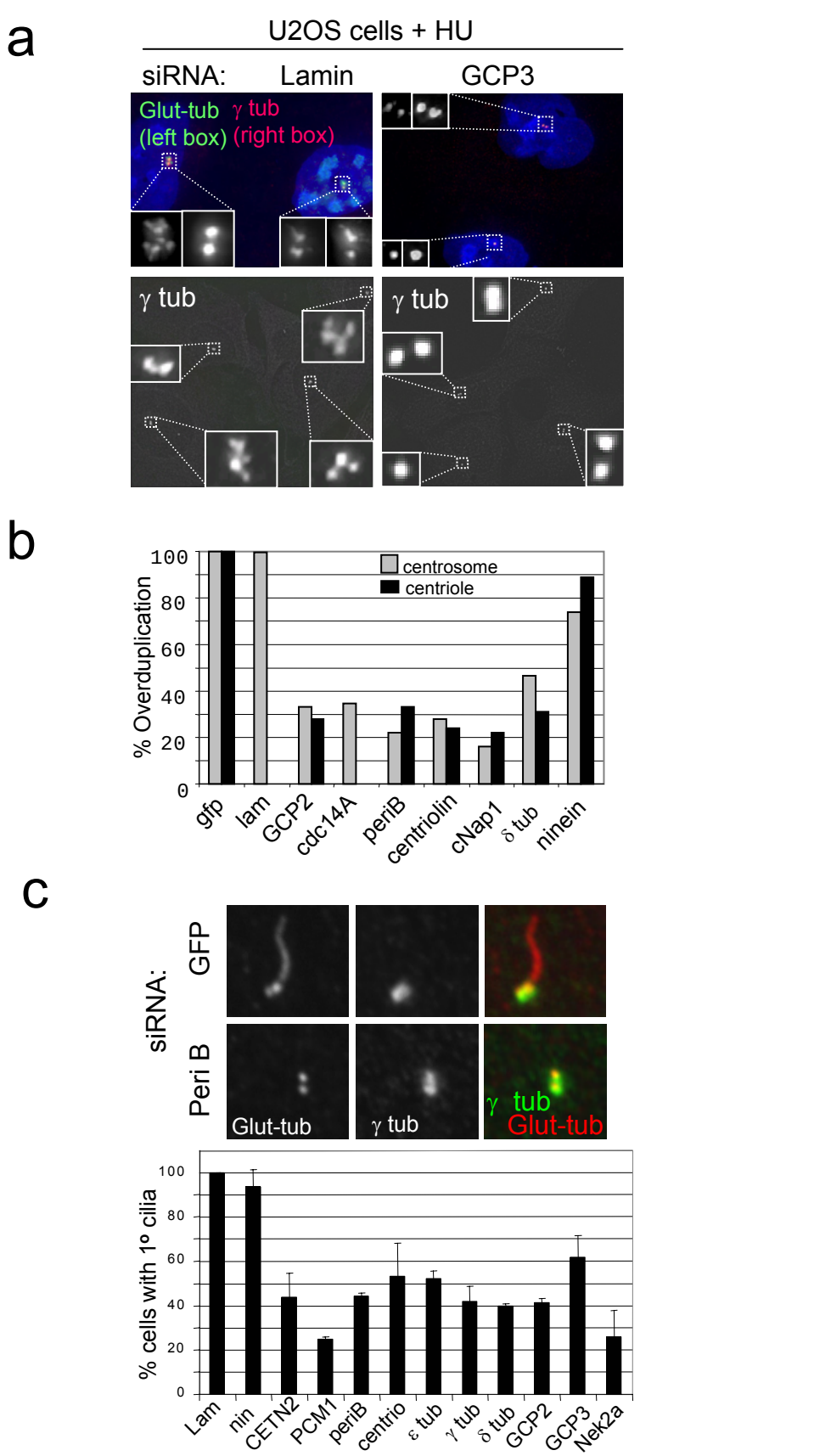
a
U2OS cells + HU
siRNA:
Lamin
GCP3
Glut-tub γ tub
(left box) (right box)
γ tub
γ tub
b
% Overduplication
100
80
60
40
20
0
centrosome
centriole
gfp
lam
GCP2
cdc14A
periB
centriolin
cNap1
δ tub
ninein
c
siRNA:
GFP
Peri B
Glut-tub
γ tub
γ tub
Glut-tub
% cells with 1° cilia
100
80
60
40
20
0
Lam
nin
CETN2
PCM1
periB
centrio
ε tub
γ tub
δ tub
GCP2
GCP3
Nek2a

Fig. 5

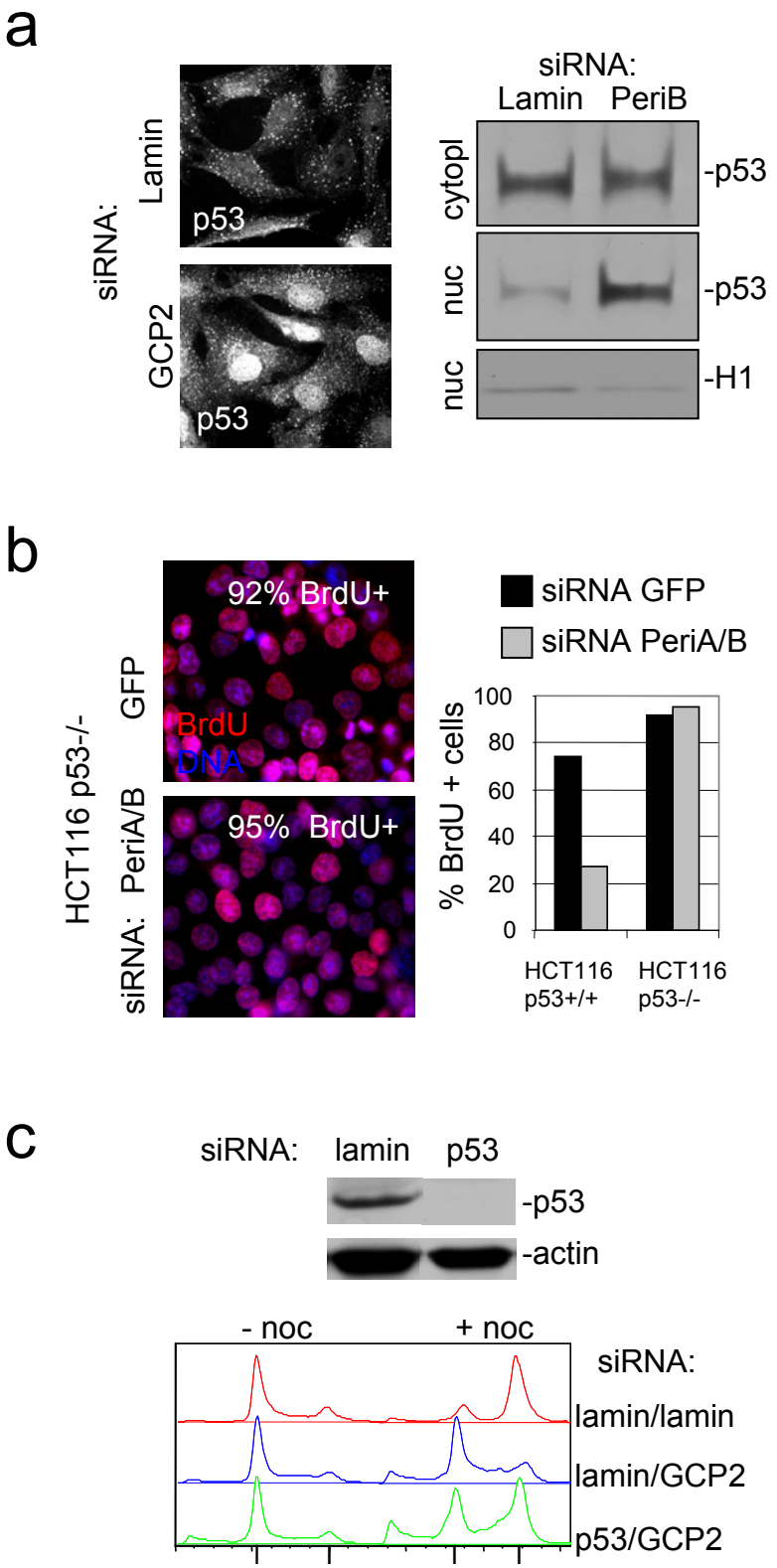
a
siRNA:
Lamin
p53
GCP2
p53
siRNA:
Lamin PeriB
cytopl
-p53
nuc
-p53
nuc
-H1
b
HCT116 p53-/-
siRNA:
GFP
PeriA/B
92% BrdU+
BrdU
DNA
95% BrdU+
siRNA GFP
siRNA PeriA/B
% BrdU + cells
100
80
60
40
20
0
HCT116 p53+/+
HCT116 p53-/-
c
siRNA: lamin p53
-p53
-actin
- noc
+ noc
siRNA:
lamin/lamin
lamin/GCP2
p53/GCP2
2N
4N
2N
4N

Fig. 6

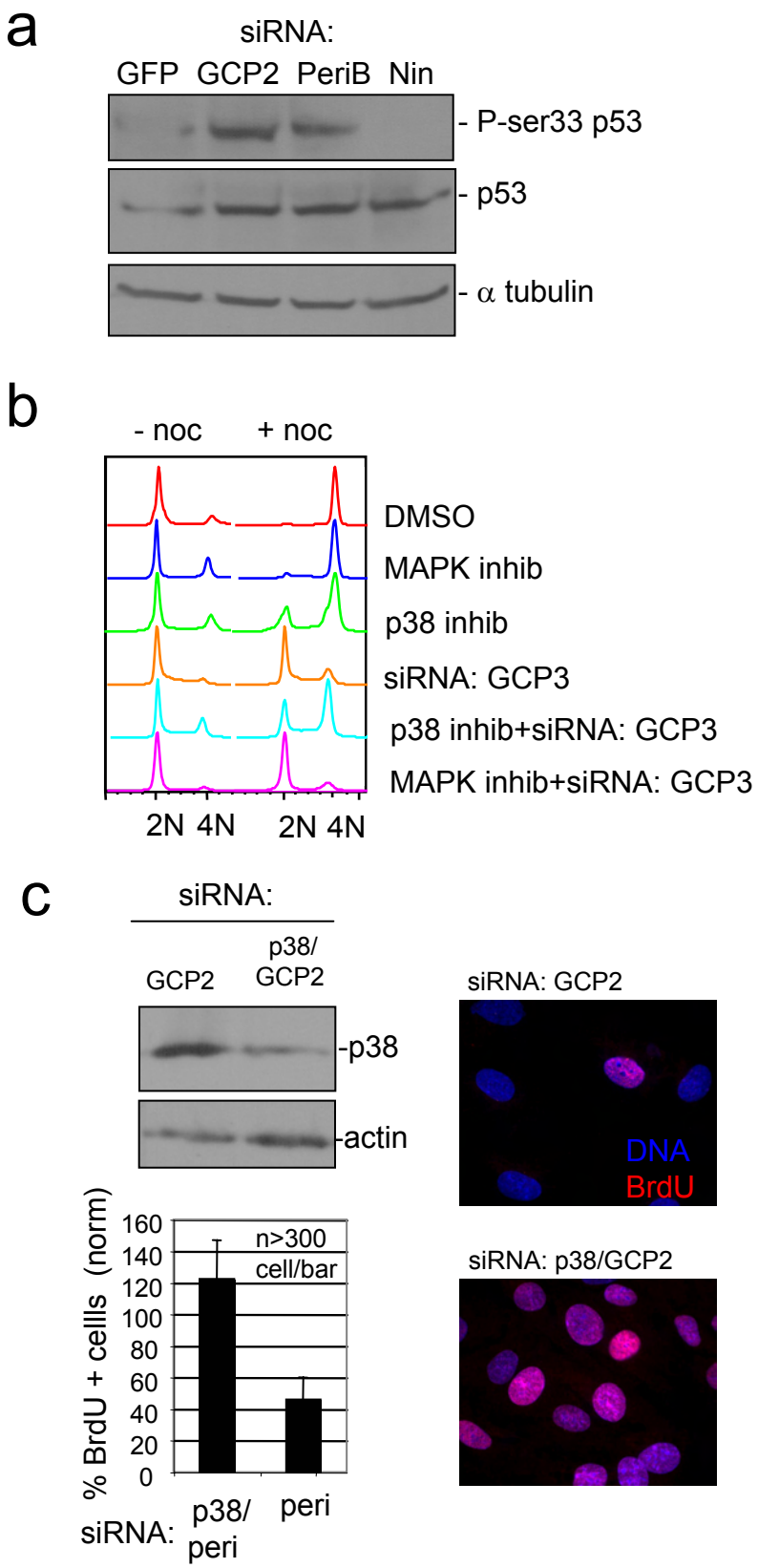
a
siRNA:
GFP GCP2 PeriB Nin
- P-ser33 p53
- p53
- α tubulin
b
- noc + noc
DMSO
MAPK inhib
p38 inhib
siRNA: GCP3
p38 inhib+siRNA: GCP3
MAPK inhib+siRNA: GCP3
2N 4N 2N 4N
c
siRNA:
GCP2
p38/ GCP2
-p38
-actin
% BrdU + cellls (norm)
160
140
120
100
80
60
40
20
0
n>300 cell/bar
siRNA: p38/ peri
peri
siRNA: GCP2
DNA
BrdU
siRNA: p38/GCP2

Fig. 7

a

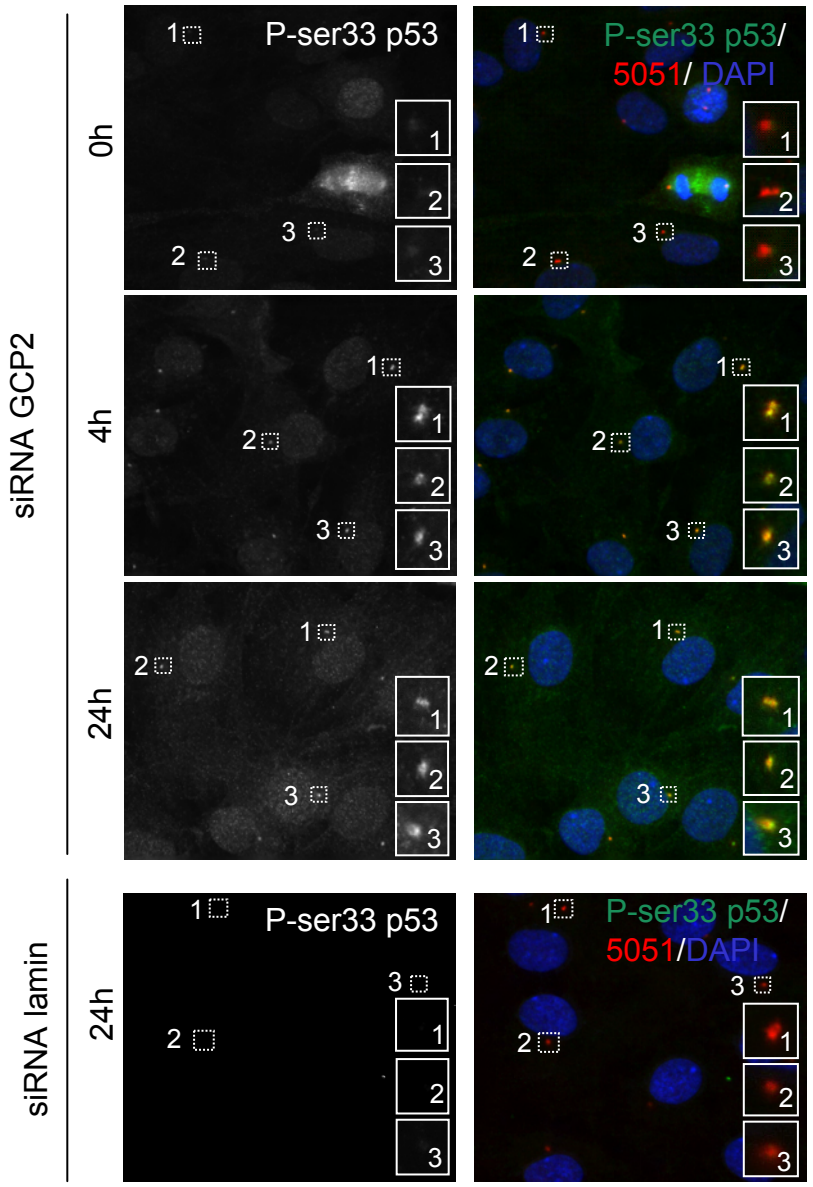
siRNA GCP2
0h
4h
24h
P-ser33 p53
P-ser33 p53/
5051/ DAPI
siRNA lamin
24h
P-ser33 p53
P-ser33 p53/
5051/DAPI

b

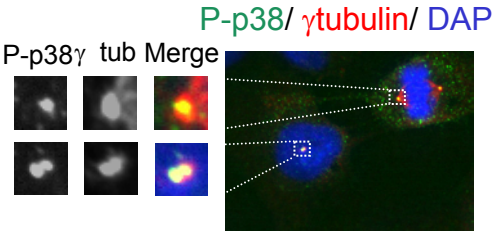
P-p38/ γtubulin/ DAPI
P-p38γ
tub
Merge

Fig. 8

Chromatin remodelling proteins interact with pericentrin and the centrosome to regulate centrosome integrity and spindle function

James Sillibourne* Manisha Singh,
Stephanie Mirabelle and Stephen Doxsey

Program in Molecular Medicine, University of Massachusetts, 373 Plantation Street, Worcester, MA 01605, USA.

* Current Address: Institut Curie, Section Recherche UMR 144 du CNRS, 26 rue d'Ulm, Paris 75248, France.

Running title: Chromatin remodeling proteins control spindle function

Abstract

Pericentrin is an integral centrosomal component that anchors both regulatory and structural molecules to this organelle. To identify novel interacting proteins a yeast two-hybrid screen was carried out using the C-terminus of pericentrin as bait. A cDNA encoding a C-terminal fragment of chromodomain helicase DNA-binding protein 4 (CHD4) or Mi2β was identified as a pericentrin-interacting protein. CHD4, and possibly another member of the CHD family, CHD3, form part of a seven member complex known as the nucleosome remodelling deacetylase (NuRD) complex. Other members of the NuRD include: histone deacetylase 1 and 2 (HDAC1/2), Rb-associated protein 46 and 48 (RbAp46/48), methyl-CpG-binding domain 3 (MBD3) and a metastasis-associated protein (MTA) subunit. Three members of the NuRD complex, CHD3, CHD4 and MTA2 were found to associate with pericentrin and, in addition, localize to the centrosome. Over-expression of the C-terminal domain of either CHD3 or CHD4 resulted in the rapid loss of both pericentrin and γ-tubulin from the centrosome, suggesting that these proteins are required for the anchoring of centrosomal components. Depletion of CHD3, but not CHD4, by small interfering RNA (siRNA) caused the loss of multiple components from the centrosome and disrupted bipolar spindle formation in mitotic cells. Time lapse imaging of HeLa cells, treated with CHD3 siRNA, showed that the majority of dividing cells failed early in mitosis, unable to segregate their chromatids and reattached to the substrate as mononucleate cells. Some cells successfully completed chromosome segregation, but failed later on in cytokinesis becoming binucleate. The data suggests that pericentrin is able to form a complex with both CHD3 and CHD4, but distinct complexes probably exist, with differing functions, and a CHD3-containing complex is essential for centrosome integrity.

Introduction

Centrosomes are the major microtubule organizing centers (MTOC) within the cell and play a pivotal role in regulating processes such as cell cycle progression, bipolar spindle formation and cytokinesis. A centrosome consists of a pair of centrioles surrounded by an array of proteins that form a lattice-like structure termed the pericentriolar matrix (PCM). Pericentrin localizes to the PCM and is responsible for anchoring both regulatory and structural proteins at the centrosome (Chen et al., 2004; Dictenberg et al., 1998; Diviani et al., 2000; Zimmerman et al., 2004). Recent work has shown that pericentrin interacts with components of the γ-tubulin small ring complex (γ-TuSC), is responsible for transporting the γ-TuSC to the centrosome and organizing the components into a lattice-like structure (Zimmerman et al., 2004). Pericentrin also binds the PKCβII and the regulatory subunit of PKA anchoring these kinases to the centrosome (Chen et al., 2004; Zimmerman et al., 2004).

Chromodomain helicase DNA-binding (CHD) proteins belong to a family of proteins that are related by the presence of two chromatin organization modifier domains (chromodomains) and a conserved ATPase helicase domain. This family contains at least six members that can be grouped into subfamilies, based on sequence homology, with CHD1 and CHD2 forming one subfamily, CHD3, CHD4 and CHD5 another and CHD6 the last (Woodage et al, 1997**;** Thompson et al., 2003). CHD1 and 2 differ from the other members of the family in that they contain a telobox-related DNA-binding within their C-termini; sequence comparison indicates that this domain is poorly conserved in other members of the family (Woodage et al, 1997).

CHD4 has been found in multiple complexes including the nucleosome remodelling deacetylase (NuRD) complex, an ATR-containing complex and a 2 MD complex involved in loading cohesin onto chromatin (Hakimi et al., 2002; Wade et al., 1998; Wang and Zhang, 2001; Zhang et al., 1998).

The NuRD complex contains, in addition to CHD4, histone deacetylases 1 and 2, retinoblastinoma associated proteins 46 and 48 (RbAp46/48), methyl-CpG-binding domain-containing protein 3 (MBD3) and a metastasis associated protein (MTA) subunit. At least four MTA isoforms, encoded by three different genes, have been identified MTA1, MTA2, MTA3 and MTA3L. It has been shown that the NuRD is able to remodel nucleosomes in an ATP-dependent manner and that this activity is required to allow HDAC1/2 to have access to histone acetyl-lysine residues and deacetylate them (Wang and Zhang, 2001). A NuRD complex containing MTA3, but neither MTA1 nor MTA2, has recently been identified that indirectly regulates E-cadherin gene expression, suggesting that MTA subunits may confer targeting specificity to the complex (Fujita et al., 2004).

A CHD4 complex containing ATR and HDAC1/2 has been purified from HeLa cell lysates using antibody affinity columns. Although the function of this complex within the cell has not elucidated, it has been suggested that it may play a role in the DNA damage response and silence genes regulating cell cycle progression (Schmidt and Schreiber, 1999).

The third CHD4 complex to be identified contains structural maintenance of chromosomes proteins 1 and 3 (SMC1 and SMC3), Scc1 and Scc3, as well as other NuRD components. This complex is involved in the loading of cohesin onto Alu repeat sequences.

It has been previously reported that MBD3, HDAC1 and CHD4 localize to the centrosome during the metaphase stage of mitosis. In this paper we show that CHD3 and CHD4 localize to the centrosome and are novel pericentrin-interacting proteins. Data is also presented showing that the depletion of CHD3 disrupts the integrity of the centrosome. Loss of CHD3, by treating cells with siRNA, displaced multiple components from the centrosome and induced defects during mitotic spindle formation and cytokinesis.

MATERIALS AND METHODS

Yeast Two-Hybrid Screen

The yeast strain AH109 was transformed with a GAL4 DNA-binding domain fusion vector, pGBKT7 (Clontech), containing residues 1340-1756 of murine pericentrin. After determining that the GAL4 DBD/pericentrin fusion failed to auto-transactivate the reporter genes, a 50 ml culture was grown overnight and then mated with the yeast strain Y187, which had been pre-transformed with a human testes cDNA library (Clontech). Diploid clones were plated out onto to synthetic defined medium lacking leucine, tryptophan, histidine and adenine to select for positive interactants.

cDNA clones, cloning techniques and expression constructs

Complementary DNAs (cDNAs) encoding CHD3, CHD4 and pericentrin were obtained from the following sources: CHD3 C-terminal sequence from IMAGE clone 642405 (IMAGE consortium); CHD4 human testis cDNA library described above; pericentrin as described before. Sequences encoding pericentrin, CHD3 and CHD4 were amplified by PCR using Pfu Turbo DNA polymerase (Stratagene), cloned into a donor vector of the Creator system (Clontech) and sequenced to verify the fidelity of the amplifying enzyme (Applied Biosystems). Coding sequences were transferred, by Cre-mediated recombination, into a range of expression vectors that included pLP-GBK-T7 (Clontech), pLP-CMV-myc (Clontech) and an existing FLAG-tagged vector that was converted for use with the system. The recombination protocol was as follows: 200 ng of each vector (donor and acceptor) were incubated at 37^{o}C for 1 hour in 1X Cre recombinase buffer with 1 unit of Cre recombinase (NEB), the enzyme was then heat inactivated at 70^{o}C for 5 min and the reaction allowed to slowly cool to room temperature.

Cell Culture and transfection

COS and HeLa cells were cultured in DMEM supplemented with L-glutamine and 10% foetal calf serum whereas, retinal pigment epithelial (RPE-1) cells (Clontech) were cultured in DMEM-F12 supplemented with L-glutamine, sodium bicarbonate and 10% foetal calf serum (Invitrogen). Cells were transfected either with Lipofectamine (Invitrogen) or by calcium phosphate precipitation. COS were transiently transfected with 5 μg of DNA using lipofectamine plus reagent (Invitrogen) according to the protocol provided by the manufacturer. Cells grown on coverslips were transiently transfected with 4 μg of DNA by calcium phosphate precipitation.

Antibodies

The following antibodies were used either for immunofluorescent staining or western blotting purposes: anti-RbAp46 (AbCam), anti-CHD3 (Orbigen), anti-CHD3 (gift from W. Wang) anti-CHD4 (Orbigen), anti-CHD3/4 and anti-MTA2 (gifts from P. Wade). Secondary antibodies for immunofluorescent staining were obtained from the following sources: anti-mouse alexa 488, anti-mouse AMCA and anti-rabbit alexa 488 (all from Molecular Probes); anti-mouse Cy3, anti-rabbit Cy3 and anti-human Cy5 (all from Jackson Immunochemicals). Horse radish perixoidase (HRP) linked anti-mouse and anti-rabbit secondary antibodies for western blotting purposes were obtained from Amersham.

Immunofluorescent staining

Cells were grown on 12 mm acid washed circular coverslips and fixed with either -20^{o}C methanol or 3.7% paraformaldehyde for 10 minutes at room temperature. Fixed cells were rehydrated by sequentially washing in PBS and then with a buffer consisting of PBS, 1% bovine serum albumin (BSA), 0.1% Triton X-100 (PBSA). Antibodies were diluted in PBSA, pipetted onto the surface of the coverslip and incubated at room temperature for 1 hour. The cells were washed with PBSA, secondary antibodies diluted

in the same buffer added and incubated for 30 minutes at room temperature. DNA was stained using DAPI (Sigma).

siRNA

The following duplexes were synthesized for the purpose of gene silencing: CHD3, AAGCGUGACAGUGAGGAGGAA and AAGGCCAUCGAUCGGUUUAAU; CHD4, AAGGAUGAUGAUGAUGAUGAU and AACAGUUACCAAGAAGACUUA ; MTA2, AACCGGUAUAUUCAGCAGAAA; lamin AACUGGACUUCCAGAAGAACA (Dharmacon). Cells were transiently transfected with siRNA at a final concentration of 200 nM using oligofectamine (Invitrogen) according to the protocol provided.

RESULTS and DISCUSSION

Identification of CHD3/4 as pericentrin-interacting proteins

A number of pericentrin-interacting proteins have been identified and include components of the γ-tubulin small complex (γ-TuSC) and the kinases PKA and PKCβII (Chen et al., 2004; Diviani et al., 2000; Zimmerman et al., 2004). To identify other pericentrin-interacting proteins a truncated C-terminal domain of the protein (residues 1340-1756) was used as bait in the yeast two-hybrid system to screen a human testis cDNA expression library. Several pericentrin-interacting clones were identified one of which encoded the C-terminal domain, residues 1577-1912, of CHD4 (Fig. 1A). This protein belongs to a family that contains at least 6 members, which are related by the presence of two chromodomains and a SWI/SNF helicase domain. To investigate the possibility that CHD3, a closely related member of the same family, might interact with pericentrin a cDNA clone was obtained from the IMAGE consortium and a sequence encoding residues 1566-1966 of CHD3 isoform 2 was cloned into a yeast two-hybrid expression vector. This fragment of CHD3 was tested and also found to interact, indicating that both the C-terminal domains of CHD3 and CHD4 have the ability to

associate with pericentrin. Deletion mapping of the pericentrin-binding site on CHD4 (supplemental figure 1) showed that amino acids 1687-1880 were required for this interaction; furthermore, sequence comparison shows that this domain is well conserved between CHD3 and CHD4 sharing 81% sequence identity and 92% similarity.

In order to determine if an interaction existed between the full length pericentrin and CHD4 proteins COS-7 cells were transiently co-transfected with HA-tagged-pericentrin and FLAG-tagged-CHD4 expression constructs and the tagged form of CHD4 immunoprecipitated with an anti-FLAG antibody. Western blotting with an anti-HA antibody showed that pericentrin specifically co-immunoprecipitated with the tagged form of CHD4 demonstrating that the full length proteins are able to interact (Fig. 1B). A second series of transient transfections were carried out where only a single FLAG-tagged protein, either pericentrin or CHD4, was expressed and immunoprecipitated and then western blotting performed, using antibodies specific to the endogenous forms of the corresponding partners. This demonstrated that endogenous forms of both CHD3 and CHD4 interacted with FLAG-tagged pericentrin (Fig. 1D). Similarly, endogenous pericentrin could be co-immunoprecipitated with FLAG-tagged CHD4 (Fig. 1C). To verify that the interaction between pericentrin and CHD3/4 was not an artifact caused by the over-expression of these proteins, endogenous CHD3 and CHD4 were immunoprecipitated from HeLa cells extracts. Western blotting detection demonstrated that pericentrin was present within the immunoprecipitate indicating that this protein forms a complex with endogenous CHD3/4 (Fig. 1E).

In order to determine if other components of the NuRD form a complex with pericentrin the FLAG tagged form of this protein was immunoprecipitated from transfected COS cell lysates and western blotting carried out. MTA2, RpAp46 and MBD3 were found to be present within the co-immunoprecipitated material suggesting that they are part of a

pericentrin/CHD3/4 complex (Fig. 1D). These results demonstrate a biochemical interaction between pericentrin and members of the NuRD complex.

NuRD components localize to the centrosome

A number of the components of the NuRD, including CHD3/4 (Mi2), MBD3 and HDAC1, have been found to localize to the centrosome during mitosis. Chadwick and Willard in their study of the localization of CHD3/4 used an antibody that recognized conserved domain and it was unclear, for this reason, whether the fraction of CHD3/4 at the centrosome was represented by one or both of these proteins. To address this issue and determine if other components of the NuRD localized to the centrosome RPE-1 cells were stained, by indirect immunofluorescence (IF), with antibodies specific for CHD3, CHD4, MTA2 or RpAp46 and a centrosomal marker (either γ-tubulin or the human autoimmune serum 5051). In interphase cells, all proteins, which were stained for, predominantly localized to the nucleus with a small pool of protein present within the cytoplasm. Surprisingly, a fraction of CHD3, CHD4 and MTA2 were found to colocalize with the centrosome markers used, indicating that these proteins localize to the centrosome during interphase (Fig. 2A, top 2 panels). During prophase CHD3/4 and MTA2 appear to be released from chromatin and become dispersed throughout the cytoplasm. Despite this large cytoplasmic pool of CHD3/4 and MTA2 a small fraction appeared to be enriched at the centrosome and remained present until metaphase (Fig. 2A, bottom 3 panels). After this point, a fraction of CHD3 remained associated with the centrosome, while the amount of CHD4 at this organelle appeared to decrease. Later on, in anaphase, CHD3/4 and MTA2 appeared to accumulate at the midbody, in a manner similar to that described for MBD3. In contrast to MTA2 and CHD3/4, RpAp46 did not localize to the centrosome during interphase and appeared to be enriched only upon the spindle during metaphase (Fig. 2A, bottom panels). Localization of CHD3,

CHD4 and MTA2 to centrosomes did not require microtubules suggesting that they were bona fide centrosome proteins (Fig. 2B).

The C-terminal domains of CHD3 and CHD4 displace pericentrin and other components from the centrosome

Data from the yeast two-hybrid system indicated that the C-terminal domains of pericentrin and CHD3/4 interacted. To ascertain if the C-terminal domains of CHD3 and CHD4 have some effect upon the function of the centrosome, cells were transiently transfected with myc-tagged versions of these domains and stained by indirect-immunofluorescence with antibodies against pericentrin and anti-myc. Both the C-terminal domains of CHD3 and CHD4 were distributed throughout the cytoplasm of the cell and excluded from the nucleus. This result can be simply explained as the nuclear localization sequences of CHD3 and CHD4 are contained within the N-termini and the over-expressed fragments lack these signal sequences. In a small number of transfected cells (4%) localization of over-expressed C-terminal fragment of CHD4 at the centrosome was observed (Fig. 3). Most cells expressing either CHD3 or CHD4 showed a reduction in pericentrin levels at the centrosome. Compare nontransfected control cell in lower right panel to all others in Figure 3 (see insets). These results demonstrate that CHD3/4 C-termini disrupt centrosome integrity.

Effect of silencing NuRD component genes on the centrosome

To determine if any of the components of the NuRD complex might play a role in regulating the activity of the centrosome, RNAi was used to silence the genes of CHD3 and CHD4. RPE-1 cells were treated with siRNA that specifically targeted CHD3 or CHD4 and were incubated for 72 hours. Western blotting showed depletion of all the

targeted proteins including lamin A/C (control), CHD3 and CHD4; pericentrin and α-tubulin levels appeared to be unaffected in CHD3 and CHD4 siRNA-treated cells (Fig. 4B). Immunofluorscence data showed that both CHD3 and CHD4 were lost from the centrosome and reduced in the nucleus when specifically targeted with siRNAs (Fig. 4A, 5). However, only the loss of CHD3 from the centrosome appeared to induce a concomitant decrease in the centrosomal proteins recognized by the human autoimmune serum 5051 and in pericentrin (Fig. 4A, 5A). No dramatic changes were observed in the levels of gamma tubulin at interphase centrosomes or in the levels of centrin-1 at centrioles (Fig. 5B). These results demonstrate that depletion of CHD3 but not CHD4 induces selective loss of pericentrin from centrosomes in interphase cells.

Silencing of CHD3 gene causes mitotic defects and cytokinesis failure

Immunofluorescence staining demonstrated that the silencing of the CHD3 gene caused mitotic defects. Cells treated with CHD3 siRNA predominantly showed a prometaphase-like configuration with chromsomes misaligned on the metaphase plate and aberrant bipolar spindles (Fig. 6A, C, supplementary Fig. 2). Microtubules within these spindles either appeared to be bundled together or fewer in number. In comparison this phenotype was rarely observed in CHD4 or lamin A/C siRNA-treated cells, although a slight increase in spindle defects was observed after CHD4 RNAi. A reduction in the amount of γ-tubulin at centrosomes during mitosis was observed in CHD3 siRNA-treated cells compared to CHD4 and lamin A/C-treated (Fig. 6B), suggesting that the effect on gamma tubulin was mitosis specific (see Fig. 5B and Zimmerman et al., 2004). We quantified mitotic stages in siRNA-treated cells (Fig. 6C). Spindle defects were grouped together to simplify the presentation of the results and included: lagging chromosomes monopolar-, tripolar- and half-spindles. CHD3 siRNA-treated cells predominantly exhibited a prometaphase-like phenotype (44% of mitotic cells versus undetectable

levels in controls) but an increase in spindle defects was also observed (15% versus 3-4%). CHD4 siRNA treated cells also showed a minor increase in prometaphase like cells and an increase in spindle defects, compared to the lamin A/C control. We conclude that CHD3 silencing severely disrupts mitotic spindle poles, spindle microtubule organization and chromosome segregation and that CHD4 has a similar but not as penetrant a phenotype. Currently, we do not know if this is due to a reduced involvement in mitosis or insufficient reduction in CHD4 protein levels.

The effect of gene silencing was further investigated by monitoring HeLa cells treated with siRNA against CHD3 by time-lapse imaging. Figure 7 shows still images from a movie that represents a 28 hour time period finishing 52 hours after the initial treatment with siRNA and shows that many cells fail in cell division. Cells treated with siRNA against CHD3 exhibited a metaphase delay, failure to segregate chromosomes and a failure to complete cytokinesis. Quantification of defects in cells treated with CHD3 siRNA and control (lamin) are shown in Fig. 7B and represent data from two experiments. The graph shows the time taken to complete nuclear envelope breakdown (NEB) to the end of metaphase transition in lamin A/C and CHD3 siRNA-treated HeLa cells. In other experiments we show that a total of 23/23 lamin siRNA treated cells progressed from NEB to metaphase with an average time of 38 minutes (range of 15-110 mins). In contrast, only 10/27 CHD3 siRNA-treated cells underwent division and took an average of 265 mins to complete the transition (range 40-435 mins); the other 17 cells failed division.

In summary, our results show that the CHD3 and CHD4 members of the NuRD complex bind the centrosome protein pericentrin. Both are involved in centrosome integrity and mitotic fidelity although CHD3 produces a more potent phenotype when depleted by

siRNAs. Pericentrin has recently been found in the nucleus and it will be interesting to determine if it is plays a role at this site (Keryer et al., 2003). It is interesting to note, that a cDNA encoding a protein that shares homology with the zinc finger transcription factor kaiso was identified as another pericentrin-interacting protein in the yeast two-hybrid screen. Kaiso belongs to a family of transcription factors that are involved in the repression of gene transcription. If this protein is a bona fide interacting protein, it would support the idea that pericentrin has a role in the nucleus, perhaps in regulating gene expression by associating with specific transcription factors and components of the NuRD complex or possibly a structural role.

ACKNOWLEDGEMENTS

This work was supported by the NIH/NCI (CA82834) and Depaartment of Defense (PC030931) to SJD. We thank Sambra Redick and Keith Mikule for careful reading of the manuscript.

REFERENCES

Chen, D., A. Purohit, E. Halilovic, S.J. Doxsey, and A.C. Newton. 2004. Centrosomal anchoring of protein kinase C betaII by pericentrin controls microtubule organization, spindle function, and cytokinesis. *J Biol Chem*. 279:4829-39.

Dictenberg, J.B., W. Zimmerman, C.A. Sparks, A. Young, C. Vidair, Y. Zheng, W. Carrington, F.S. Fay, and S.J. Doxsey. 1998. Pericentrin and gamma-tubulin form a protein complex and are organized into a novel lattice at the centrosome. *J Cell Biol*. 141:163-74.

Diviani, D., L.K. Langeberg, S.J. Doxsey, and J.D. Scott. 2000. Pericentrin anchors protein kinase A at the centrosome through a newly identified RII-binding domain. *Curr Biol*. 10:417-20.

Fujita, N., D.L. Jaye, C. Geigerman, A. Akyildiz, M.R. Mooney, J.M. Boss, and P.A. Wade. 2004. MTA3 and the Mi-2/NuRD complex regulate cell fate during B lymphocyte differentiation. *Cell*. 119:75-86.

Hakimi, M.A., D.A. Bochar, J.A. Schmiesing, Y. Dong, O.G. Barak, D.W. Speicher, K. Yokomori, and R. Shiekhattar. 2002. A chromatin remodelling complex that loads cohesin onto human chromosomes. *Nature*. 418:994-8.

Keryer, G., B. Di Fiore, C. Celati, K.F. Lechtreck, M. Mogensen, A. Delouvee, P. Lavia, M. Bornens, and A.M. Tassin. 2003. Part of Ran Is Associated with AKAP450 at the Centrosome: Involvement in Microtubule-organizing Activity. *Mol Biol Cell*. 14:4260-71.

Schmidt, D.R., and S.L. Schreiber. 1999. Molecular association between ATR and two components of the nucleosome remodeling and deacetylating complex, HDAC2 and CHD4. *Biochemistry*. 38:14711-7.

Thompson, P.M., T. Gotoh, M. Kok, P.S. White, and G.M. Brodeur. 2003. CHD5, a new member of the chromodomain gene family, is preferentially expressed in the nervous system. *Oncogene*. 22:1002-11.

Wade, P.A., P.L. Jones, D. Vermaak, and A.P. Wolffe. 1998. A multiple subunit Mi-2 histone deacetylase from Xenopus laevis cofractionates with an associated Snf2 superfamily ATPase. *Curr Biol*. 8:843-6.

Wang, H.B., and Y. Zhang. 2001. Mi2, an auto-antigen for dermatomyositis, is an ATP-dependent nucleosome remodeling factor. *Nucleic Acids Res*. 29:2517-21.

Zhang, Y., G. LeRoy, H.P. Seelig, W.S. Lane, and D. Reinberg. 1998. The dermatomyositis-specific autoantigen Mi2 is a component of a complex containing histone deacetylase and nucleosome remodeling activities. *Cell*. 95:279-89.

Zimmerman, W.C., J. Sillibourne, J. Rosa, and S.J. Doxsey. 2004. Mitosis-specific anchoring of {gamma} tubulin complexes by pericentrin controls spindle organization and mitotic entry. *Mol Biol Cell*.

Figure 1

Components of the NuRD interact with pericentrin.

A) An image of the yeast strain AH109, transformed with the C-terminus of either CHD3 (residues 1566-1966) or CHD4 (residues 1577-1912) and the C-terminus of pericentrin (residues 1340-1756), growing on selective media to demonstrate a positive interaction. No interaction could be detected between the C-termini of CHD3 and CHD4 and the GAL4 DNA-binding domain alone. The domain of pericentrin used in the study has previously been shown not to interact with gamma tubulin complex members (Zimmerman et al., 2004). **B**) COS cells were co-transfected with HA-pericentrin and FLAG-CHD4 expression constructs. Anti-FLAG or anti-GFP (nIgG) antibodies were used to immunoprecipitate (IP) FLAG-CHD4 (lower western blot) and an anti-HA-antibody was used to detect pericentrin and found to be present only when both proteins were co-expressed. **C**) Co-IP of endogenous pericentrin with FLAG-CHD4 from transfected COS cell lysates. **D**) Interaction between pericentrin and components of the NuRD: western blotting with antibodies against CHD3, CHD4, MTA2, RpAp46 and MBD3 was carried out to test for their ability to co-IP with FLAG-tagged pericentrin immunoprecipitated from transfected COS cell lysates. CHD3, CHD4 and MTA2 appeared to be present within the IP, indicating that these proteins associate with pericentrin, while the abundancy of RpAp46 and MBD3 was exceptionally low, suggesting that these proteins are either not present within the complex or associate only transiently. **E**) CHD3/4 were IP from HeLa cell lysates and western blotting for pericentrin carried out to demonstrate an interaction between the endogenous proteins.

Figure 2 Localization of NuRD components

A) RPE-1 cells were stained with antibodies against CHD3, CHD4, MTA2, RbAp46 (green) and a centrosomal marker, either γ-tubulin or the human autoimmune serum 5051 (red). In interphase cells all antibodies against the different NuRD components

gave a strong nuclear labeling, but in the case of CHD3, CHD4 and MTA2 a fraction of protein was found to co-localize with the centrosomal marker. Localization of RbAp46 at the centrosome was not observed in interphase cells. During the early stages of mitosis the NuRD components dissociated from the chromosomal DNA and dispersed throughout the cytoplasm. Later on the NuRD components appeared to accumulate on the central spindle and the midbody. CHD3 and MTA2 remained associated with the centrosome throughout mitosis while the amount of CHD4 at the centrosome appeared to decrease during the later stages of mitosis. In the case of RbAp46 enrichment upon the mitotic spindle was observed but the majority of the protein was dispersed throughout the cytoplasm. **B**) RPE-1 cells were treated with nocodazole for 90 minutes at 37^{o}C to depolymerize microtubules and then stained with antibodies against CHD3, CHD4, MTA2 and centrosomal marker. A fraction of CHD3, CHD4 and MTA2 were found to be present at the centrosome indicating that these proteins are stable components.

Figure 3 Over-expression of the C-termini of CHD3 and CHD3 cause centrosomal defects

HeLa cells were transiently transfected, by electroporation with myc-tag constructs expressing the C-terminus of either CHD3 or CHD4, plated out onto fibronectin/collagen-coated coverslips and 6 hrs later fixed in -20^{o}C methanol. IF staining with an anti-myc to detect the fusion proteins and an anti-pericentrin antibody was carried out to determine the effect of over-expression on pericentrin localization. Over-expression of the C-terminus of either CHD3 or CHD4 caused the rapid loss of pericentrin from the centrosome. See insets in ‘merge’ panels. Compare centrosome in control cell that is not transfected (bottom panel upper cell) with other transfected cells. In a small population of cells (4%) over-expressing the C-terminus of CHD4 localization of the fusion protein at

the centrosome was observed (boxed region in left image). Insets in the merged images show enlargements of pericentrin centrosomal staining.

Figure 4

CHD3 and CHD4 are lost from the centrosome upon RNAi

A) RPE-1 cells were treated with siRNA that specifically targeted CHD3 or CHD4 for 72 hrs, fixed in -20^{o}C methanol and stained by IF with CHD specific antibodies and 5051. Both CHD3 and CHD4 were lost from the centrosome upon RNAi treatment in addition to a reduction in the nuclear staining of the proteins. Loss of CHD3 from the centrosome also appeared to cause a concomitant decrease in centrosomal proteins recognized by the human autoimmune serum 5051. Compare centrosome staining levels to cells with higher levels of CHD3 or 4. Lower cell in both CHD3 and 4 panels has reduced centrosome (5051) staining. **B**) Western blotting was carried out to determine the level of protein reduction in lamin A/C (control), CHD3 and CHD4 siRNA-treated cells. Pericentrin and α-tubulin levels appeared to be unaffected in CHD3 and CHD4 siRNA-treated cells.

Figure 5 Centrosomal components are lost after silencing of the CHD3 gene

A) HeLa cells were treated with siRNA against CHD3, CHD4 or lamin A/C for 48 hrs, the cells fixed in -20^{o}C methanol and then stained with an anti-CHD3/4 monoclonal antibody (red) and an anti-pericentrin antibody (green). Silencing of the CHD3 gene resulted in the loss of pericentrin from the centrosome while CHD4 RNAi appeared to have no affect. See intensity profiles for more quantiative data (below images). **B) upper panels**. HeLa siRNA-treated cells from the experiment described in A were stained with anti CHD3/4 specific (red) and anti-γ-tubulin (green) antibodies (upper panels). Insets show enlarged images of centrosomal γ-tubulin staining. The amount of γ-tubulin present at the centrosome in CHD3 siRNA-treated interphase cells was no different compared to

CHD4 or lamin A/C siRNA-treated cells. **B) lower panels.** RPE-1 cells were treated with CHD3, CHD4 and lamin A/C siRNA for 72 hrs, fixed and stained with CHD3/4 specific (red) and centrin-1 (green) antibodies to determine of centrioles were present after gene silencing. Insets show enlarged images of centrin-1 staining. Centrin-1 staining was observed under all siRNA conditions indicating that silencing of either the CHD3 or CHD4 genes did not affect the centriole structure.

Figure 6

Mitotic failure in cells treated with siRNA against CHD3

A) HeLa cells treated with CHD3, CHD4 or lamin A/C siRNA for 48 hrs were fixed with -20^{o}C methanol and stained with anti-α-tubulin (red) and 5051 (green) antibodies. Mitotic cells treated with CHD3 siRNA predominantly displayed a prometaphase-like phenotype with unaligned chromosomes and poorly formed bipolar spindles. Microtubules within these spindles either appeared to be bundled together or lesser in number. In comparison this phenotype was rarely observed in CHD4 or lamin A/C siRNA-treated cells, although a slight increase in spindle defects was observed after CHD4 RNAi. **B**) IF staining of gamma tubulin in HeLa cells treated with siRNA against CHD3, CHD4 or lamin A/C. A reduction in the amount of γ-tubulin at centrosomes during mitosis was observed in CHD3 siRNA-treated cells compared to CHD4 and lamin A/C-treated. **C**) Quantification of mitotic stages in siRNA-treated cells. Spindle defects were grouped together to simplify the presentation of the results and included: lagging chromosomes monopolar-, tripolar- and half-spindles. CHD3 siRNA-treated cells predominantly exhibited a prometaphase-like phenotype (44% of mitotic cells) but an increase in spindle defects was also observed. In CHD4 siRNA treated cells an increase in spindle defects, compared to the lamin A/C control, was observed.

Figure 7

Depletion of CHD3 causes metaphase delay and cytokinesis failure

Images taken from time-lapse imaging of HeLa cells treated with siRNA against either lamin A/C siRNA (**A**) or CHD3 (**B**). Imaging was started 24 hrs after initial siRNA treatment and monitored cell division for >22 hours. **A**) Arrowheads point to cells undergoing mitosis, the average time taken for the transition from NEB to the end of metaphase was 38 minutes after treatment with lamin A/C siRNA. **B**) Cells treated with siRNA against CHD3 exhibited a metaphase delay, failure to segregate chromosome and a failure to complete cytokinesis. Dotted lines encircle cells that fail to completely divide. At time 0 hrs the cell in the upper left corner appears to have divided but later on the daughter cells rejoin and form a binucleate cell. A second cell that appears to be in metaphase at 0 hrs enters into anaphase a 2 hrs 45 min but fails to complete cytokinesis and ultimately becomes binucleate. Further examples of this phenotype are seen later on in the movie, starting at times 13 hrs 20 min and 19 hrs 40 mins. At 12 hrs 35 min a cell (labeled with black arrowhead) starts to undergo mitosis and after spending 375 min in metaphase the cell enters into anaphase, 18 hrs 50 mins. A total of 6 cells in the movie fail to segregate their chromosome and an example of this phenotype is shown by the cell marked with a white arrowhead. After a prolonged period spent in metaphase (280 mins) the cell eventually reattaches to the substrate and is mononucleate. **B**) Graph showing the time taken to complete nuclear envelope breakdown (NEB) to end of metaphase transition in lamin A/C and CHD3 siRNA-treated HeLa cells. A total of 23 cells completed this process after treatment with lamin A/C siRNA with an average time of 38 minutes (range of 15-110 mins). In contrast, only 10 CHD3 siRNA-treated cells underwent division taking on average 265 mins to complete the NEB to end of metaphase transition (range 40-435 mins).

Supplemental Figure 1

Mapping of the pericentrin-binding domain on CHD4 using the yeast two-hybrid system

A series of GAL4-TAD CHD4 deletion constructs, covering the pericentrin-interacting fragment identified in the yeast two-hybrid screen, and a GAL4-DBD pericentrin expression construct were used to transform the yeast strain AH109. Colonies were streaked onto selective media to test for an interaction. A region between residues 1687-1880 of CHD4 was required for this interaction. Comparison shows that this domain is conserved between CHD3 and CHD4 sharing 81% sequence identity and 92% similarity.

Supplemental figure 2

Mitotic defects after CHD3 gene silencing

HeLa cells were stained 48 hrs after siRNA treatment with anti-α-tubulin and 5051 antibodies. These panels shows additional defects than those shown in Figure 6A.

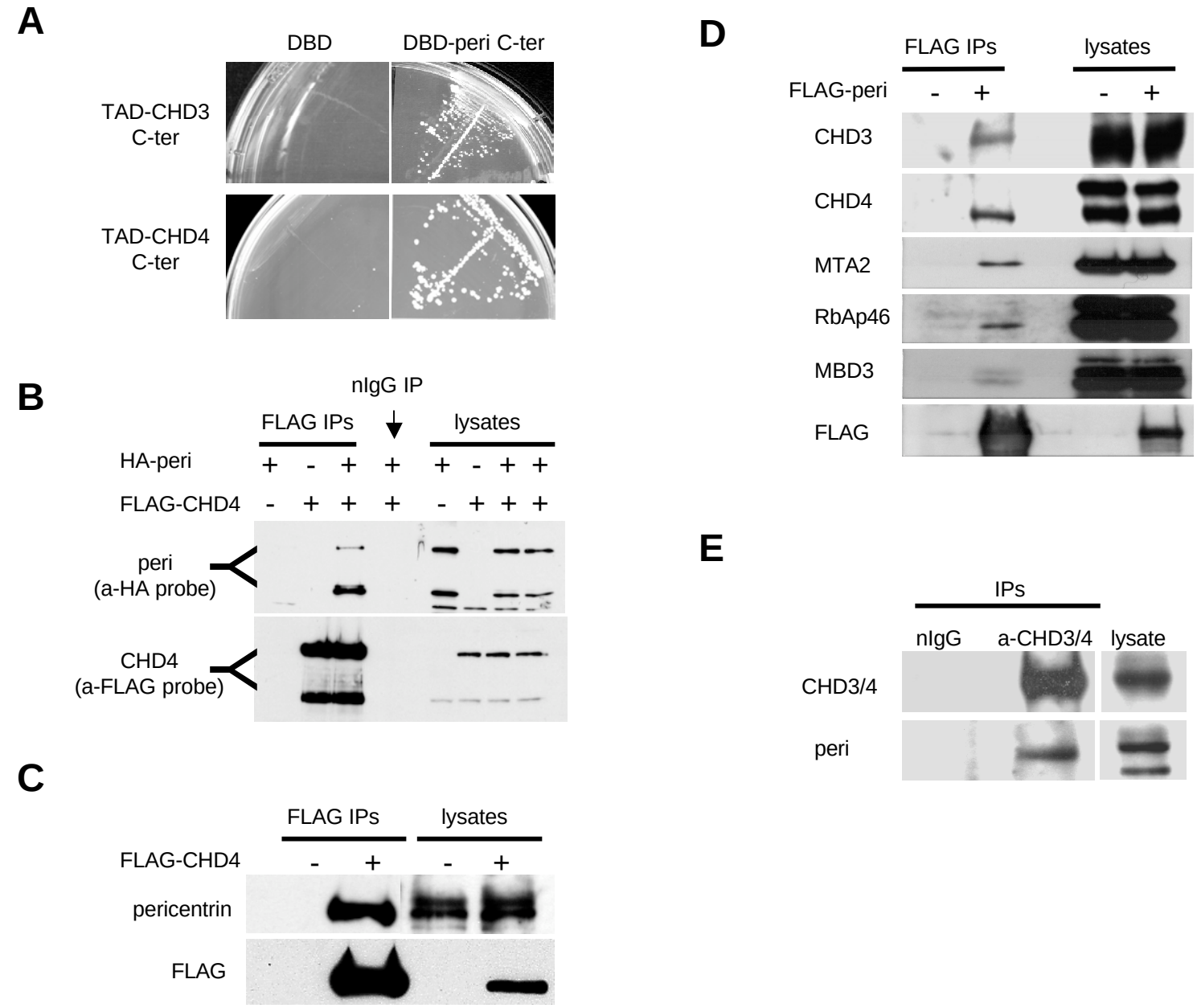
A
DBD
DBD-peri C-ter
TAD-CHD3
C-ter
TAD-CHD4
C-ter
B
nIgG IP
FLAG IPs
lysates
HA-peri
+ - + + + - + +
FLAG-CHD4
- + + + - + + +
peri
(a-HA probe)
CHD4
(a-FLAG probe)
C
FLAG IPs
lysates
FLAG-CHD4
- + - +
pericentrin
FLAG
D
FLAG IPs
lysates
FLAG-peri
- + - +
CHD3
CHD4
MTA2
RbAp46
MBD3
FLAG
E
IPs
nIgG
a-CHD3/4
lysate
CHD3/4
peri

Fig 1

A

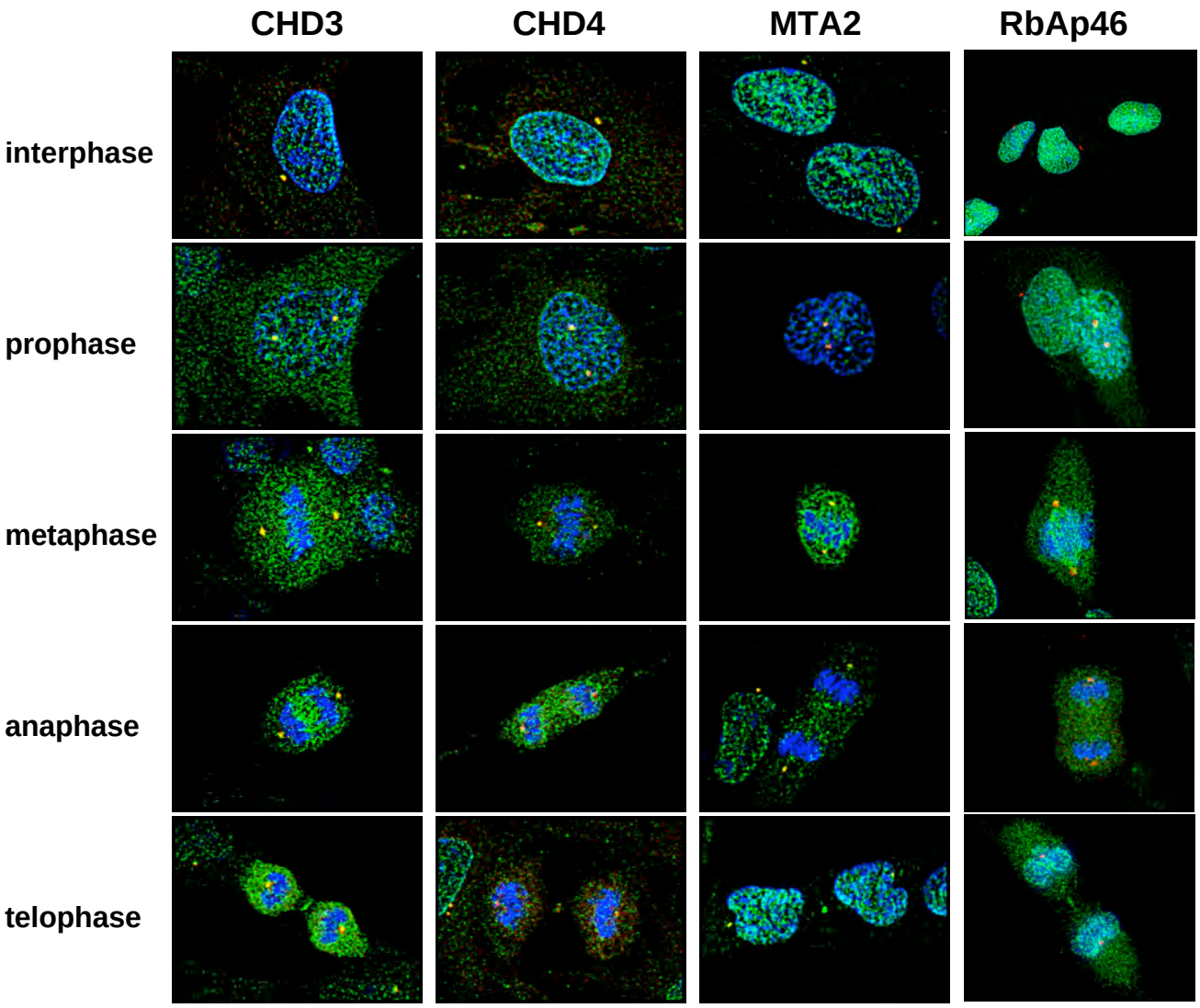
CHD3
CHD4
MTA2
RbAp46
interphase
prophase
metaphase
anaphase
telophase

B

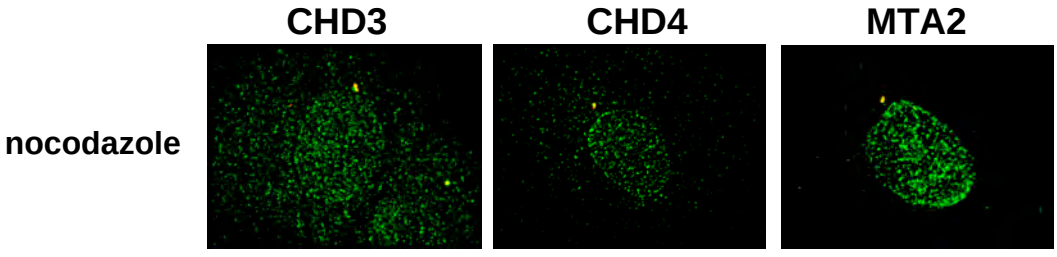
CHD3
CHD4
MTA2
nocodazole

Fig 2

A

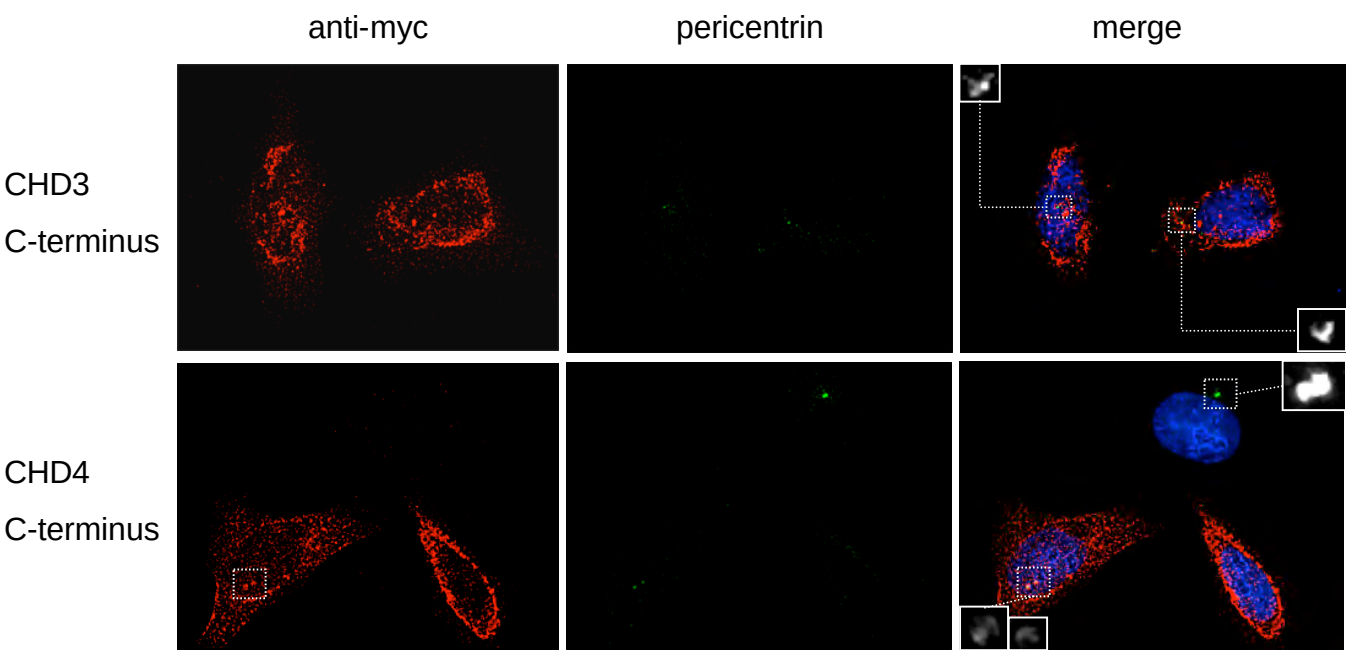

B

Graph quantifying defects

Fig 3

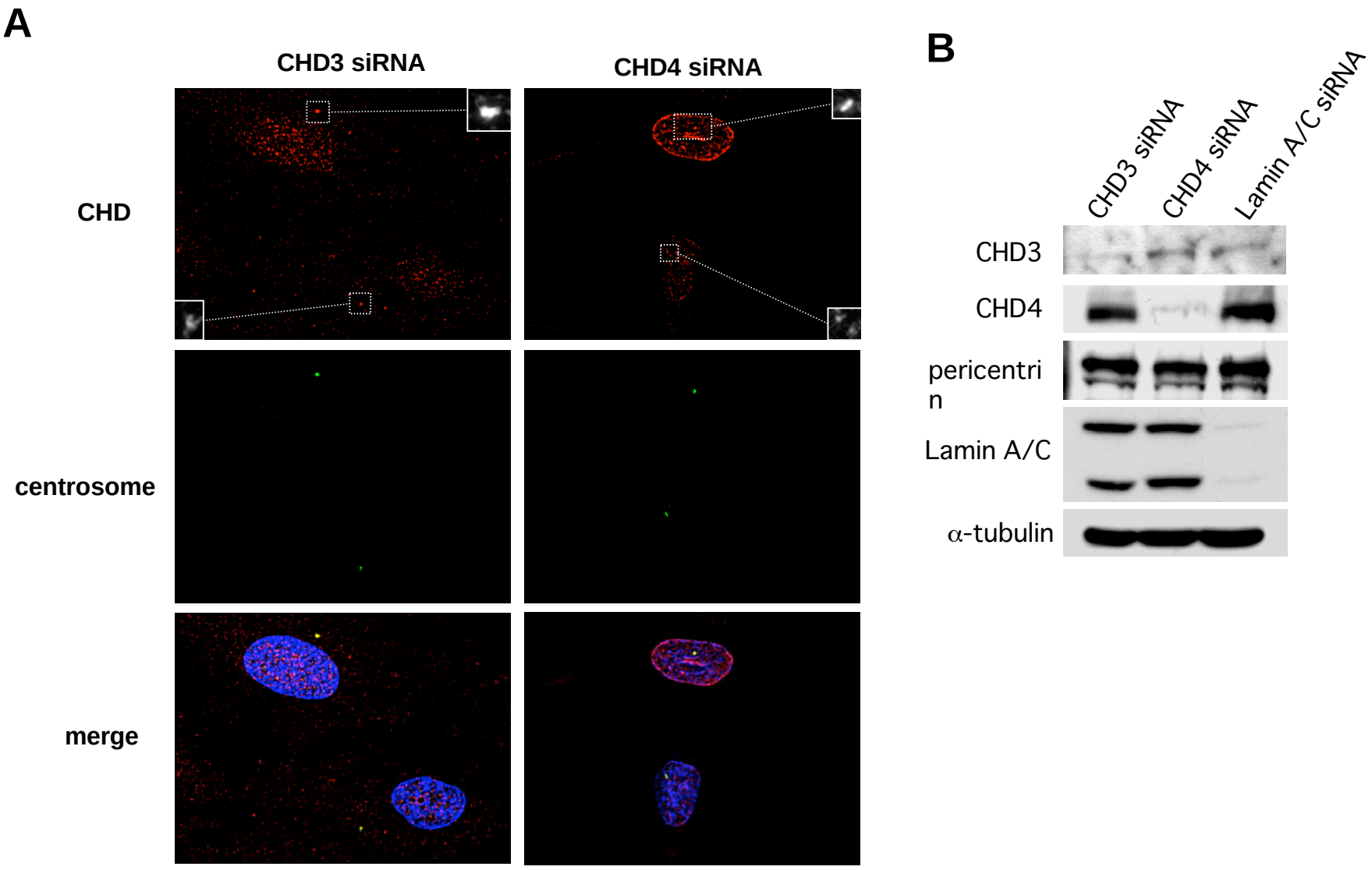
A
CHD3 siRNA
CHD4 siRNA
CHD
centrosome
merge
B
CHD3 siRNA
CHD4 siRNA
Lamin A/C siRNA
CHD3
CHD4
pericentri
n
Lamin A/C
α-tubulin

Fig 4

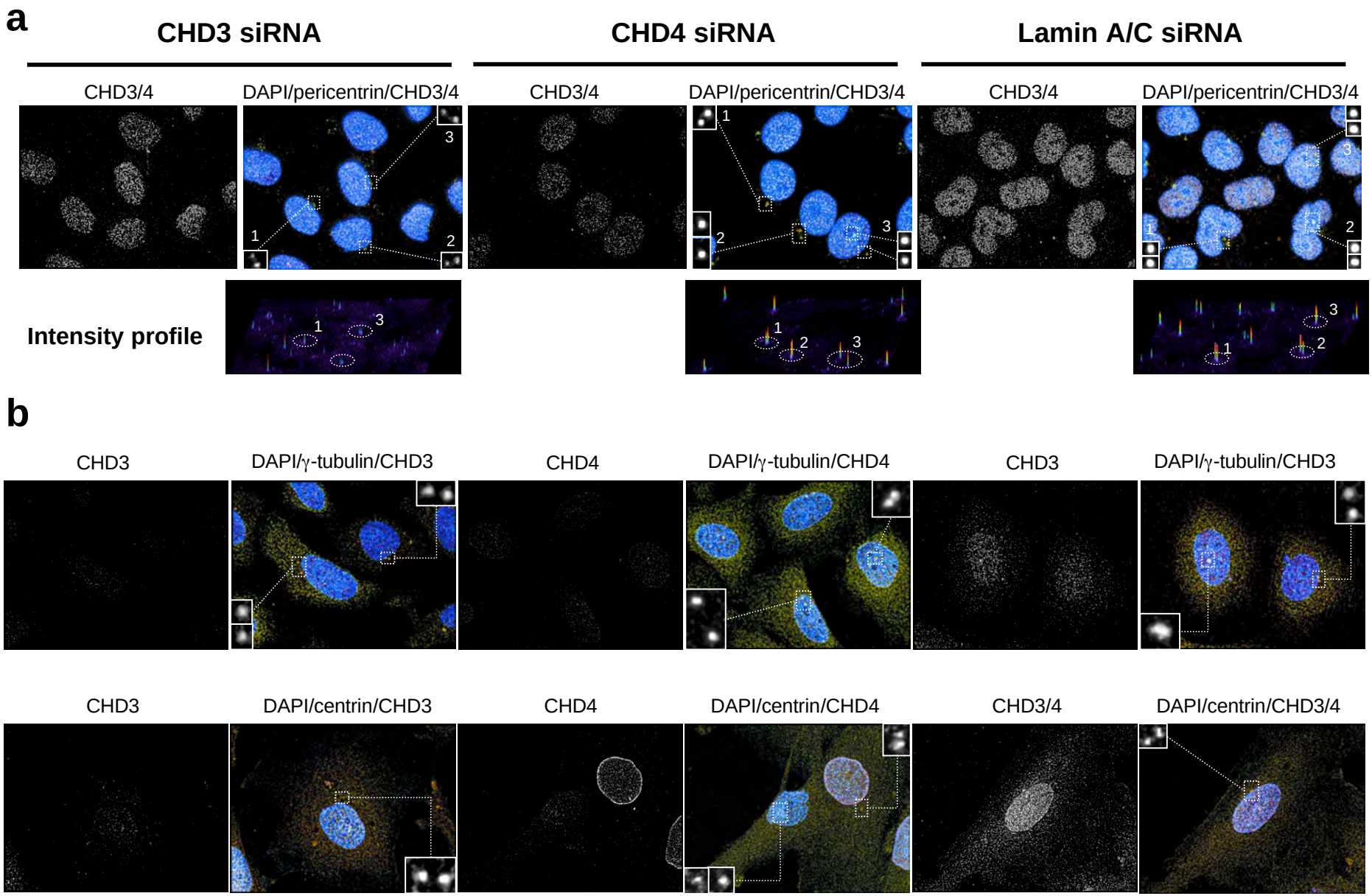
a
CHD3 siRNA
CHD4 siRNA
Lamin A/C siRNA
CHD3/4
DAPI/pericentrin/CHD3/4
CHD3/4
DAPI/pericentrin/CHD3/4
CHD3/4
DAPI/pericentrin/CHD3/4
Intensity profile
b
CHD3
DAPI/γ-tubulin/CHD3
CHD4
DAPI/γ-tubulin/CHD4
CHD3
DAPI/γ-tubulin/CHD3
CHD3
DAPI/centrin/CHD3
CHD4
DAPI/centrin/CHD4
CHD3/4
DAPI/centrin/CHD3/4

Fig 5

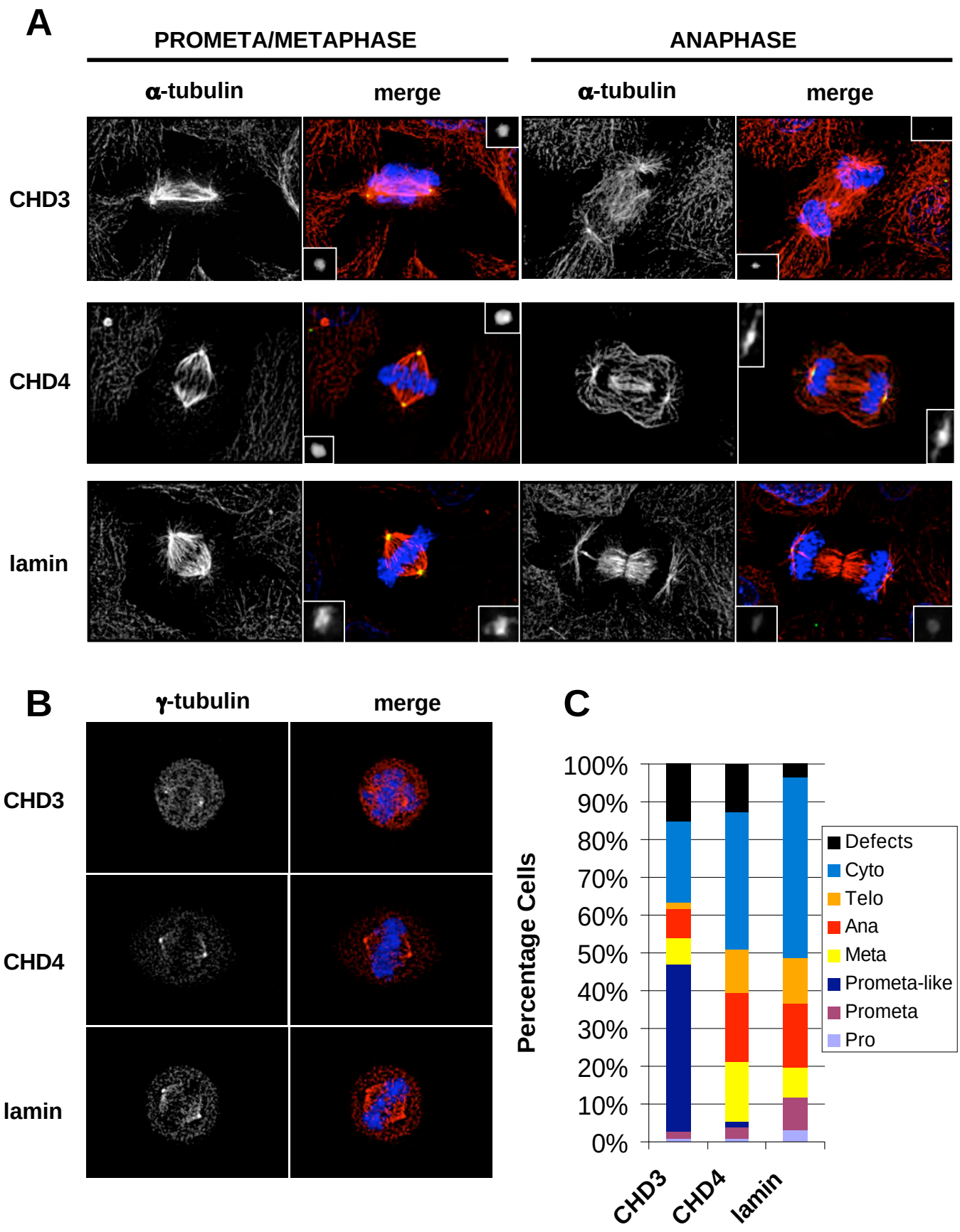
A
PROMETA/METAPHASE
ANAPHASE
α-tubulin
merge
α-tubulin
merge
CHD3
CHD4
lamin
B
γ-tubulin
merge
CHD3
CHD4
lamin
C
Percentage Cells
100%
90%
80%
70%
60%
50%
40%
30%
20%
10%
0%
CHD3
CHD4
lamin
Defects
Cyto
Telo
Ana
Meta
Prometa-like
Prometa
Pro

Fig 6

A

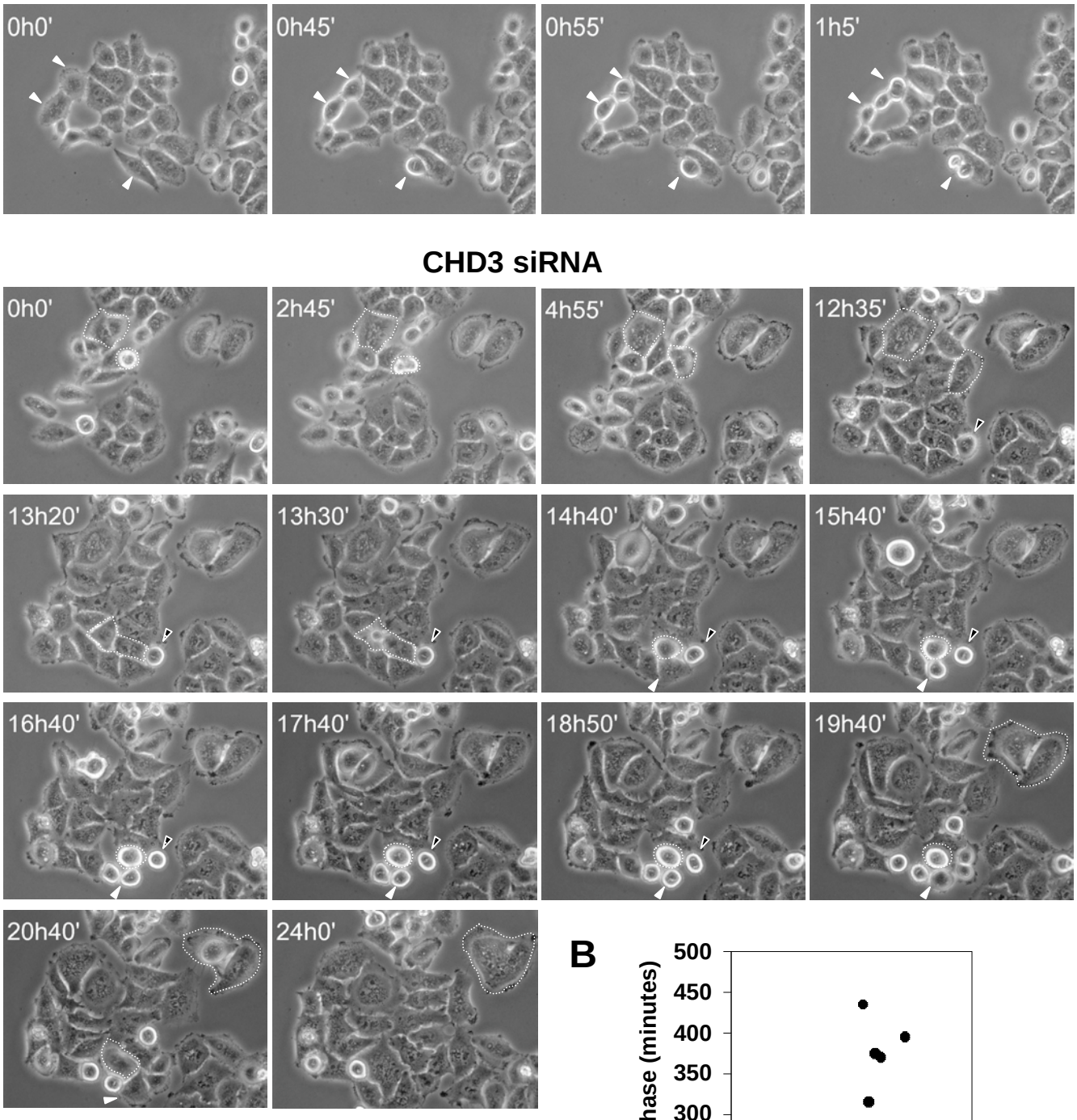
lamin siRNA
0h0'
0h45'
0h55'
1h5'
CHD3 siRNA
0h0'
2h45'
4h55'
12h35'
13h20'
13h30'
14h40'
15h40'
16h40'
17h40'
18h50'
19h40'
20h40'
24h0'

B

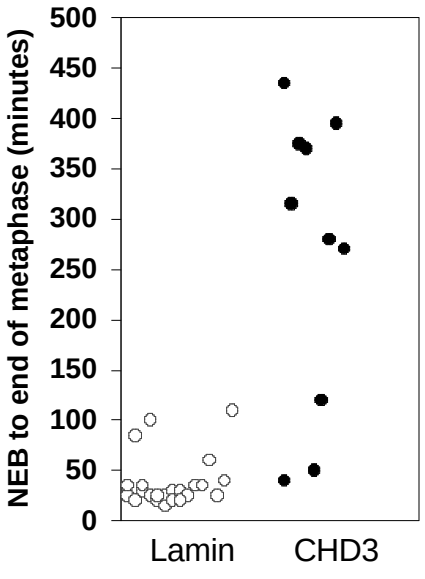
NEB to end of metaphase (minutes)
500
450
400
350
300
250
200
150
100
50
0
Lamin
CHD3

Fig 7